UNIVERSITAT DE BARCELONA

Final degree project

Biomedical engineering degree

"MECHANICAL REGULATION OF NUCLEOCYTOPLASMIC TRANSPORT IN NEURONS"

Barcelona, 11 June 2025

Author: MAR ALTADILL CORDERO

Director: JORGE OLIVER de la CRUZ

Tutor : PERE ROCA-CUSACHS SOULERE

Abstract

Brain stiffness changes with aging and is further altered in neurodegenerative diseases such as Alzheimer's disease (AD). It is now well established that cells are capable of sensing mechanical cues from their environment and adapting their behaviour accordingly — a process known as mechanosensing. One of the processes affected by mechanical forces is nucleocytoplasmic transport (NCT), where extracellular mechanical inputs can modulate nuclear tension and impact molecular trafficking through nuclear pores. Interestingly, NCT has been shown to be disrupted in AD and other neurodegenerative disorders. However, whether neurons can directly sense changes in brain stiffness and whether this affects NCT remains unclear.

In this project, we addressed this question by combining a neuronal model (SH-SY5Y cells differentiated into neuron-like cells), polyacrylamide (PAA) hydrogels of defined stiffness, and a mechanosensitive synthetic reporter of NCT (SeNCYT). We also validated the system using osmotic shocks and compared undifferentiated and differentiated cells. Our results show that neuron-like cells respond to changes in substrate stiffness with alterations in cell morphology and NCT dynamics, supporting the idea that mechanosensing may contribute to the regulation of nuclear transport in the context of neurodegenerative disease. These findings provide a potential link between brain mechanics and neuronal dysfunction in aging and AD.

Key words: Stiffness, Alzheimer Disease, Mechanosensing, Nucleocytoplasmic Transport, cell differentiation, SH-SY5Y cell line, SeNCYT

Resum

La rigidesa del cervell varia amb l'envelliment, i s'observa substancialment alterada en trastorns neurodegeneratius, com per exemple l'Alzheimer. Avui dia, està àmpliament acceptat el fet que les cèl·lules són capaces de detectar i respondre a estímuls mecànics de l'entorn, en un procés conegut com a '*mechanosensing'*. Un dels mecanismes més sensibles a les forces mecàniques és el transport nucleocitoplasmàtic (TNC), on els impulsos mecànics externs són capaços de modular la tensió nuclear de les cèl·lules, com també de causar un impacte sobre el tràfic molecular a través dels porus nuclears. A més a més, s'ha evidenciat que el TNC està alterat en patologies com l'Alzheimer o en altres malalties neurodegeneratives. No obstant això, encara es desconeix si les neurones poden detectar canvis en la rigidesa cerebral, afectant al transport entre el nucli i el citoplasma conseqüentment.

Aquest projecte respon aquesta qüestió mitjançant la combinació d'un model neuronal (cèl·lules SH-SY5Y diferenciades en neurones), hidrogels de poliacrilamida (PAA) d'una rigidesa determinada, i un sensor sintètic mecano-sensitiu (SeNCYT) capaç de reportar canvis en el TNC. Per validar els resultats, s'han aplicat xocs osmòtics i s'han comparat els efectes sobre cèl·lules diferenciades i cèl·lules i no diferenciades. Els resultats indiquen que les cèl·lules neuronals són sensibles a la rigidesa del substrat, incloent-hi alteracions en la morfologia cel·lular i en la dinàmica del TNC, fet que suporta la idea que el '*mechanosensing'* contribueix a la regulació del transport nuclear en patologies neurodegeneratives. Aquestes conclusions permeten enllaçar la mecànica cerebral amb la disfunció neuronal.

Paraules clau: Rigidesa, Alzheimer, *Mechanosensing,* Transport nucleocitoplàsmic, diferenciació cel·lular, cèl·lules SH-SY5Y, SeNCYT

Acknowledgements

I would like to begin by expressing sincere gratitude to Jorge Oliver de la Cruz, the director of this project. His constant dedication and guidance have been essential throughout this journey. I am especially thankful for the patience he showed in the initial stages and the trust he had in me as the work progressed. Under his mentorship, I have been able to understand that research and academia is a journey defined by experience, and that with the proper attitude, solutions can always be found.

My genuine thanks also go to Professor Pere Roca for giving me the opportunity to develop this project within his research group. Being a part of this team has given me the possibility to explore the field of cellular mechanobiology, particularly in relation to neurodegenerative diseases. In addition, I equally appreciate the warm welcome and guidance of all the members of his group. Their passion and dedication have been really inspiring and valuable during my stay.

A very special thanks goes to Valeria Venturini, whose help was key in understanding the complexities of confocal microscopy imaging. Honestly thank her experience and disposition to share with me a version of her ImageJ macro – which I furtherly could adapt to my project –. Her collaboration enhanced and eased crucial points of my analysis. In addition, her support, both practical and personal, made a significant difference in the success of this work.

Finally, I also want to show gratitude to all my family and friends. Their constant support and encouraging words have been a source of strength. Their presence has not only eased the process and the struggles I might have faced but also gave me the motivation to progress.

LIST OF FIGURES

LIST OF TABLES

LIST OF EQUATIONS

GLOSSARY

IBEC	Institute for Bioengineering of Catalonia
WBS	Work Breakdown Structure
PERT	Program Evaluation and Review Technique
AD	Alzheimer's Disease
ECM	Extracellular Matrix
FA	Focal Adhesions
APP	β-Amyloid precursor protein
PHF	Paired Helical Filaments
YAP	Yes-Associated Protein
TAZ	WW Domain-Containing Transcription Regulator Protein 1
MS	Multiple Sclerosis
TBI	Traumatic Brain Injury
LINC	Linker of nucleoskeleton and cytoskeleton complex
NPCs	Nuclear Pore Complexes
ATP	Adenosine Triphosphate
NCT	Nucleocytoplasmic transport
Nups	Nucleoporins
FG	Phenylalanine-Glycine
NTR	Nuclear Transport Receptor
NLS	Nuclear Localization Sequence
NES	Nuclear Export Sequence
NGF	Nerve Growth Factor
iPSC	Induced Pluripotent Stem Cells
vhCOs	Vascularized human Cortical Organoids
AJs	Adherens Junctions
MA-ion channel	Mechanical Activated Ion Channel
CNS	Central Nervous System
CAMs	Cell Adhesion Molecule
RBPs	RNA Binding Proteins
WHO	World Health Organization
US	United States
EU	European Union
PET	Positron Emission Tomography
MRI	Magnetic Ressonance Imaging
CSF	Cerebrospinal Fluid
NGN2	Neurogenin 2
rtTA	Reverse-Tetracycline Transactivator Protein
tetO	Tet-Operator
dox	Doxycycline
FBS	Fetal Bovine Serum
RA	Retinoic Acid
BDNF	Brain Derived Neurotrophic Factor
KCl	Potassium Chloride
GFP	Green Fluorescent Protein
PrA	Protein A
MRTFA	Myocardin-related transcription factor A
NFAT	Nuclear factor of activated T-cells
WT	Wild Type

UV	Ultraviolet
NE	Nuclear Envelope
LSCM	Laser Scanning Confocal Microscope
SeNCYT	Sensor of Nucleocytoplasmic Transport
RT	Room Temperature
FACS	Fluorescent Activated Cell Sorting
S/N	Sign to Noise
N/C	Nuclear to Cytoplasm
BPI	BrainPhys
NB	Neurobasal
PAA	Polyacrylamide
CO_2	Carbon Dioxide
CO	Carbon Oxide
DMEM/F12	Dulbecco's Modified Eagle Medium (DMEM) and Ham's F-12 Nutrient Mixture
Pen/Strep*L-Glut	Penicillin and Streptomycin (Pen/Strep), with L-Glutamine
SD	Standard Deviation
N2 gun	Nitrogen spray gun
PBS	Phosphate Buffered Saline
TEMED	Tetramethylethylenediamine
APS	Ammonium Persulfate
EDC	1-Ethyl-3-(3-dimethylaminopropyl) carbodiimide
NHS	N-Hydroxysuccinimide
HEPES	4-(2-hydroxyethyl)-1-piperazineethanesulfonic acid
PLL-G PEG	Poly(L-lysine)-graft-poly (ethylene glycol)
DNA	Deoxyribonucleic Acid
LED	Light-emitting Diode

TABLE OF CONTENTS

1. INTRODUCTION

1.1. MOTIVATION

For as long as I can remember, I have been fascinated by biology, the human body behaviour and, specially, the brain. To keep learning about them I decided to pursue Biomedical Engineering, which allowed me to attend lessons in biomechanics and biophysics. Among all subjects, the seminars and lectures on mechanobiology were the most fascinating to me, and that is why, when I saw the opportunity to participate in a research project in IBEC, I did not hesitate for a second.

Alzheimer's Disease (AD) has been widely studied over the years. However, there are still many aspects of its pathology that remain unexplored. This increased my interest in neurobiology, and particularly in AD. Since my interests were growing, I really wanted to get into the subject and learn as much as possible. Motivated by this curiosity, I ended up developing a project based on understanding the relationship between brain stiffness and nucleocytoplasmic transport, and its effects on AD. The research was carried under the supervision of Jorge Oliver de la Cruz, a senior researcher at the Professor Pere Roca-Cusachs' research team. The ultimate goal of the project is to expand our understanding about brain mechanics in AD and hopefully contribute to further advancements and therapeutic strategies.

1.2. OBJECTIVES

The main aim of this research is to study whether nucleocytoplasmic transport in neurons is regulated by substrate stiffness. To investigate this phenomenon, we will develop a novel in vitro model using neuronal-like cells equipped with a genetically encoded fluorescent sensor. These cells will be cultured on substrates with controlled mechanical properties.

This primary objective can be divided into the following specific aims:

- To generate a cell line constitutively expressing a validated genetically encoded sensor for nucleocytoplasmic transport.
- To assess the sensor responsiveness to cellular tension using osmotic stress assays.
- To generate an in vitro model combining differentiated neuron-like cells, the sensor, and hydrogels of defined stiffness.
- To analyse the nucleocytoplasmic distribution of the sensor across the different rigidities using live-cell imaging microscopy.

In addition to these scientific goals, efficient project coordination was essential to ensure smooth progress and high-quality results. The project management objectives included:

- Designing an exhaustive research plan, which included dividing the research into achievable milestones aligned with the time available and experimental complexity.
- Staying in close contact with the research supervisor for guidance, troubleshooting, and critical feedback.
- Anticipating possible experimental or logistical setbacks and preparing backup strategies.
- Ensuring timely access to materials, reagents, and instrumentation by coordinating reservations and orders.
- Maximizing the reliability and reproducibility of the results by using validated protocols and performing appropriate replicates.

1.3. LIMITATIONS

As in any research project, several limitations must be taken into account, as they may impact the reliability or scope of the results. This constrains might be related to organizational challenges or external factors beyond our control.

One potential limitation is the availability of basic resources, such as reagents, equipment or laboratory spaces.

Another relevant factor is the complexity of the methods involved in this research project. Despite the director, Dr. Jorge Oliver, having extensive knowledge and experience with the required techniques, it also necessary to fine-tune protocols and optimize experimental conditions. Likewise, although the student is already familiar with general laboratory procedures (e.g. cell culture, microscopy), additional training is required to ensure the correct handling of specialized techniques (e.g. neuronal differentiation, live-imaging microscopy). This learning process may initially affect the rhythm and precision of the experiments.

Despite the importance of the limitations proposed above, the restricted number of substrate stiffness conditions tested was a crucial constraint throughout the development of the project. Although the two selected rigidities were carefully chosen based on prior studies — where they showed clear effects on neuronal-like cells — they only represent a simplified model of brain tissue mechanics. The use of static hydrogels, without dynamic modulation over time, further constrained the ability to mimic the progressive mechanical changes that occur during aging or neurodegeneration.

Another significant limitation was the technical complexity of using the genetically encoded SeNCYT sensor in live-cell imaging. Because fixation alters the distribution of the sensor, all experiments had to be performed in live cells, which added constraints in terms of timing, reproducibility, and environmental control. The success of each experiment depended heavily on selecting cells with optimal expression levels and fluorescence signal, which significantly reduced the usable sample size. Consequently, while trends were observable, some results could not reach statistical significance due to limited replicate numbers.

Furthermore, given the complexity of the biological systems involved (neurons, nuclear transport, tissue rigidity) and the difficult questions being investigated, the results of the project and their interpretation are inherently limited, only barely exploring the effects of rigidity on the transport of an artificial sensor. Consequently, to further validate the extent of the results and understand their implication, it will be necessary posterior experiments to confirm the findings and asses their biological relevance in the context of brain and AD.

Finally, the most constraining factor was the limited time available to complete the entire project. The long duration of differentiation protocols, combined with the need for real-time imaging and access to high-end microscopy platforms, demanded a strictly organized workflow. In some cases, compromises had to be made in experimental scope to ensure that key comparisons could be completed with sufficient quality and control.

Taken together, these limitations highlight the technical and logistical challenges of studying mechanosensitive processes such as nucleocytoplasmic transport in live neuron-like cells. However, they also lay the groundwork for future experiments with expanded conditions, dynamic mechanical models, and complementary methods to further validate and extend these findings.

1.4. STRUCTURE

This report is organized into four major sections, each reflecting a different stage of the development of the project, as illustrated in Figure 1.

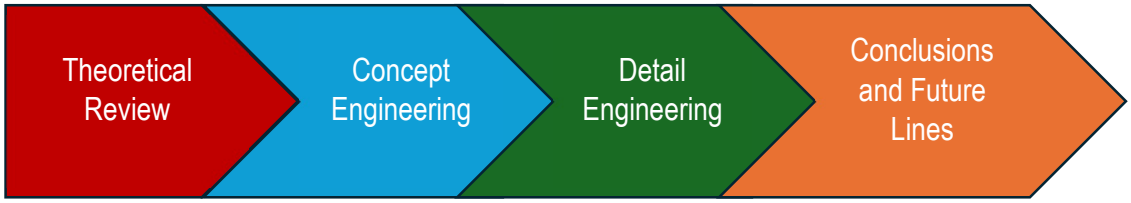

Figure 1. Flowchart of the different sections of the project

The **first section** provides the theoretical framework of the project. It includes a comprehensive review of the most relevant scientific literature to the topics of the research project, including background concepts on Alzheimer's disease, cellular mechanobiology, and nucleocytoplasmic transport, as well as a review of current models and tools used in the field. A market analysis and an overview of relevant regulations are also included, see Sections 2,3 and 9.

The **second section** covers the aspects related to conception engineering detailed in Sections 4, 6, 7 and 8. It includes a comparative evaluation of techniques, media optimization, the development of PAA substrates, and the selection of imaging protocols. It also covers all decisions related to cell model development, sensor integration, and image analysis strategies. A Work Breakdown Structure (WBS) is presented to explain the division of the full research into specific work packages, along with the duration and cost for each one of them. Furthermore, a PERT and a GANTT diagram are also included to provide a comprehensive overview of the project timeline and workflow.

The **third block**, which comprises Section 5, presents the experimental results. This includes the generation of the sensor-expressing SH-SY5Y line, its characterization pre- and post-differentiation, and quantification of nucleocytoplasmic transport under different mechanical conditions.

The final **fourth section** contains the main conclusions and future research directions. It reflects on the significance of the results in relation to the original hypothesis and proposes possible extensions of the study (Section 10) .

1.5. IBEC: Cellular and molecular mechanobiology group

This project was carried out in the **Cellular and molecular mechanobiology group** at the **Institute for Bioengineering of Catalonia (IBEC) [1],** led by Professor Pere Roca-Cusachs. The main research focus of this group is to uncover the molecular mechanisms that enable cells to detect physical forces-such as tissue stiffness or tension- and how these signals lead to changes in cellular behaviour. Molecular mechanobiology, as a general discipline, seeks to explain the basis of how cells sense, respond, and adapt to mechanical stimulation in their environment [2].

One of the group key research areas is nuclear mechanotransduction: the process by which mechanical stimuli are transmitted to the nucleus, influencing gene expression and cell function. Their findings have shown that cells not only sense the rigidity of their environment but also respond to the spatial arrangement of ligands and neighbouring cells. These mechanisms are essential in processes such as development, regeneration, and disease [3]. The group combines biophysical techniques (e.g., force microscopy, optical tweezers) with molecular biology, advanced imaging,

and computational models to study the connections between extracellular forces and intracellular signalling.

In recent years, with the incorporation of Dr. Jorge Oliver into the team, a new research line has emerged focusing on neuronal mechanobiology. This includes studying how mechanical cues influence neuronal behaviour and how these processes may be altered in neurodegenerative diseases like Alzheimer's.

1.5.1. INSTALLATIONS

This project was carried out mainly in the laboratory facilities shared by the Cellular and molecular mechanobiology group and the Integrative Cell and Tissue Dynamics group, located at the Helix building, one of the buildings integrated in the Parc Científic de Barcelona (PCB), as shown in Figure 2. Workplaces included the cell culture room, the microscope room, and the general laboratory area with benches and computer workstations. Additional infrastructures in the building included -80ºC freezers and liquid nitrogen tanks used for cell cryopreservation.

Moreover, the specialized facilities at the common cell culture of the PCB, located in Cluster I, were used for lentiviral production and for generating the stable cell line used in this project. The most relevant instruments for the study included optical and confocal microscopes, laminar flow hoods, cell culture incubators, -80ºC freezers and liquid nitrogen tanks.

Figure 2. Situation of Helix building, location of the laboratory and other amenities [4]

2. BACKGROUND

This section provides the conceptual and scientific background necessary to understand the rationale and design of the project. It begins with a summary of general concepts, including the main pathological and clinical features of Alzheimer's disease (AD), key principles of cellular mechanobiology, and the mechanical regulation of nucleocytoplasmic transport.

The second part reviews the current state of the art, focusing on the cellular models commonly used to study AD — such as primary cultures and cell lines — and on the tools available to investigate mechanosensitive regulation of nucleocytoplasmic transport. Finally, a brief assessment of the current research landscape is presented, with particular emphasis on the links between brain tissue mechanics, nucleocytoplasmic transport dysfunction, and neurodegeneration. This background serves as the foundation for the experimental approach developed in this project.

2.1. GENERAL CONCEPTS

2.1.1. ALZHEIMER'S DISEASE

Alzheimer's Disease (AD) is progressively becoming one of the most lethal and burdening causes of dementia. AD is characterized by progressive cognitive impairment affecting several domains, or by neurocognitive disfunctions leading to a functional impact on the person life. Apart from clinical diagnosis based on symptomatology, AD may also be detected thanks to the presence of certain biomarkers.

Two main pathological hallmarks define AD pathology: the accumulation of extracellular plaques formed by the accumulation of β-amyloid protein, and the intracellular aggregation of hyperphosphorylated TAU protein.

Neuroinflammation, ageing, and disfunction of the glymphatic system impact in conjunction to produce the accumulation of β-Amyloid. Cryo-electron microscopy and has allowed gaining insight on how the destabilized interactions between the β-Amyloid precursor protein (APP) and catalytic subunits of *γ*-secretase (one of the enzymes responsible for the protein shedding) can lead to a premature release of aggregation-prone β-Amyloid peptides.

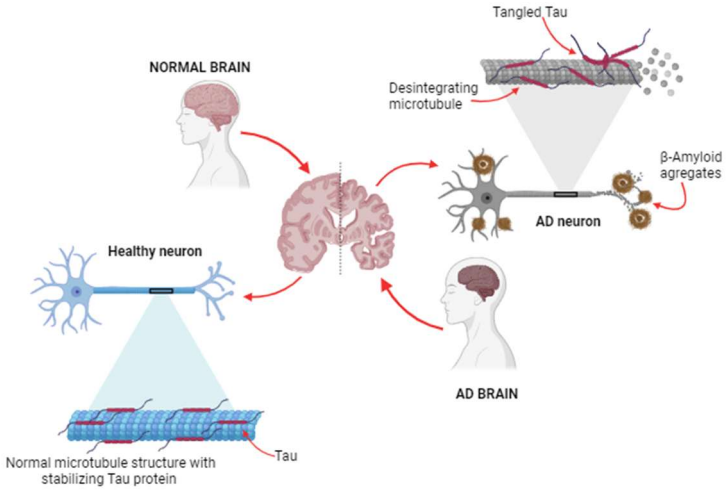

Figure 3. Illustration of the difference between a healthy neuron and AD neurons. Created with www.biorender.com

On the other hand, Tau most known function is to stabilize the microtubule structure in the neuronal axon. In a neurodegenerative context, Tau is hyperphosphorylated, loses the stabilization and assembly abilities, and aggregated into intraneuronal neurofibrillary tangles of paired helical filaments (PHF), finally leading to neurofibrillary degeneration.

Despite the progress made in understanding AD, there is not still a defined cause. However, some factors that increase the likelihood of its appearance have been described. Among the most important ones are an advanced age and carrying the APOEε4 allele. Furthermore, an unhealthy lifestyle and cardiovascular risk factors have also been related to the appearance of neurodegenerative diseases [5],[6]. Although identifying these AD-boosting factors might suggest that finding a cure should be straightforward, in fact, there is still a lot to figure out and learn. Currently, only palliatives treatments exist to delay its progression. In addition, a clear relationship between AD and the mechanobiology there has not yet been described, which might help clarify the underlying causes of AD [7].

2.1.2.CELLULAR MECHANOBIOLOGY

Cell mechanotransduction is defined as the process by which cells translate mechanical inputs from the extracellular environment into biochemical signals inside the cell.

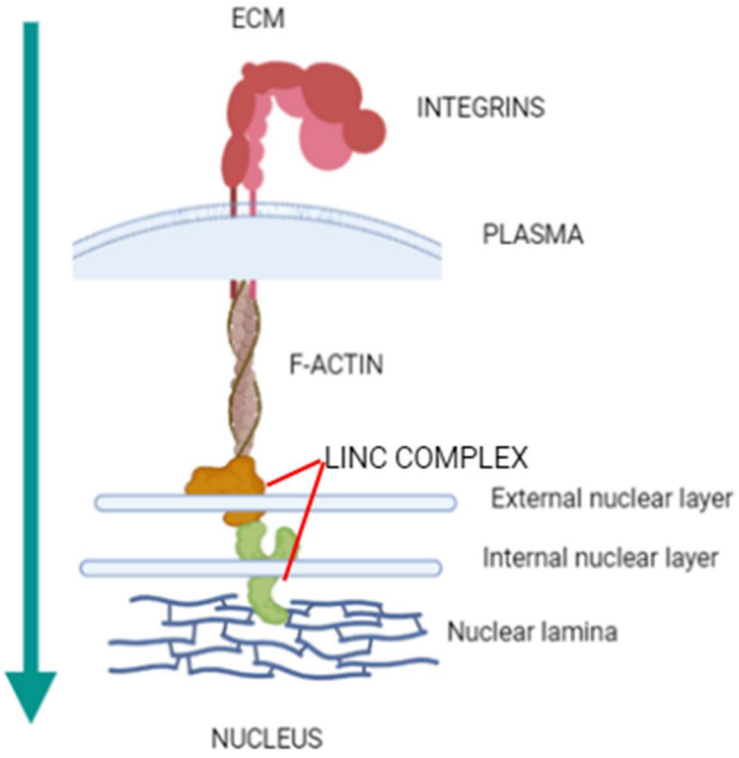

Figure 4. Force transmission pathway from the ECM to the nuclear lamina. Made with: https://www.biorender.com/

As reflected in Figure 4, a prototypical mechanotransduction pathway begins with the extracellular matrix (ECM), which provides structural and biochemical support to surrounding cells. Integrins, transmembrane receptors, mediate the attachment between the ECM and the cellular cytoskeleton. When mechanical forces are applied, integrins transmit these signals to the actin cytoskeleton, a network of actin filaments that provides structural integrity and facilitates intracellular signalling. Nesprins, which are part of the linker of nucleoskeleton and cytoskeleton (LINC) complex, connect the cytoskeleton to the nucleus. This connection allows mechanical signals to be transmitted to the nucleus, influencing gene expression and other nuclear functions, thereby enabling the cell to respond and adapt to its mechanical environment. These changes altered the nuclear lamina, which, in physiological conditions is very dynamic and highly responsive to changes in mechanical stimuli from the ECM, providing protection and structural support to the nucleus [8].

Neurons have been shown to express several mechanosensitive proteins/mechanoreceptors, including several integrins subunits as well as mechanosensitive transmembrane proteins such as PIEZO or TRPVs channels [9]. When PIEZO1 channels are activated, they induce the release of adenosine triphosphate (ATP), directly modulating cellular processes. For instance, recent research found that PIEZO1 channels located at the tip of growth of neuron cones regulate signalling events involved in axonal pathfinding and cell migration [9]. Additionally, neurons also express several TRP mechanosensitive channels, such as TRPV4, which among different stimuli can react to force application. When activated, they have been shown to induce pathologically neuroinflammation and cell death in epilepsy models [10]

Taken together, these findings highlight the importance of mechanical communication between the ECM and the nucleus in neuronal function. Disruption of this communication, particularly through the impairment of the nuclear scaffold, can lead to the malfunction of the Nuclear Pore Complexes (NPCs), which will be addressed in more detail later. For example, the altered conformation and aggregation of hyperphosphorylated TAU contributes to NPCs dysfunction. This may result in synaptic impairment and the abnormal release of neurotransmitters, triggering the progression of neurodegenerative conditions such as AD [10].

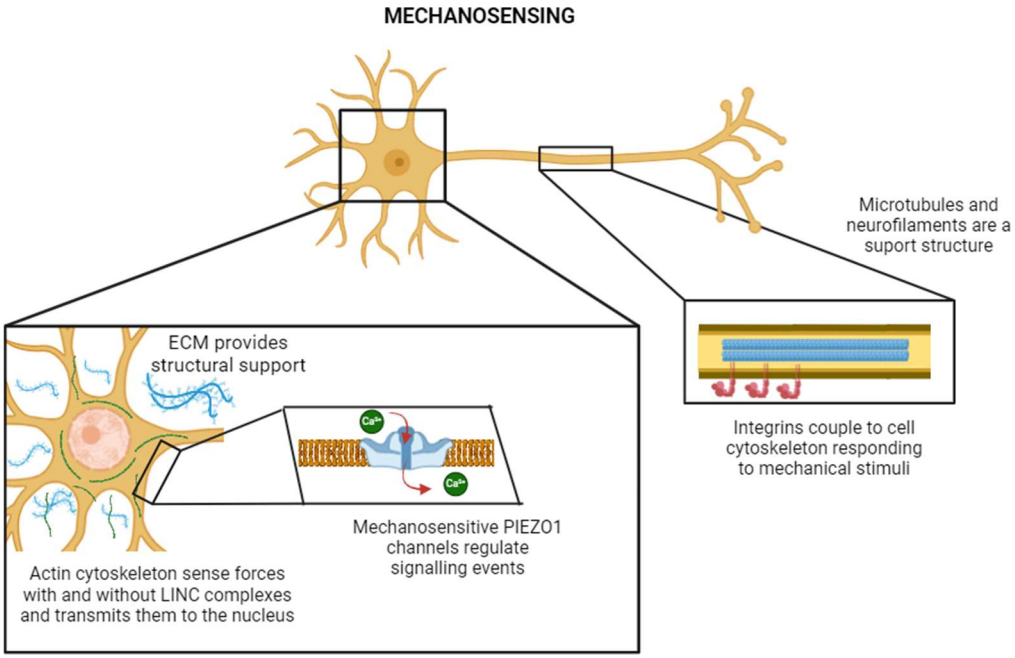

Figure 5. Physiological mechanosensitive hallmarks. Made with: https://www.biorender.com/

Nevertheless, most of the studies have been conducted in the developing brain, with immature neurons/axons, and in animal models, which do not accurately resemble the human AD condition. Hence, there is still plenty of research to be done in adult brain [11].

2.1.3. MECHANICAL REGULATION OF NUCLEOCYTOPLASMIC TRANSPORT

Nucleocytoplasmic transport (NCT) refers to the bidirectional movement of molecules between the nucleus and the cytoplasm. This highly complex process takes place through the nuclear pore complexes (NPCs), large protein complexes embedded in the nuclear envelope.

NPCs are symmetrically structured complexes that span both the inner and the outer nuclear membrane. Each NPC is composed of approximately 30 different proteins known as nucleoporins (Nups), arranged in multiple copies to form a cylindrical channel with octagonal symmetry. The full complex has an estimated molecular weight of around 120 MDa.

The permeability and selectivity of the NPC are regulated by a subset of Nups known as FG-nucleoporins (FG-Nups), which contain intrinsically disordered domains rich in phenylalanine-glycine (FG) repeats. These FG-Nups create a selective barrier that allows small molecules to diffuse passively, while restricting the passage of larger macromolecules. The efficiency of passive diffusion decreases with increased molecular weight (MW). Proteins above ~40-60 KDa generally require active, facilitated transport. In such cases, cargo proteins interacting with nuclear transport receptors (NTR), including exportins and importins, to be efficiently translocated through the NPCs.

For nuclear import, these large molecules must carry a nuclear localization sequence (NLS) which allows its binding to α-importins, that, in turn can interact with β-importins. β-importins are the NTR mediating fast passages within the NPCs by interacting with the FG-nups. Various NLS motifs with differing affinities for importins have been described.

For nuclear export, proteins containing nuclear export sequences (NES) are recognized by exportins, which facilitate their passage through the NPC via interactions with FG-nups.

Nucleocytoplasmic transport is an energy-dependent process, and its directionality is controlled by the Ran GTPase system. The hydrolysis of Ran-GTP to Ran-GDP provides the energy necessary for macromolecular trafficking through NPC. A gradient of Ran-GTP and Ran-GDP is maintained across the nuclear envelope, with Ran-GTP concentrated in the nucleus and Ran-GDP in the cytoplasm. This gradient is essential for regulating the transport cycle: nuclear Ran-GTP promotes cargo release from import complexes and drives the assembly of export complexes [12], [13].

Mechanical forces are able to influence NCT via effects on the NPCs structure and function. Forces transmitted through the cytoskeleton to the nucleus may induce conformational changes in NPCs, altering their pore diameter, nucleoporin composition, and molecular arrangement [12]. These modifications in turn affect the efficiency and selectivity of the transport, in a way dependent on factors such as the molecular weight of the cargo, its mechanical stability, and its binding affinity for the importins and exportins. Mechanosensitive regulation of the NPC function plays a crucial role in cellular adaptation to mechanical cues, impacting processes such as gene expression and cellular adaptation to the physical environment.

2.2. STATE OF THE ART

Improving Alzheimer's Disease understanding requires enhancement of accurate and physiologically relevant in vitro models. This section reviews the current cellular options to study AD pathology, including 2D traditional systems, modern 3D models, and iPSC-derived neurons. In addition, emerging tools for investigation the mechanoregulation of nuclear transport are introduced, as well as the need for gaining mor interest in neurodegeneration research field.

2.2.1. CELLULAR MODELS TO STUDY ALZHEIMER'S DISEASE

The ideal model to study AD needs to reproduce its development by demonstrating the amyloid plaques, Tau tangles, and the progression of neurodegeneration [14]. Some studies that were promising because of their pre-clinical studies, have ended failing in human-clinical trials. Hence, innovative 3D cell culture models have been developed enhancing accuracy in testing models as they allow mimicking AD environment, cell interaction, and blood flow [15]. Nevertheless, in this block different 2D models will be explained as well as the cutting-edge 3D ones.

2.2.2. PRIMARY CULTURES

The generation of primary cultures have been a major advancement during the early stages of AD research, and they allowed to study AD key hallmarks, such as neurofibrillary degeneration or granulovascular neuronal degeneration. Primary neurons are typically obtained from embryos or early postnatal rodents, depending on the required type of neurons and the specific experimental needs. These cells provide a valuable model for understanding disease mechanisms, testing drug efficacy, and observing neuronal behaviour in a controlled environment. Moreover, they can be isolated from transgenic mice carrying human mutations associated with AD, such as those on APP or PS1 genes, to better mimic the genetic background of the disease. These models can recapitulate important AD pathological events, such as β-Amyloid plaques and Tau tangles [14].

However, the use of animal-derived cells has significant limitations. They cannot fully replicate human physiopathology, and important species differences affect the translatability of findings to humans. For instance, many animal models only partially reproduce AD features, often lacking extensive neuronal loss or the development of mature neurofibrillary tangles. Moreover, mice models present a short life span of the animals which, indeed, does not allow the necessary time for the development of the events that in human take for years, even decades. Finally, obtaining primary neurons from animals involves ethical considerations and can be technically challenging, requiring precise techniques to ensure cell viability, and a new extraction for each experiment. Despite these drawbacks, primary neurons remain an essential tool in AD research, offering mechanistic insights that are not easily achievable through other in vitro systems.

2.2.3.CELL LINES

Neuronal cell lines are widely used in in vitro neurobiology studies, mainly because they are ready to use and can be expanded almost indefinitely. Moreover, they can be quite easily genetically modified. In some cases, through proper stimulation, they can be transformed into neuron-like cells that exhibit neuronal traits such as biomarker expression and neurite formation. Several immortalized cell lines have been established over the years, such as PC12, SH-SY5Y, bEnd3, TR-BBB, HBMEC, BV2 with the first two being the most commonly used ones due to their neurogenic properties. Both cell lines can be differentiated into neuron-like cells, presenting neuronal features such as neurotransmitters secretion, neuron morphology, as well as ion and neurotransmitter receptors. However, they differ in origin and differentiation characteristics.

On the one hand, PC12 are derived from a pheochromocytoma of a rat adrenal medulla. Under normal conditions, they present morphological and physiological features of adrenal cells. PC12 are among the most widely used neuronal models because its short differentiation process. In the presence of nerve growth factor (NGF), these cells differentiate and start to show the morphological and functional traits of sympathetic ganglion neurons. For example, some studies have cultured PC12 cells on microelectrodes to understand the synapse formation and function in a non-invasive way [15].

On the other hand, SH-SY5Y cell line is derived from infant human neuroblastoma. They can be differentiated into various types of neuronal-like cells (excitatory, inhibitory, etc) depending on the biochemical stimulation. SH-SY5Y-derived neuronal-like cells display many features resembling mature neuronal morphology, and have therefore been extensively used in AD studies, such as in neurodegeneration models induced by exposition to β-Amyloid oligomers. Despite its popularity, this cell line does not completely resemble mature neurons, and cancerous origin may interfere with certain experimental outcomes [14].

2.2.3.1 IPSC-DERIVED NEURONS

Induced pluripotent stem cells (iPSC) are becoming the gold standard for in vitro study due to their ability of differentiating into several cell types, including neural cells. They are obtained by reprogramming mature somatic cells; thereby avoiding the ethical concerns associated with the use of embryonic stem cells.

Most importantly, iPSC lines can be generated from AD patients, allowing researchers to reproduce in vitro neuronal cells carrying the genetic background of AD patients. For example, in 2011 and in 2012, researchers who differentiated iPSC from AD patients with PS1 and PS2 mutations observed changes in neuronal physiology which are considered important hallmarks of the disease, such as higher levels of β-Amyloid and phosphorylated Tau [14].

More recently, CRISPR/Cas9 technology has been used in iPSC lines to generate knock-in human neurons carrying AD mutations either heterozygously or homozygously. These models reproduce multiple features of the disease, providing valuable tool to improve our understanding of AD [1].

The main disadvantage of iPSC-derived neurons are their higher costs and the longer time required to generate both the cell lines and the derived neurons. Moreover, the resulting neural cells are not fully mature, typically displaying embryonic or foetal characteristics.

2.2.3.2 ADVANCED CELL CULTURES MODELS

In recent years, several advanced models have been developed to overcome the actual constraints of transgenic animals. For instance, cerebral organoids represent one of the newest incorporation into AD research. Organoids allow the formation of structures resembling the human cortex, one of the most affected brain regions in AD. An even more innovative model is the use of vascularized human cortical organoids (vhCOs), which, unlike conventional organoids, are coupled to a perfusion system to mimic cortical vasculature. vhCOs also exhibit properties of the blood-brain barrier (BBB) and nutrient transporters, enhancing the reproduction of the physiological environment found in AD. Even though cerebral organoid cultures feature well some neurodegenerative AD hallmarks, they still present limitation, not fully recapitulating of recreating pathological events and having high costs.

Additionally, several models based on a triculture system have been developed, incorporating neurons, astrocytes, and microglia within a microfluidic platform. Just as organoids, these models have been improved by simulating BBB properties. This 3D model offers more accurate drug-screening methods and eases the research of individual phenotype variations, allowing a personalized approach to disease treatment.

While undoubtably representing a major improvement over classical 2D models, these systems require a long-term culture and the use of expensive reagents, which may limit their use in high-throughput studies [17].

2.2.4. TOOLS TO STUDY THE MECHANOREGULATION OF NUCLEOCYTOPLASMIC TRANSPORT

Throughout the previous sections, an important relation between mechanical stimuli and nuclear behaviour has been highlighted. Hence, studying these interactions is essential to improve our understanding of the underlying mechanisms. Several methods are available to investigate them, which are reviewed in the following paragraphs.

2.2.4.1 STAINING OF SHUTTLING PROTEINS

Several proteins have their nuclear and cytoplasmic distribution naturally altered according to the physical stimuli coming from the extracellular milieu, such as substrate stiffness, shear stress, and cell stretching, allowing the transduction of mechanical signals into changes in gene expression and cellular behaviour. The mechanoregulation of these shuttling proteins stands at the forefront of cellular mechanobiology, offering a profound understanding of how cells perceive and respond to mechanical cues.

Some of the most notable examples are YAP (Yes-associated protein), its paralog protein WWTR1/TAZ (Transcriptional coactivator with PDZ-binding motif), MRTFA (Myocardin-related transcription factor A) or NFAT (Nuclear factor of activated T-cells).

For instance, high substrate stiffness promotes YAP to translocate into the nucleus, where it activates genes associated with cell proliferation and survival, thus dictating cellular fate in response to tissue rigidity. Force transmission leads to nuclear flattening, which stretches nuclear pores, reduces their mechanical resistance to molecular transport, and increases YAP nuclear import [18]. Conversely, MRTFA activity is inhibited by mechanical forces, resulting in its cytoplasmic sequestration and inhibition of transcriptional activity. This delicate balance between nuclear and cytoplasmic localization of YAP and MRTFA is pivotal for maintaining cellular homeostasis and ensuring proper tissue development.

Therefore, analysing the nuclear and cytoplasmic localization by immunostaining can be used as read out of the mechanical state of the nuclei under specific conditions. Nevertheless, this process does not allow to study the process dynamics, as it requires the fixation of the cells. Another limitation is the total expression of these proteins, which can be low in several cell types and therefore reduce the sensitivity of the readout. Finally, given the central role of these proteins in cell homeostasis, they serve as a hub of several inputs. This means that their localization is not only regulated by mechanical cues, but also biochemical signals, such as growth factor paracrine signalling, ECM composition, or energetic status. As a result, their nucleocytoplasmic ratio reflects a combination of these factors rather than cell tension alone.

2.2.4.2 TRANSFECTION OF FLUORESCENT-CONJUGATED SHUTTLING PROTEINS

To overcome some of the limitations of intrinsic shuttling proteins, researchers have overexpressed chimeras which contain covalently attached fluorescent proteins, such as Green Fluorescent protein (GFP). This strategy helps overcome the low levels of expression in some cells and permits live imaging, and therefore the calculation of the kinetics of shuttling. As a drawback, these molecules are still subjected to a mixture of mechanical and biochemical regulations, and therefore they cannot straightforwardly be used as a direct measure of the nuclear tension. Unfortunately, the expression of such important transcription factors can impair normal cell behaviour and cause artifacts, due to the saturation of the cell mechanisms controlling their localization. The recent development of tagging endogenous proteins using CRISPR technology could avoid these issues; however, the inclusion of the fluorescent tag may also alter the molecular weight, the mechanical stability, and the possible interactions of the protein, therefore altering the natural shuttling.

2.2.4.3 SYNTHETIC MOLECULES

DEXTRAN-BASED

Dextran-based assays are commonly used to study nuclear cytoplasmic transport, particularly for assessing the permeability of the nuclear envelope to macromolecules. Dextran molecules are polysaccharides of varying molecular weights that can serve as tracers to mimic the behaviour of larger molecules, such as proteins, within the cell. These assays typically involve the use of fluorescently labelled dextrans of different sizes, allowing researchers to track their movement between the nucleus and cytoplasm.

The molecular weights of dextran molecules used in these assays can vary widely, ranging from a few kilodaltons to several megadaltons. Dextrans with smaller molecular weights (e.g., 3-10kDa) are often used to assess passive diffusion through nuclear pores, while larger dextrans (e.g., 40-70kDa) may be employed to investigate active transport mechanisms or potential barriers to nuclear import/export.

This technique has several advantages. It is versatile and adaptable, given that dextrans of various sizes can be used to probe different aspects of nuclear transport. Moreover, dextran assays are relatively straightforward to perform and can be adapted for use in different cell types and experimental conditions. Finally, fluorescently labelled dextrans enable quantitative and dynamic measurement of nuclear transport, such as transport rates and equilibrium distribution between the nucleus and cytoplasm. Nevertheless, there are some concerns to be considered. To introduce them into the cell, it is necessary to either permeabilize the cells, which can alter their homeostasis, or perform microinjections, which heavily limits the high throughput analysis. Moreover, they are not fully inert: dextrans may exhibit non-specific interactions with cellular structures or components, or aggregate, leading to background signal and complicating data analysis [19].

PROTEIN BASED

Another technique to overcome the issue regarding the protocols described above is the generation of synthetic, protein-based molecules. Contrary to dextrans, they can be genetically encoded, thus allowing the production of cell lines expressing the constructs and not requiring the permeabilization. By modifying the molecular weight of the protein, both passive and facilitated transport can be studied, in a similar way to dextrans. This can be achieved by expressing different number of repeats of non-interactive proteins, such as the 7kDa bacterial Protein A (PrA), therefore offering a net readout of the changes in the nucleocytoplasmic transport independently of other biochemical signalling. Other similar molecules can be used to play with the mechanical stability of the protein, which may affect its ability to unfold as required to pass through the nuclear pore. Their affinity to importins and exportins can be further tuned up or down by including nuclear localization signals (NLS) or nuclear export signals (NES) with different affinity for them [19].

2.3. STATE OF THE SITUATION

Recent findings in mechanobiology have revealed potential relation between mechanical inputs and neurodegenerative processes, which include AD. Variations in brain stiffness, cell tension, and cytoskeletal integrity seem to be influencing crucial pathological features such as Tau aggregation. This section inspects the ongoing knowledge of how mechanotransduction pathways, mechanosensitive proteins, and nuclear-cytoskeletal interactions might affect to AD origin and evolution.

2.3.1. ALZHEIMER'S DISEASE AND MECHANOBIOLOGY

Recent studies have related mechanotransduction to the development of pathological events related to neurodegenerative disorders and AD. Changes in brain stiffness have been reported during brain maturation, normal aging, and pathological conditions such as AD, multiple sclerosis (MS), or stroke. The application of forces, such as Traumatic Brain Injury (TBI), are also risk factors [18].

Throughout the research changes in brain's mechanical properties and their relationship with the development or onset of Alzheimer's Disease have attempted to be found. Indeed, some characteristics display that there must be a relation.

Introducing in neurodegenerative illnesses field, channels as Piezo1 or Hippo pathway are recently described to be crucial for the investigation and understanding on many neuronal disorders [20].

Focusing on AD, brain presents viscoelasticity irregularities, which might be due to molecular mechanisms that degrade and disrupt ECM and cytoskeletal integrity. For instance, neuroglia and microglia are affected by environmental stiffening due to β-Amyloid plaques deposition, as exposed

before. Some studies defense that the response to this stimulus upregulates Piezo1 channel, certainly linked with central neuronal system (CNS) demyelination. Another, mechanical change effect over AD is extracted from some post-mortem human brain studies, where one of the Hyppo pathways components, YAP1 is downregulated in the onset of the disorder. YAP downregulation has found to be related with β-Amyloid plaques aggregation and Tau tangles formation, common AD hallmarks.

More than that, in AD, cell adhesion molecules (CAMs) altered expression might be related to neuroinflammation and amyloid metabolism. Is remarkable because these molecules are crucial for healthy intracellular signalling. Additionally, is pertinent to remember that cytoskeletal structure in a physio-pathological AD state ends up deteriorating. In fact, it is also related to β-Amyloid plaques aggregation and microtubule disassembling. Nevertheless, this last system deterioration may also be caused by microtubule-associated protein 2 (MAP2) abnormally phosphorylated, source of cell death in AD.

Regarding the cytoskeleton, it ensures a proper microtubule and intermediate filament organisation, which is completely lost throughout AD. Further, cell mechanics are also regulated by the nucleoskeleton, which abnormalities consequentially are related to neurodegenerative disease progression. Lamins A, C, B1, and B2 form a mesh of intermediate filaments that take part in chromatin stabilization and give nucleus shape and rigidity. Hence, when they are distorted, cell changes and neurodegenerative hallmarks emerge. To end up, some studies reveal how nucleoskeletal variations directly affect AD evolution, actually, Lamin A increased expression results in an increase of nucleus stiffness and decrease of chromatin mobility [21].

2.3.2. NUCLEOCYTOPLASMIC TRANSPORT AND ALZHEIMER'S DISEASE

Neurodegeneration is characterized by nuclear protein deposits. As an example, RNA binding proteins (RBPs) TDP43 are depleted from the nucleus and found aggregated in the cytoplasm of affected neurons. Also, Tau protein tangles and extracellular β-amyloid plaques are specifically characteristic of AD symptomatology. Nevertheless, protein aggregates in the nucleus or cytoplasm are different for each neurological disease.

As said, these last years, nucleocytoplasmic transport has been linked to disease-associated protein aggregates and dysfunctionality of nucleocytoplasmic structures. To exhaustively study it, transport assays measuring nuclear import or export, and functional studies that monitor the localization of reporter proteins have been run. From them, it was observed that reduced nuclear import and export signals (NLS/NES), which are protein dependent, in AD is due to the presence of pathological Tau. Further, cytosolic protein deposits caused by β-amyloid layers agglomeration have, also, been related to impaired nucleocytoplasmic transport, thus leading to neurodegenerative diseases.

NPCs regulate bidirectionally protein flow between nucleus and cytoplasm. They are large multiprotein complexes of nucleoporins (Nups). Nups can be classified into scaffold or FG-Nups, which are rich in phenylalanine glycine motifs. Nups are affected in several neurodegenerative states. Dysfunction, and Nups mislocalization induce nucleocytoplasmic transport impairment. For instance, Nup98 and Nup62 mislocalization is related to Tauopathies like AD. As an example, some hypotheses say that pathological Tau state causes transport defects by depleting Nup98 and Nup62 from the NPC. Moreover, Nup98 interferes in gene expression by regulating transcription and chromatin organization, as well as plays a role on the nucleocytoplasmic transport of disease-linked mislocalized proteins. Also, invaginations of the nuclear envelope (NE) have been found in

neurodegenerative disorders, particularly in AD and Huntington Disease (HD), and related to Nups pathological conformation. In addition, NE malformations correlated with nuclear integrity and loss of crucial Nups are also persistent in physiological ageing.

Besides, nuclear transport receptors (NTRs) mislocalization or aggregation has been reported in AD conditions. They are classified into importins and exportins, which mediate protein and specific RNAs transport. In fact, Impα- and Impβ-like NTRs are the most affected proteins in neurodegenerative disorders. In AD, Impα localize to intracellular actin aggregates, known as Hirano bodies.

Eventually, the RanGTP/GDP gradient concentration between nucleus and cytoplasm potentially interferes in the directionality of nucleocytoplasmic transport. Alterations in Ran levels or the regulators that control its state, have a noticeable effect on neurodegeneration. Ran-GAP was first discovered as a crucial protein that becomes functionally impaired in C9-associated neurodegeneration due to its binding with C9-RNA. Changes in cellular distribution or expression levels of Ran have been reported in Tauopathies. Indeed, it has been demonstrated that Ran localization changes under different stress exposition, hence, being affected by ageing. Finally, mention that RanGDP import is dependent on NTF, which is mislocalized in AD, indicating that RanGDP import is affected by nucleocytoplasmic transport.

Despite having described all these important results to understand better nucleocytoplasmic transport, many fields have still to be studied to help improving the actual information on the topic [11].

3. MARKET ANALYSIS

The increasing prevalence of AD has positioned this disease as major worldwide health challenge, as well as target of investment in diagnostic, therapeutics, and care services. This block studies the actual state of AD-related healthcare sector, its historical development, and future trends. With the market analysis and technological advancements study, we outline both opportunities and needs in AD research.

3.1. SECTOR

According to the World Health Organization (WHO) September 2023 report, around 55M people suffer from neurodegenerative diseases, dementia, worldwide. Alzheimer's disease is one of the most common diseases with a prevalence between the 60-70% of those cases.

Moreover, due to Alzheimer's disease high incidence, governmental and non-governmental entities are investing a lot in research of new diagnosis AD treatments which may lead to an increase in the market sector. For example, there has been a growth in the funding for research and development of AD between 2021 of 2022, being of USD 3,059 M and USD 3,348 M respectively [22].

As said before, AD therapeutics market has risen exponentially in recent years thanks to the discovery of new drug, techniques and treatment progresses. The AD therapeutic market is divided into Drug Class and Distribution Channel. Drug Class refers to medication distribution while Distribution channel concerns to the supplying of these drugs.

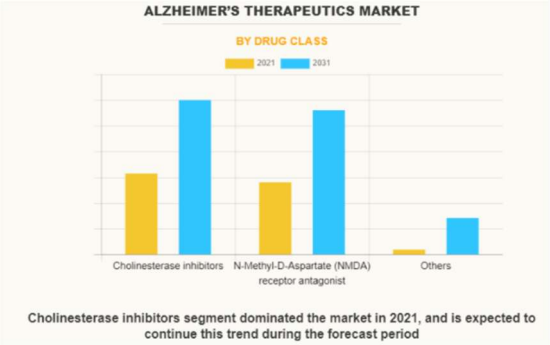

Figure 6. Forecast of the evolution of Drug Class therapeutic market [23]

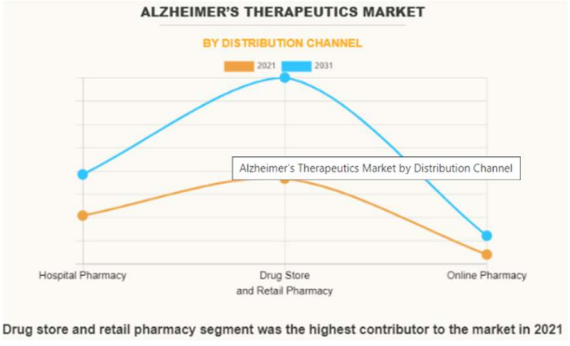

Figure 7. Forecast of the evolution of Distribution Channel therapeutic market [23]

Both Figures 6, and 7 expose the increase in the two of the therapeutic AD market's field [23].

However, official death certificates recorded 121.499 death owing to AD in 2019, and the disease was listed to be the fifth-leading death cause in the United States (US) between 2020-2021. Furthermore, more than 18 billion hours have been dedicated to the assistance of AD and other type of dementia in 2022 by family members or unpaid caregivers, which means there has been a decrease in the number of caregivers and, sequentially, an increase in the number of hours dedicated by each caregiver. In addition, unrewarded caregivers work has been valuated over 339,5 billion in 2022. This can be translated to a huge increase of family members assistance, which may lead to an exponential growth of mental health assistance needs or similar.

Hence, despite the need of investment in drug development and new treatment techniques, there is also a noticeable demand for health workers related to AD assistance [24].

3.2. HISTORICAL MARKET EVOLUTION

The recognition of age-related cognitive decline dates back thousands of years, but it wasn't until the early 20th century that Alzheimer's disease (AD) was clinically and pathologically defined. Dr. Kraepelin (1856-1926) classified dementia into two forms: senile and presenile, He names Alzheimer's disease after his colleague and student, Alzheimer, who in 1906 described the characteristic pathological features in presenile dementia [25]. Around the same time, Czech psychiatrist Oskar Fischer also studied senile dementia and described similar plaques in the brains of elderly patients, contributing independently to the early understanding of AD pathology Since then, both the understanding of the disease and the strategies to diagnose and treat it have advanced significantly.

In the first half of the 20th century, AD was considered a rare condition, mostly associated with early-onset dementia. As life expectancy increased in the second half of the century, cases of dementia became more frequent, and the disease began to be recognized as a major public health issue. During this period, initial research efforts began to emerge, primarily within academic and public health institutions.

By the 1990s and early 2000s, Alzheimer's disease had become a strategic target for pharmaceutical companies. This era saw the development and approval of the first symptomatic treatments (e.g., acetylcholinesterase inhibitors such as donepezil and rivastigmine), as well as the emergence of diagnostic tools like positron emission tomography (PET) and cerebrospinal fluid (CSF) biomarkers. These advances helped shape the first real therapeutic market for AD.

In the past decade, technological innovations have transformed the AD research and development landscape. Advanced techniques such as patient-derived induced pluripotent stem cells (iPSCs), organ-on-a-chip platforms, 3D organoid models, and gene editing tools like CRISPR have allowed for more accurate in vitro modelling of the disease. At the same time, AI-powered diagnostic algorithms, wearable monitoring devices, and large-scale omics data analysis have accelerated the identification of early biomarkers and treatment targets. The recent introduction of monoclonal antibody therapies targeting β-amyloid further signals a shift toward disease-modifying approaches. These advances aim to help society increase its awareness of dementia and improve the quality of life for affected individuals [26].

3.3. FUTURE MARKET PERSPECTIVES

It is estimated that nowadays 50 million people are leading with dementia, number that may rise to 150 million in 2050. AD is typically diagnosed with a multidisciplinary work up depending on the clinical history of each patient: clinical symptoms, neuropsychiatric, physical, and functional assessments, imaging techniques, blood tests, and, in some European countries, cerebrospinal fluid (CSF) biomarkers.

An early diagnosis of AD it is crucial to reduce the risk of ending with dementia development and to slow AD progression. Hence, in an effort to improve the understanding and enhance the abilities of diagnosis the 15th International Conference on Alzheimer's and Parkinson's Diseases and related neurological disorders was hold in 2021. Biomarkers were determined to be the most accurate diagnosis method. However, the availability of these molecules is limited, and this technique cannot be implanted worldwide due to differences in availability [27].

Despite biomarkers are a solution, there have been depicted new ways to improve the understanding, diagnosis, and treatment of AD. It seems that the implantation of a personalized treatment is the future of AD, where prevention and diagnosis are extremely studied for each case, leading to a better description of each patient's situation. On the one hand, enhancement of prevention is based on a more involucrate society, which has a lot of information to look at, on lifestyle and pharmacological interventions. On the other hand, to better precision and diagnosis, all techniques mentioned before are being improved and focused on diverse therapeutic targets that may not be considered before, like amyloid and tau pathologies [28].

4. CONCEPT ENGINEERING

In this section, an analysis is presented to explain the strategic and technical decisions made to carry out the experimental work of the project. The goal is to define the most appropriate combination of techniques, protocols, and materials to investigate how mechanical cues affect nucleocytoplasmic transport in neuronal-like cells. Although some parameters are constrained by time, reagent availability, or laboratory infrastructure, several aspects of the workflow allow for optimization and require careful consideration before implementation.

4.1. SOLUTIONS STUDY

To select the final experimental strategy, different methodological options were explored in relation to five key components of the study: (i) the selection of techniques suitable to investigate mechanobiology, (ii) the choice of an appropriate neuronal cell model and differentiation strategy, (iii) tools to quantitatively monitor nucleocytoplasmic transport, (iv) evaluation of imaging conditions to preserve and detect fluorescence signal, and (v) image processing methods for quantitative analysis. Each subsection presents the alternatives considered, their advantages and drawbacks, and the rationale behind the final choices made for the execution of the project.

4.1.1. TECHNIQUES TO STUDY MECHANOBIOLOGY

To explore how neurons respond to mechanical forces—particularly in the context of nucleocytoplasmic transport (NCT)—it is crucial to apply controlled physical inputs that mirror physiological or pathological conditions. Several methodologies have been developed for this purpose, each offering unique advantages and limitations depending on the research focus.

One widely used strategy to study how cells respond to mechanical stimuli is to modulate the **stiffness of the substrate** they grow on. By culturing neural cells on materials with defined elastic properties, such as polyacrylamide (PAA), polyethylene glycol (PEG), polydimethylsiloxane (PDMS), or agarose, researchers can explore how physical cues influence their ability to modulate mechanosensitive pathways.

Another complementary approach involves applying **osmotic stress** to induce rapid changes in cell and nuclear volume. These shifts can alter nuclear membrane tension and permeability, ultimately impacting NTC and protein localization.

Methods for **localized mechanical stimulation**, such as atomic force microscopy (AFM), magnetic tweezers, and micropipette aspiration, can be also applied to stimulate neurons. These techniques allow the application of forces at subcellular resolution, permitting the evaluation of neuronal elasticity and traction forces. In combined AFM–TFM experiments on cortical neurons cultured on PAA hydrogels, researchers were able to map traction stresses and stiffness changes (with cortical stiffness reaching ~1–2 kPa), demonstrating how neurite outgrowth correlates with local mechanics [29].

Another tool is **impulse stretch**, which consists in the application of rapid, high-strain mechanical deformations. These changes induces measurable nuclear movement and deformation in cells, offering a way to probe nuclear mechanotransduction dynamics [30].

Furthermore, **computational models** can be developed to replicate the behaviour of such complex systems. With the performance of these computer simulations, scientist use many different variables to adjust and predict the behaviour of cells and tissues facing different environments and stages [31].

Taken together, these techniques can offer complementary insights into neuronal mechanobiology. This project has centred on the analysis of cells exposed to two different strategies. First, osmotic shock, because despite their simplicity, they are widely used due to their immediate and observable effects on cell shape and volume. However, while useful, this approach does not represent the most physiologically relevant and sustained mechanical cue. Therefore, this work also includes studies with substrates of different rigidities. As substrate stiffness is known to impact cytoskeletal

organization and NCT, its analysis is essential to understanding how neurons integrate mechanical signals from their environment.

4.1.1.1. OSMOTIC SHOCKS

Osmotic pressure plays a critical role in several physiological processes, including cell proliferation, wound healing and disease progression. However, the relationship between the ECM and cell response to osmotic shocks has not been completely deciphered. It has been proposed that ECM acts as a pressure sensor, helping to sense and transmit osmotic changes to the cell, which is valuable for understanding the mechanical response of cells to osmotic pressure.

Osmotic shocks cause water flux exchange across the plasma membrane, causing variations in cell volume and cortical tension. Moreover, due to the tight connection between ECM transmembrane proteins and cells, cell volume changes caused by osmotic shocks evoke the deformation of the ECM inherently [32]. Hyper-osmotic stress shrinks the nucleus, whereas hypo-osmotic stress swells it. These alterations in structure can cause potential changes in the nuclear pores complexes (NPC) , therefore influencing nucleocytoplasmic transport (NCT) and gene transcription, the focus of this research project [33], [34]. Hyperosmotic stress applied to neuronal models has been shown to disrupt the RanGTP gradient [33]. This methodology has already been successfully implemented in our laboratory, where osmotic shocks have been used to induce controlled changes in cell and nuclear volume, confirming expected effects on solute concentration and cellular morphology [34]. Due to their rapid and highly reproducible effects, often occurring within minutes, osmotic shocks provide a powerful approach to investigate how mechanical stress influences nucleocytoplasmic transport and cellular stress responses in neurons. Previous studies have shown that osmotic pressure can influence the nuclear export of RNA-binding proteins such as TDP-43 and FUS, proteins that have been implicated in neurodegenerative diseases [35], [36].

4.1.1.2 SUBSTRATE STIFFNESS

The mechanical properties of the cellular microenvironment are known to play a pivotal role in regulating neuronal behaviour. Among the various mechanical cues, substrate stiffness is one of the most consistent and biologically relevant stimuli influencing processes such as neuronal differentiation, polarity, and neurite outgrowth. To mimic these mechanical inputs in vitro, hydrogels are widely used as substrates due to their tissue-like water content and tuneable elasticity.

In the laboratory, there have been established protocols for the reliable fabrication of hydrogels with precisely controlled stiffnesses. These protocols enable the production of hydrogels ranging from soft (~0.5 kPa) to stiff (~30 kPa). Among the options considered, which included Polydimethylsiloxane (PDMS), Polyethylene glycol (PEG) hydrogels, and natural biopolymers like collagen or hyaluronic acid, Polyacrylamide (PAA) has been selected as the substrate for this project.

PAA gels allows reliable modulation of gel stiffness by adjusting the concentration of acrylamide and bis-acrylamide. Its simplicity and reproducibility make it a common choice for standard applications. The use of PAA gels in neuronal studies is well supported in the literature. PAA has been successfully employed in the culture of primary neurons, neural stem cells, and SH-SY5Y cells, offering a chemically inert background with a high degree of control over stiffness. Unlike naturally derived hydrogels, PAA does not present inherent biological signals, making it a neutral platform for testing the effects of specific mechanical properties and surface functionalization. Furthermore, its compatibility with microscopy and image-based analyses, especially confocal

imaging, makes it especially attractive for high-content studies of cell morphology and protein localization [37].

For the current study, stiffness values of 0.5 kPa and 15 kPa were selected. These values span the range most commonly associated with mechanosensitive behaviour in other cell types. Moreover, previous works have shown that SH-SY5Y cells, as well as primary neurons and neural stem cells, display distinct morphological and transcriptional profiles when cultured on soft (0.1–1 kPa) versus stiffer (10–30 kPa) substrate [38], [39], [40].

To ensure proper cell adhesion and differentiation on the otherwise non-adhesive PAA surface, it is necessary to perform a surface functionalization with ECM proteins. Laminin is the most used protein in this context due to its role in neuronal development and its ability to support neurite outgrowth (e.g. [41]). Other proteins used for neuronal adhesion and signalling include fibronectin, collagen I, collagen IV, and vitronectin.

Different protocols to covalently bind the ECM proteins in the PAA gel preparation have been described, having been two successfully implemented in the laboratory.

The first protocol follows a simpler and more established workflow, based on the use of sulfo-SANPAH, a heterobifunctional crosslinker activated by UV light. This approach enables the covalent binding of amine-containing proteins, such as laminin, to the PAA surface,

In contrast, the second method incorporates acrylic acid into the gel matrix during polymerization. This approach enables pH-controlled activation of carboxylic groups, allowing for more flexible and precise control over protein conjugation and potentially higher customization of the gel surface. Such control can be advantageous in more complex or demanding experimental setups where protein density and spatial distribution are critical but also have been experimentally teste din the lab to induce a higher incorporation of proteins such as laminin to the hydrogel surface.

In both cases, the selected strategy allows functionalization of the gels with biologically relevant ECM, which have all been shown to influence adhesion, differentiation, and neurite outgrowth in neuronal and neuron-like cells. Thus, the choice between protocols should be guided by the specific experimental needs, balancing convenience, reproducibility, and surface complexity.

In summary, functionalized PAA gels present a robust and versatile platform for mechanobiological studies in neuronal-like cells. By integrating tuneable stiffness with defined biochemical cues, this system enables the systematic investigation of mechanosensitive pathways involved in neuronal differentiation, maturation, and response to microenvironmental stimuli.

4.1.2. CELLULAR MODEL

As described in previous sections, various in vitro models have been developed to study Alzheimer's disease (AD), each offering different advantages depending on the specific research goals. In the laboratory, currently work two models developed by Dr. Jorge Oliver-De La Cruz are in use: iPSC-derived neurons and the SH-SY5Y neuroblastoma cell line, both engineered to allow inducible neuronal differentiation through NGN2 overexpression.

The first model consists of human induced pluripotent stem cells (iPSCs) derived from the UKiBio11-A3 line, which carries the APOE4/E4 genotype, a major genetic risk factor for AD. An isogenic APOE3/E3-corrected line is also available, enabling comparative studies. These iPSCs have been stably modified to express Neurogenin-2 (NGN2) under a doxycycline-inducible Tet-On system, following the differentiation approach described by Song et al. (2021), [42]. Upon NGN2

induction, the cells differentiate into mostly glutamatergic neurons over a period of 21 to 28 days. Despite their high relevance for modelling AD, iPSC-derived neurons pose several experimental challenges. The differentiation process is lengthy and costly, requiring expensive media and reagents. Additionally, these cells are fragile and cannot be detached and reseeded beyond day 7 without compromising viability or maturation. As a result, their final differentiation must occur directly on the hydrogel substrates used for experimentation, potentially introducing variability due to the influence of substrate composition on maturation. Moreover, although non-cancerous, iPSC-derived neurons often exhibit a foetal-like transcriptional profile, which may limit their ability to fully replicate adult AD phenotypes.

In parallel, we evaluated the use of SH-SY5Y cells, a well-characterized neuroblastoma-derived cell line frequently used in neurodegeneration studies. In our lab, this model has been optimized through the introduction of NGN2 under doxycycline control, enabling synchronized neuronal induction. Compared to iPSC-derived neurons, SH-SY5Y cells offer a faster, more affordable, and easier-to-handle system. They can be expanded efficiently, differentiated within a shorter timeframe, and detached and reseeded after differentiation, a crucial feature for mechanobiological experiments involving substrate stiffness planned in this project.

Several protocols exist for the differentiation of SH-SY5Y cells into neuron-like cells. Among these, we considered two commonly used methods: the protocols described by Dravid et al. (2021) [43] and Overbaugh, Mangold, and Szpara (2016) [44]. Both involve sequential exposure to retinoic acid (RA) and neurotrophic factors, but differ in complexity, duration, and culture conditions. Based on its simplicity, reproducibility, and compatibility with available reagents, we adopted the Dravid et al. protocol as our foundation. The differentiation strategy was further enhanced by Dr. Oliver's NGN2-based system, which accelerates and improves the neuronal commitment of SH-SY5Y cells.

Still, both approaches present concerning limitations that can be optimized. A key component in the early stages of neuronal differentiation in both methodologies is the presence of RA. This molecule is photo-unstable and has short storage stability, needing fresh stock preparation for each experiment. To overcome this issue, a synthetic analogue known as EC23 has been developed. EC23 is photostable and has demonstrated efficiency in promoting neural differentiation of human pluripotent stem cells and the cell line ReNcell 197VM [45], [46].

Considering all the above, and balancing biological relevance, practicality, and experimental requirements, we ultimately selected the NGN2-modified SH-SY5Y model for this study. It offers a reliable, reproducible, and flexible platform ideally suited for investigating how neuronal-like cells respond to mechanical stimuli, particularly substrate stiffness.

4.1.3. QUANTITATIVE ANALYSIS OF NUCLEOCYTOPLASMIC TRANSPORT

4.1.3.1 SELECTION OF THE REPORTER FOR NCT: SeNCYT

Among the tools used to quantify nucleo-cytoplasmic transport (NCT) dynamics in response to mechanical cues, a key approach developed and validated by Dr. Roca-Cusachs' group is the synthetic construct SeNCYT (Sensor of NucleoCYToplasmic ratio) [47]. This GFP-tagged protein was rationally engineered to enable mechanosensitive readout of NCT by systematically tuning two main parameters: its molecular weight and the affinity of its nuclear localization signal (NLS) for importins [48].

As illustrated in Figure 8 (a), the construct is modular and composed of three parts: (i) an NLS of high, medium, or low affinity for importin α, (ii) a GFP tag for visualization, and (iii) a variable number

of protein A (PrA) domains that increase the molecular weight without introducing additional nuclear transport signals. This design allows the generation of a full matrix of constructs with defined combinations of NLS affinity and molecular weight, ranging from 27 to 67 kDa. These constructs were used to dissect how mechanical signals affect active nuclear import.

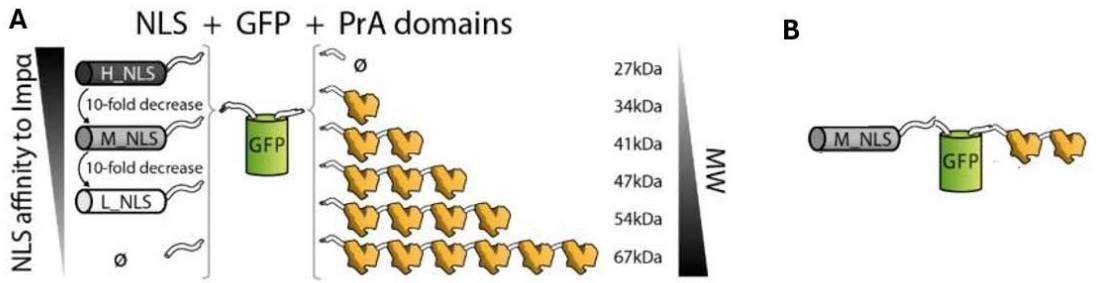

Figure 8. Design of the SeNCYT construct toolbox. (A) Schematic representation of a modular library of GFP-tagged constructs combining nuclear localization signals (NLS) of varying affinity for importin α (high, medium, low) with an increasing number of protein A (PrA) domains to tune molecular weight. (B) Example of the construct selected as SeNCYT (L_NLS–41kDa), optimized for mechanosensitive quantification of nucleo-cytoplasmic transport. Images were obtained from Andreu, Granero-Moya et al. 2022 [48].

The system was validated in various experimental conditions. Its nucleocytoplasmic distribution was shown to be sensitive to inhibition of the import machinery, to cytoskeletal disruption, and to changes in substrate stiffness. Constructs with higher importin affinity or lower molecular weight accumulated more efficiently in the nucleus, while increasing molecular weight or reducing NLS affinity led to predominant cytoplasmic localization. Importantly, these shifts were reversible and could report mechanical changes in a dynamic and quantitative manner.

From this toolbox, the construct combining a low-affinity NLS with a molecular weight of 41 kDa (L_NLS-41kDa) was selected and renamed SeNCYT (Figure 8b). This version exhibits a near-balanced distribution between nucleus and cytoplasm under basal conditions, making it particularly suitable as a sensitive and dynamic reporter for mechanosensitive regulation of nucleo-cytoplasmic transport. Given these characteristics, we decided to employ this same construct for the SH-SY5Y cells.

The next key consideration was how to introduce the SeNCYT sensor into SH-SY5Y cells. Two strategies were evaluated: transient transfection and the generation of stable cell lines using lentiviral particles.

Transient transfection would need to be performed after neuronal differentiation, as the expression typically does not persist long enough to span the entire differentiation process. However, differentiated neurons are notoriously difficult to transfect, and the expected transfection efficiency would likely be low and heterogeneous.

In contrast, **generating stable cell lines** via lentiviral transduction ensures long-term expression and allows for SeNCYT to be present throughout the differentiation process. While this approach requires more time upfront, access to additional facilities, and carries the risk of interfering with neuronal differentiation, it offers the advantage of consistent expression across the population. Since the construct does not include an antibiotic resistance marker, fluorescence-activated cell sorting (FACS) [49]. may be necessary to isolate a homogeneously expressing population. For all this reasons, this was the chosen method.

4.1.3.2 IMAGING TECHNIQUES

Fluorescence microscopy is the method of choice for monitoring nucleocytoplasmic transport (NCT), as it allows specific visualization of fluorescently tagged proteins within the nuclear and cytoplasmic compartments. To analyse SeNCYT localization, it is essential to distinguish these compartments reliably and in live cells, since fixation alters the sensor distribution and leads to artifacts.

We performed our imaging taking advantage of the Access to a laser scanning confocal microscopy (LSCM), which enables optical sectioning by rejecting out-of-focus light using a pinhole. This improves spatial resolution and signal-to-noise ratio, allowing accurate quantification of GFP intensity in nucleus and cytoplasm [50], [51].

In addition, LSCM is well suited for live-cell imaging, as it allows for real-time observation and acquisition of z-stacks across the cell volume. All imaging was carried out under controlled CO_2 and temperature conditions, ensuring cellular viability and physiological relevance during acquisition.

4.1.3.3 OPTIMIZATION OF MEDIA FOR FLUORESCENCE LIVE IMAGING

During initial experiments, we observed a low signal-to-noise (S/N) ratio when imaging SeNCYT, which compromised the accuracy of nucleocytoplasmic transport (NCT) quantification. After discussions with Dr. Jorge Oliver, we hypothesized that the issue might be partly due to autofluorescence from the culture medium, and that reducing background fluorescence could significantly improve the quality of live-cell imaging.

To address this, we systematically tested several medium formulations with the dual goal of minimizing autofluorescence while preserving cell viability and differentiation capacity. The media tested included:

- **Neurobasal-A complete:** The standard differentiation and maintenance medium, supplemented with B27. However, B27 is known to contain components with intrinsic autofluorescence, potentially interfering with GFP signal detection.
- **Neurobasal-A basal:** The same medium but without B27. While this reduces background fluorescence, the absence of essential supplements may impair cell viability and neuronal differentiation over time.
- **BrainPhys™ (BPI) complete:** A commercially available neuronal medium specifically optimized for live imaging, primarily in iPSC-derived neurons [52]. It includes N2 and SMI1 supplements, which are formulated to support imaging without introducing significant background signal.
- **BrainPhys™ (BPI) basal:** The same formulation as above but lacking N2 and SMI1, thus reducing background further but potentially compromising neuronal support.

Each formulation was tested by culturing SH-SY5Y cells, followed by live-cell confocal imaging to evaluate both background fluorescence and cellular behaviour. The medium providing the best balance between low background signal and support for neuronal differentiation was selected for all subsequent imaging experiments.

4.1.3.4 IMAGE ANALYSIS TOOLS

There are many programs available for image analysis. In our laboratory, the two most commonly used are CellPOSE and ImageJ, both of which are open-source and widely adopted in the scientific community.

CellPOSE is an anatomical segmentation algorithm written in Python 3. It is designed to segment both isolated cells and densely packed ones that are otherwise difficult to distinguish. One of its main strengths lies in its generalizability: it does not require model training or parameter adjustment, as it comes pre-trained on a large, diverse dataset of segmented cell images [53], [54]. In addition, CellPOSE incorporates an innovative approach by converting training set masks into vector gradients that can be predicted by a neural network, which enhances its segmentation accuracy. More recently, 3D segmentation capabilities have been introduced, broadening its applicability to volumetric image stacks.

ImageJ, by contrast, is a Java-based image processing program that runs on various platforms, including Windows, macOS, and Linux, in both 32-bit and 64-bit modes [55]. It is widely used for basic image processing tasks such as visualization, zooming, scrolling, filtering, and adjusting brightness and contrast. ImageJ allows for manual or semi-automated selection of regions of interest (ROIs), making it especially useful for routine tasks and user-guided quantification. Its intuitive interface and broad plugin ecosystem make it a versatile tool for daily image analysis workflows.

4.1.4.IMAGE ANALYSIS

There are lots of programs which can be employed to analyse images. The ones used in our laboratory are ImageJ and CellPOSE, both distinguished image analysis software's and open-source platforms. On the one hand, CellPOSE is an anatomical segmentation algorithm written in Python 3 which is commonly used to segment those cells which are widely spread within the sample and, hence, easy to analyse, but also those who are more packaged between them and present difficulties to be distinguished. Moreover, apart from presenting an innovative 3D method for segmentation, CellPOSE includes a reversible transformation from training set masks to vector gradients that can be predicted by a neural network and a large, segmented dataset of varied images of cell. In other words, CellPOSE does not require model training or parameter adjustments [53],[54]. On the other hand, ImageJ is written in Java, which allows it to run on different platforms such as Linux, Mac OS X and Windows, in both 32-bit and 64-bit modes. The program is widely used to display images as tools for zooming and scrolling are provided. Also, allow proper image selection and enhancing by the display of different filters and brightness adjustment. Thus, ImageJ is a tool more commonly used for daily image processing and analysis by offering an easy-use program [55].

4.2. FINAL SOLUTION

This section offers a precise explanation of the chosen solution for the methods employed in this project. Figure 9 below, depicts the workflow of the different steps carried out.

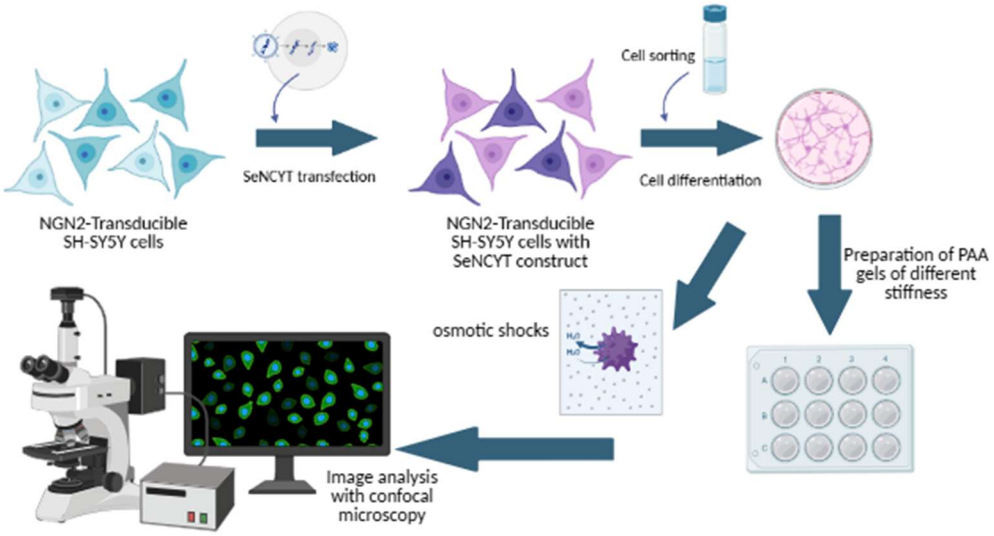

Figure 9. Workflow of the solution followed for the project. Made with www.biorender.com

In brief, the first part of the project involved the generation of an SH-SY5Y cell line that already contained a doxycycline-inducible cassette for NGN2 differentiation, and was further modified to stably express the SeNCYT construct via lentiviral transduction. These cells were expanded, and high-expressing SeNCYT-positive cells were selected through cell sorting. After expansion, backup cryopreserved vials were generated.

Some of these cells were later subjected to the neuronal differentiation protocol previously optimized in the laboratory. Once differentiation into neuron-like cells was achieved, the culture was divided into two experimental conditions. One group was exposed to osmotic shocks to investigate SeNCYT behaviour in relation to nuclear–cytoplasmic transport (NCT), while the second group was seeded onto PAA hydrogels of varying stiffness to assess the cells response to mechanical properties of the substrate.

In both cases, nuclei were counterstained with Hoechst, and live-cell confocal imaging was performed. The resulting images were then analysed using ImageJ software. All methodologies described in this workflow are detailed in Section 4.2.

4.2.1. SH-SY5Y CELL CULTURE

The SH-SY5Y parental cell line was a kind gift from D. Pozo-Devoto (Brno, Czech Republic). These cells had already been transduced with a doxycycline-inducible NGN2 expression cassette, as described in Yara's work [Yara, et al.], enabling their differentiation into neuron-like cells upon doxycycline treatment. To maintain selective pressure and preserve the expression of this cassette, cells were routinely cultured with 0.5 µg/mL puromycin, particularly during early passages.

Cells were maintained and expanded in sterile 75 cm² culture flasks under standard conditions: 37 °C, 95% humidity, and 5% CO_2 in a dedicated incubator. The culture medium consisted of DMEM/F12 supplemented with heat-inactivated foetal bovine serum (FBS), Penicillin-Streptomycin (Pen/Strep), and L-Glutamine (L-Glut), providing essential nutrients, growth factors, and antibiotics to support proliferation and prevent contamination. Cultures were routinely tested for mycoplasma contamination using PCR-based assays.

For thawing cryopreserved cells, cryovials were briefly immersed in a 37 °C water bath, disinfected, and diluted in prewarmed medium. After centrifugation, the cell pellet was resuspended and seeded into fresh flasks. For passaging, adherent cells were detached using TrypLE™, collected, centrifuged, and reseeded at a typical 1:20 ratio in prewarmed medium. Medium was refreshed every 2–3 days, and cells were subcultured when they reached approximately 80% confluence (see Annex 1 for the full protocols)

4.2.1.1 SeNCYT TRANSFECTION AND CELL SORTING

To proceed with the project, SH-SY5Y cells, already containing the doxycycline inducible NGN2 cassette, were transduced with the SeNCYT construct via lentiviral transduction, following the protocol described in this section and outlined in Figure 10, and detailed in Annex 2.

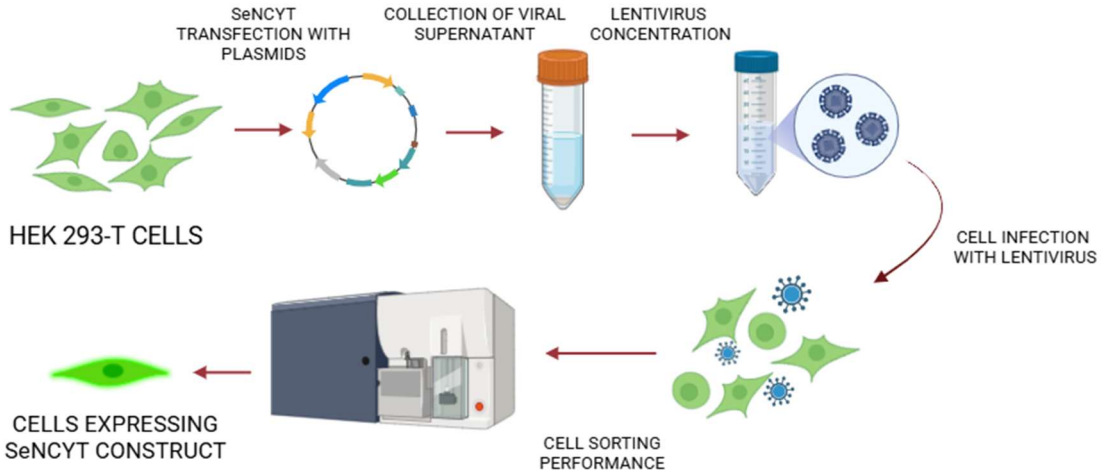

Figure 10. Workflow with the steps followed to transfect SeNCYT by means of lentivirus. Created with: www.biorender.com

Briefly, lentiviral particles were generated by culturing HEK293 cells to 40–50% confluence and co-transfecting them with the plasmid of interest, pLenti PGK-SV40A4-eGFP-2PrA, provided by the Jacco van Rheenen group at the Netherlands Cancer Institute, together with the packaging plasmids pMD2.G and psPAX2, using Lipofectamine 3000 in OptiMEM. The construct includes eGFP to allow monitoring of transduction efficiency. Viral supernatants were collected over three consecutive days, centrifuged, filtered, and concentrated using Lenti-X Concentrator. The final viral pellet was resuspended in OptiMEM for infection.

SH-SY5Y cells were incubated overnight with the viral suspension in the presence of Polybrene, 8 µg/mL. The following day, the medium was replaced with fresh culture medium. This procedure was carried out at the Lentiviral Facility of the Parc Científic de Barcelona. Transduced cells were expanded, and once a sufficient number was reached, they were subjected to fluorescence activated cell sorting, FACS, to isolate the population with high SeNCYT expression based on eGFP fluorescence. FACS was performed at the Cell Sorting Facility of the Centros Científicos y Tecnológicos de la Universidad de Barcelona, CCiTUB, with the support of their technicians. Sorted cells were expanded, and several cryovials were prepared and stored in liquid nitrogen for subsequent experiments.

4.2.2. SH-SY5Y DIFFERENTIATION INTO NEURONAL-LIKE CELLS

Despite the existence of multiple protocols to induce morphological changes and gene expression changes in SH-SY5Y, in other words, differentiating them into neuron-like cells, we adapted the

protocol described by Dravid et al. (2021) [43], with slight modifications to improve media stability and differentiation efficiency. The most important change was the incorporation of **doxycycline**, which induces NGN2 expression in our SH-SY5Y cells carrying a doxycycline-inducible cassette. NGN2 is a proneural transcription factor that enhances neuronal differentiation. Additionally, we replaced Retinoic Acid (RA) with EC23, a photostable synthetic analogue shown to enhance neural differentiation [43]. A visual summary of the differentiation timeline, including key medium transitions and approximate timing of each step, is shown in **Figure 11**.

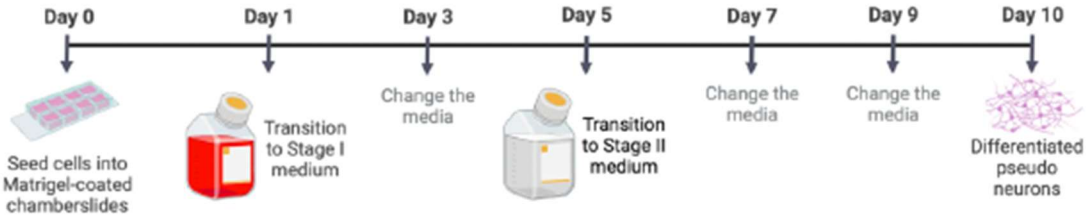

Figure 11. Timeline of the differentiation protocol used to induce SH-SY5Y cells into neuron-like cells, indicating media transitions and key procedural steps. Extracted from: http://hdl.handle.net/2445/199965

The differentiation procedure begins on day 0 by seeding approximately 10,000 cells/cm² in Matrigel-coated 6-well plates. Cell counting was performed using a LUNA-II™ Automated Cell Counter (Logos Biosystems) (see Annex 1.5).

On the following day (day 1), cells are transitioned to Stage 1 Medium, consisting of DMEM:F12 supplemented with heat-inactivated FBS, penicillin-streptomycin, L-glutamine, EC23, and doxycycline. Cells are maintained in this medium for three days, with a medium change on day 3 to replenish nutrients and remove metabolic byproducts.

On day 5, the medium is switched to Stage 2 Medium, composed of Neurobasal-A supplemented with BDNF, KCl, B27, penicillin-streptomycin, and L-glutamine. This medium is refreshed on days 7 and 9.

By day 10, cells are expected to be fully differentiated into neuron-like cells. Differentiated cells are maintained in Stage 2 Medium until used for experiments. A full list of media compositions is provided in Table 1.

Table 1. Table with the reagents needed for each medium, the concentration of the stock, and the final concentration needed

	REAGENT	[STOCK]	[FINAL]
STAGE 1 MEDIUM	DMEM: F12	-	-
	P/S-L-Glut	100x	1x
	iFBS	100%	2.5%
	EC23	10 mM	10 µM
	Doxycycline	10 mg/mL	2 µg/mL
STAGE 2 MEDIUM	Neurobasal medium	-	-
	B27	50x	1x
	BDNF	10 mg/mL	20 µg/mL
	P/S-L-Glut	100x	1x
	KCl	2 M	20 mM

.

4.2.3. OSMOTIC SOLUTIONS

Osmotic solutions were prepared to optimize the response of SH-SY5Y cells expressing the SeNCYT construct to mechanical stimuli, specifically under hypoosmotic and hyperosmotic conditions.

To guide the formulation of these solutions, we referenced the study by a former lab member, Dr. Granero-Moya [56], which reported an approximate osmolarity of about 340 mOsm for the standard culture medium. Based on this value, we established target osmolarities of around 113 mOsm (66%) for hypoosmotic and around 695 mOsm (204%) for hyperosmotic conditions.

It is important to note that neuronal culture media often have tailored osmolarities to mimic the in vivo neuronal environment, and even small deviations can significantly affect cell behaviour and viability. For this reason, precise osmolarity adjustment and validation were critical in our experimental design.

Two neuron-compatible media, Neurobasal-A Complete and BrainPhys Imaging (BPI) Complete, were selected as the basis for the osmotic treatments. In agreement with our supervisor and following reference [56], we used Mg^{2+} and Ca^{2+} salts to reduce osmolarity in hypoosmotic solutions, and D-mannitol to increase osmolarity in hyperosmotic ones. Stock solutions were prepared in Milli-Q water (100 mL total volume) after calculating the required solute concentrations (detailed in Annex 4).

Table 2. Composition of both medias to prepare osmotic solutions

Neurobasal-A(NB) Complete (1mL)			BrainPhys imaging (BPI) complete (1mL)		
REAGENT	**[STOCK]**	**[FINAL]**	**REAGENT**	**[STOCK]**	**[FINAL]**
NB	-	-	**BPI**	-	-
P/S-L-Glut	100x	1x	**P/S-L-Glut**	100x	1x
KCl	2M	20mM	**N2**	100x	1x
B27	50x	1x	**SMI1**	50x	1x

In total, six solutions were generated: hypoosmotic, hyperosmotic, and unmodified controls for each medium type. To verify whether the desired osmotic conditions were achieved, we measured the osmolality of each solution using a freezing point osmometer from the BIMPS group at IBEC, and we thank Dr. Adriano Caliari for providing access and guidance with the equipment.

Although osmolarity (mOsm/L) and osmolality (mOsm/kg) are technically distinct—osmolarity depends on volume and osmolality on mass—they are nearly equivalent in aqueous solutions, such as culture media, where the density is close to that of water. For this reason, osmolality readings from the osmometer were considered valid for comparison with the target osmolarity values derived from the literature. However, we express all measured values in mOsm/kg, the actual units provided by the instrument.

To ensure measurement accuracy and reproducibility, three independent readings were performed for each condition. We then calculated the mean, standard deviation (SD), and percent deviation relative to the target osmolarity. These validation steps were essential to confirm that osmotic stress conditions were adequately applied while maintaining cell viability for downstream experiments.

4.2.4. PAA GEL PREPARATION AND FUNCTIONALIZATION

Completely differentiated SH-SY5Y cells were seeded onto polyacrylamide (PAA) gels with stiffness levels of 0.5 kPa and 15 kPa, in order to study their mechanosensitive responses. The

final protocol used for fabricating these hydrogels on glass surfaces is summarized below; a full step-by-step description is provided in Annex 6.

We stated by preparing the **glass substrate preparation** to promote gel attachment. To do this, MatTek 35 mm glass-bottom dishes were first incubated for 1 hour with a solution of acetic acid, Bind-Silane, and 96% ethanol, followed by three washes with ethanol and drying using a nitrogen spray gun.

Then, **PAA hydrogels** were prepared by mixing PBS, 40% acrylamide, 20% bis-acrylamide, and acrylic acid, adjusting the pH to 7–8 with NaOH. Formulations were adjusted to obtain the desired stiffness levels (see Table in annex 6, section 12.6), previously validated by indentation-based measurements. After degassing for at least 15 minutes, latex beads, TEMED, and APS were added to initiate polymerization. A 12 µL drop of the gel solution was pipetted onto the treated glass and covered with a 12 mm coverslip. Gels polymerized at room temperature for at least 1 hour before being immersed in PBS and carefully uncovered.

Gels were exposed to **surface functionalization** with laminin (50 µg/mL) to support cell adhesion. Activation was performed using EDC/NHS chemistry in HEPES buffer (20 mM) for 20 minutes at 37 °C, followed by PBS washes. Laminin was then applied and incubated overnight at 4ºC. Gels were washed again, sterilized under UV light for 15 minutes, and incubated in cell culture medium until cell seeding.

4.2.5. NEURON-LIKE CELL SEEDING FOR EXPERIMENTAL ASSAYS

Both fully differentiated neuron-like SH-SY5Y cells and undifferentiated SH-SY5Y cells were seeded onto experimental substrates depending on the assay.

For neuron-like cells, after differentiation was completed, cells were washed with PBS for 4 minutes and then incubated with Accutase at 37 °C for 5 minutes to achieve gentle detachment. Cells were collected, centrifuged, and the resulting pellet was resuspended in 1 mL of Stage 2 medium.

For undifferentiated SH-SY5Y cells, which were used in parallel osmotic shock experiments, detachment was carried out using TrypLE Express, following standard passaging procedures.

Cells were then seeded onto either Matrigel-coated 35 mm glass-bottom dishes (for single-cell analysis under osmotic conditions) or onto polyacrylamide (PAA) gels with defined stiffness (for mechanotransduction assays). Approximately 100,000 cells were seeded per glass-bottom dish, while 25,000 cells were seeded per PAA gel due to the reduced surface area. Cell concentrations were determined using an automated counter, and the appropriate volume of cell suspension was added to each substrate along with Stage 2 medium.

After seeding, all cultures were maintained in the incubator for at least 24 hours to allow cell attachment and recovery before initiating any experimental procedures.

4.2.6. NUCLEAR COUNTERSTAINING

Before imaging, cells seeded on PAA gels or glass-bottom dishes were stained with Hoechst 33258 to visualize nuclei during live-cell imaging. Hoechst is a DNA-binding dye that attaches to the minor groove of double-stranded DNA and is permeable to live cells, making it suitable for both live and fixed samples [57]. This staining enables accurate distinction between nuclear and cytoplasmic regions during image analysis.

Hoechst was diluted 1:2000 in Stage 2 medium and incubated with the cells at 37 °C for at least 30 minutes. After incubation, cells were washed at least once with fresh Stage 2 medium to remove unbound dye prior to imaging.

4.2.7. MEDIA SELECTION AND OPTIMIZATION FOR IMAGING

As stated in Section 4.1.4, various media were evaluated to determine which provided the best signal-to-noise (S/N) ratio under live-cell imaging conditions. This optimization step, combined with the prior selection of the brightest SeNCYT-GFP–expressing cells, was designed to maximize the quality and consistency of the imaging signal.

Two culture systems were tested: the BrainPhys Imaging (BPI) kit and the Stage 2 differentiation medium based on Neurobasal-A. Given that several supplements in these media could contribute to autofluorescence, photobleaching, or even exhibit photoreactive behaviour, each system was tested both with and without supplements to assess their contribution to background signal.

Experiments were carried out using undifferentiated SH-SY5Y cells seeded on Matrigel-coated chamber slides. Imaging was performed using a Zeiss LSM880 inverted confocal microscope equipped with Zeiss ZEN2.3 SP1 FP3 software (black, version 14.0.24.201), and a 20× objective.

For each condition, several images were acquired, including z-stacks to allow for maximum intensity projection and to evaluate the accumulated effect of autofluorescence across the Z-axis. This approach helped minimize variability caused by differences in focus, cell positioning, and potential differences in fluorescence intensity between focal planes. More technical details can be found in Annex 3.

4.2.8. CONFOCAL MICROSCOPY

To acquire the images of fluorescent prepared samples, a Zeiss LSM900 inverted confocal microscope objective and using Zeiss ZEN 2.3 SP1 FP3 (black, version 14.0.24.201). The objective used for examining both samples on regular culture plates and on hydrogels was a 20x Plan-Apochromat objective. Florescent excitation was performed with Carl Zeiss Colibri 7LED system, suing a 430nm (V) LED for Hoechst stained-nuclei and a 511nm (C) LED for GFP-SeNCYT detection. A plot with the emission and excitation spectra of both the fluorophores and excitation lasers is depicted in Figure 12. Prior to imaging, the microscope environment was equilibrated to 37 °C with 5% CO_2 to maintain physiological conditions during live imaging. Each channel was acquired separately to ensure minimal spectral overlap and optimal signal clarity. Images were obtained at a resolution of 1024x1024, 16 bits dept, and saved in a *.czi* format. Z-stacks were obtained to capture three-dimensional information of the samples. For time-lapse experiments, the built-in position selection tools of the ZEN software were used to track multiple predefined positions across time.

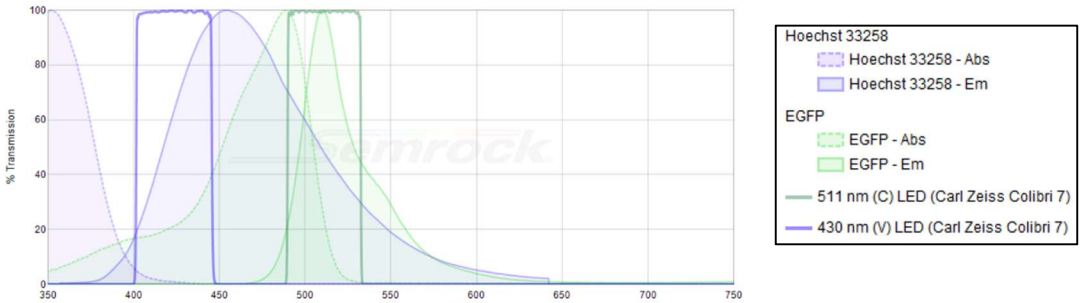

Figure 12. Plot representation of the excitation and emission spectra of the fluorophores used in imaging as well as the lasers. Graph made with: https://searchlight.idex-hs.com/

4.2.9.IMAGE ANALYSIS

Image J software was used for detailed analysis of the acquired images. A *macro* developed in the laboratory was further adapted to generate a mask able to distinguish between nucleus and cytoplasm, thereby enabling the obtention of both region intensities. Z-stacks were used to identify the planes with the highest signal intensity for each sample. The blue Hoechst channel was used to label and define nuclear regions. This nuclear mask was then used on the GFP channel to define regions on the nuclear and cytoplasmic compartments within the same cell. Given the irregular shape of the cells and the need to track them over time, results were manually curated to ensure accurate segmentation and to avoid including background signal. In addition, a background region was selected in each image and used as a reference to subtract background fluorescence from the measured intensities. Once these intensities were obtained, different calculations were performed using Microsoft, Excel. including nucleus-to-cytoplasm (N/C) ratio (Equation 1) and the evolution of nuclear and

$$N/C = \frac{Nucleus\ Intensity - Background\ Intensity}{Cytoplasm\ Intensity - Background\ Intensity}$$

Equation 1. Formula to calculate the Nuclear to Cytoplasmic SeNCYT intensity ratio

4.2.10. STATISTCAL ANALYSIS

All statistical analyses were performed using GraphPad Prism version 10. For paired comparisons of nuclear-to-cytoplasmic SeNCYT intensity ratios and nuclear projected areas before and after treatment, a **paired t-test** was used. For comparing cell behaviour on different stiffness gels, **unpaired t-tests** were applied. A **p-value < 0.05** was considered statistically significant. Results are presented as mean ± standard deviation unless otherwise stated.

5. DETAIL ENGINEERING

This section presents the key results obtained from the experimental procedures described in the Concept Engineering section, with a focus on the quantitative imaging and analysis of the SeNCYT sensor in SH-SY5Y-derived neurons. Using live-cell confocal fluorescence microscopy, we assessed SeNCYT localization under different substrate stiffnesses and media conditions to evaluate their impact on nucleo-cytoplasmic transport (NCT). Image analysis was carried out using ImageJ, enabling accurate segmentation and quantification of nuclear and cytoplasmic GFP signal. The resulting data provide valuable insights into the mechanosensitive regulation of NCT and the optimization of imaging workflows. The implications of these findings will be discussed in relation

to current understanding of neuronal mechanotransduction and cellular adaptation to the microenvironment.

5.1. CELL LINE PRODUCTION AND DIFFERENTIATION

5.1.1. GENERATION OF SENCYT SH-SY5Y

To ensure that all SH-SY5Y cells used in the study contained the SeNCYT construct required for the analysis of nuclear-cytoplasmic transport (NCT), we performed lentiviral transduction followed by fluorescence-activated cell sorting (FACS). The goal was to obtain a homogeneous population of transduced cells and, within it, to enrich for those with the highest expression levels, thereby facilitating downstream imaging and analysis.

As a first step, we sorted a control population of non-infected SH-SY5Y cells. This allowed us to establish baseline fluorescence levels and confirm the absence of GFP signal in untransduced cells. As shown in Figure 13 upper panels, these cells fall entirely outside the GFP-positive gate, validating the specificity of the fluorescent signal associated with SeNCYT expression.

Following SeNCYT transduction, we sorted the same cell line to evaluate the distribution of GFP fluorescence. As depicted in the lower panels of Figure 13, transduced SH-SY5Y cells exhibit a broad and continuous range of fluorescence intensities, rather than forming two distinct populations (GFP-positive vs. GFP-negative). This pattern indicates that most cells have been transduced but with varying levels of expression.

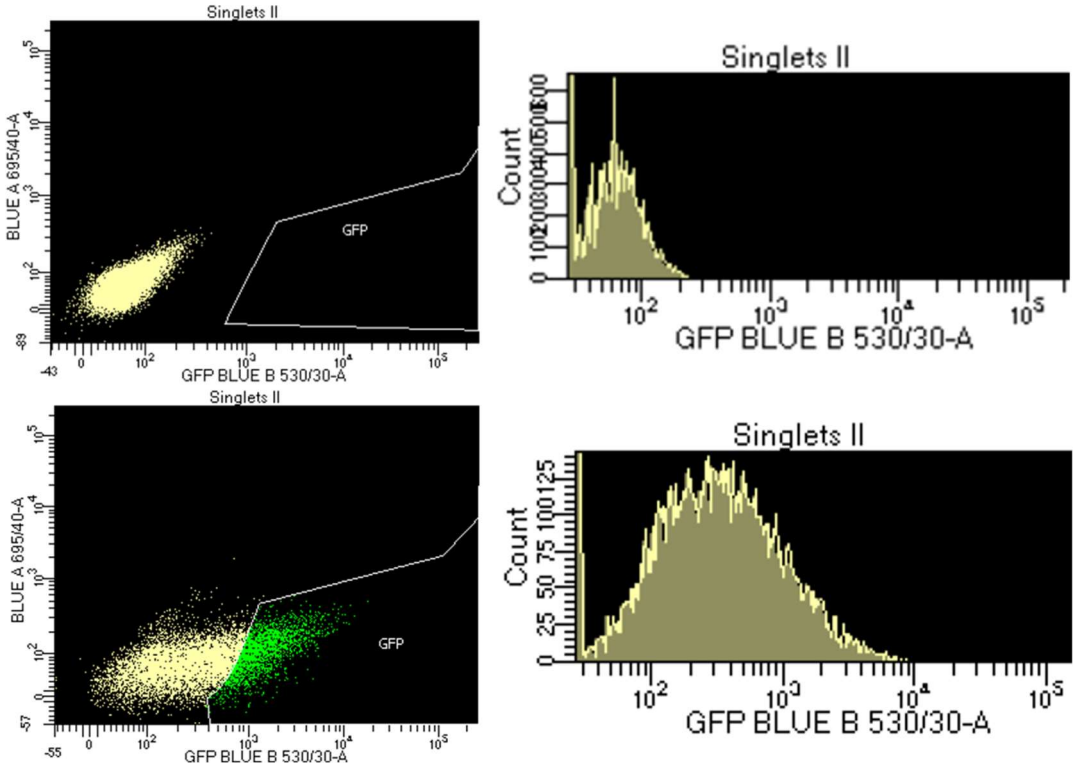

Figure 13. FACS. GFP expression in SH-SY5Y cells before and after SeNCYT transduction. Upper panels: non-transduced control cells, showing no GFP signal as shown in the dot plot (left) and corresponding histogram (right). Lower panels: transduced cells displaying a continuous range of GFP intensities in same representations.

Crucially, this variability allowed us to select and retain only the brightest cells, ensuring high construct expression and maximizing visibility in imaging applications. This strategy not only guarantees that all selected cells carry the SeNCYT construct but also addresses the common

challenge of low signal during microscopy. The final sorted population, therefore, consisted exclusively of highly fluorescent SeNCYT-expressing cells, which were subsequently used for all experimental procedures.

5.1.2. MORPHOLOGICAL ASSESSMENT OF SH-SY5Y DIFFERENTIATION

The morphology of SH-SY5Y cells was assessed at day 0 and day 10 of the differentiation protocol to evaluate structural changes associated with neuronal differentiation. Bright-field images were acquired before the initiation of differentiation and after completing the 10-day process.

At day 0, cells exhibited the typical morphology of undifferentiated SH-SY5Y cells, with irregular shapes and limited process extension. By day 10, marked morphological changes were observed, including the appearance of rounded somas and neurite-like projections forming interconnected networks across the culture surface.

These features, shown in Figure 14, were consistently observed across replicates. When compared to differentiated SH-SY5Y cells from the lab not carrying the construct, no morphological differences were observed. This indicates that SeNCYT expression did not interfere with the differentiation process or affect the acquisition of neuron-like morphology.

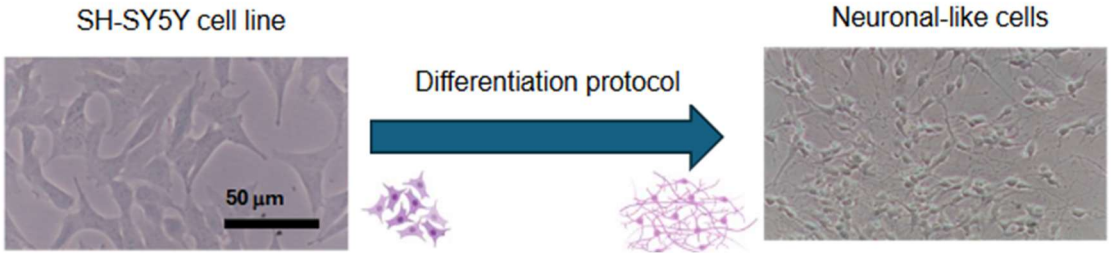

Figure 14. Bright field images of SH-SY5Y cells at day 0 and day 10 (first and final stages) of the neuronal differentiation process.

5.2. OPTIMIZATED PROTOCOL FOR LIVE IMAGING

5.2.1. MEDIA AUTOFLUORESCENCE

Previous experiments indicated that SeNCYT exhibits **low fluorescence intensity** under standard imaging conditions. To improve signal detection, an experiment was conducted to evaluate how different **imaging media compositions** affect the visibility of SeNCYT in SH-SY5Y cells.

Cells from the same culture were seeded in parallel across different wells, and after 24h, medias were replaced. As stated before, two main formulations were tested Neurobasal-A (NB) (used in differentiation media stage 2) and BrainPhys Imaging (BPI), which is specifically formulated for neuronal live imaging. Versions with and without the corresponding supplements (B27 for the Neurobasal-A), N2 and SM1 for the BrainPhys Imaging), were tested. In addition, one of the wells media was maintained in PBS as a control. Multiple images were acquired to compare SeNCYT (GFP) signal across the different conditions to reduce variability and allow for signal averaging.

As shown in Figure 15, single-plane confocal images show that the highest Signal to Noise (S/N) ratio are (b) and (d), which used BrainPhys as imaging media. The difference in signal detection between BrainPhys complete and basal was minimal, as quantified in Figure 16 (a). In contrast, cells imaged in PBS (Figure 15e), exhibited lower and more diffuse SeNCYT signal, indicating that the buffer solution cannot maintain cells due to the lack of nutrients.

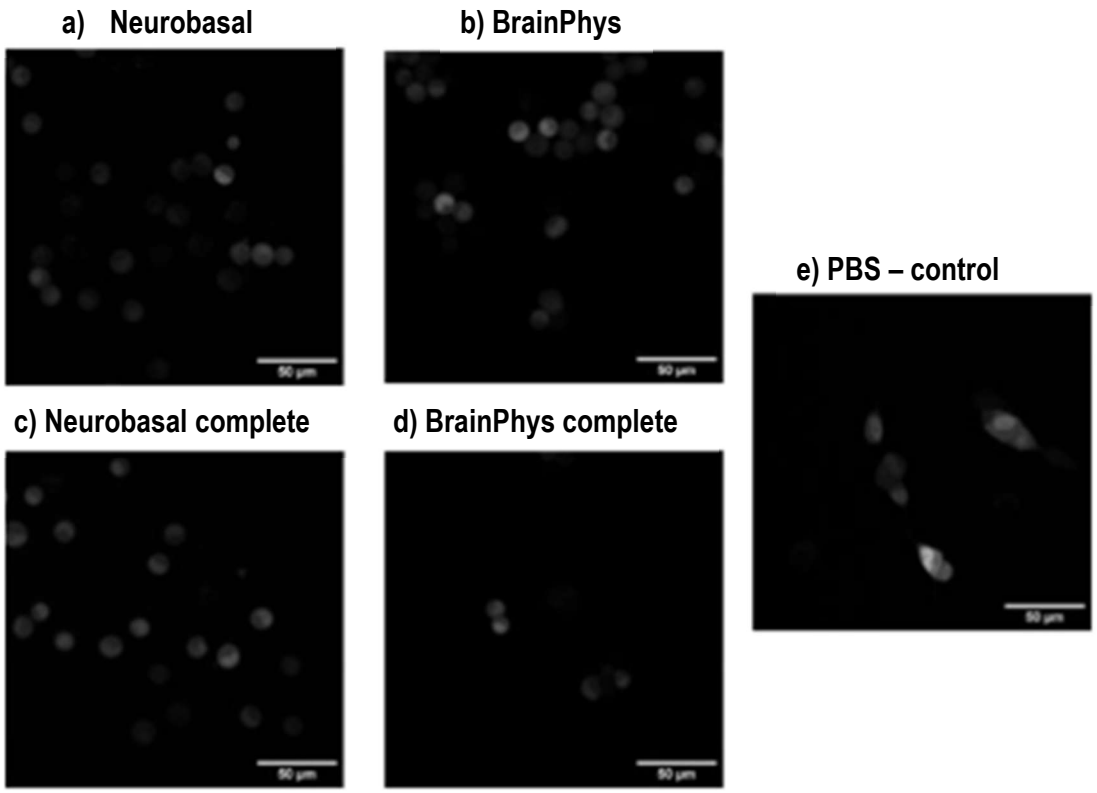

Figure 15. Single-plane confocal images of SH-SY5Y cells imaged in (a) Neurobasal, (b) BrainPhys, (c)Neurobasal Complete, (d) BrainPhys complete, (e) PBS, Scale bars: 50 µm

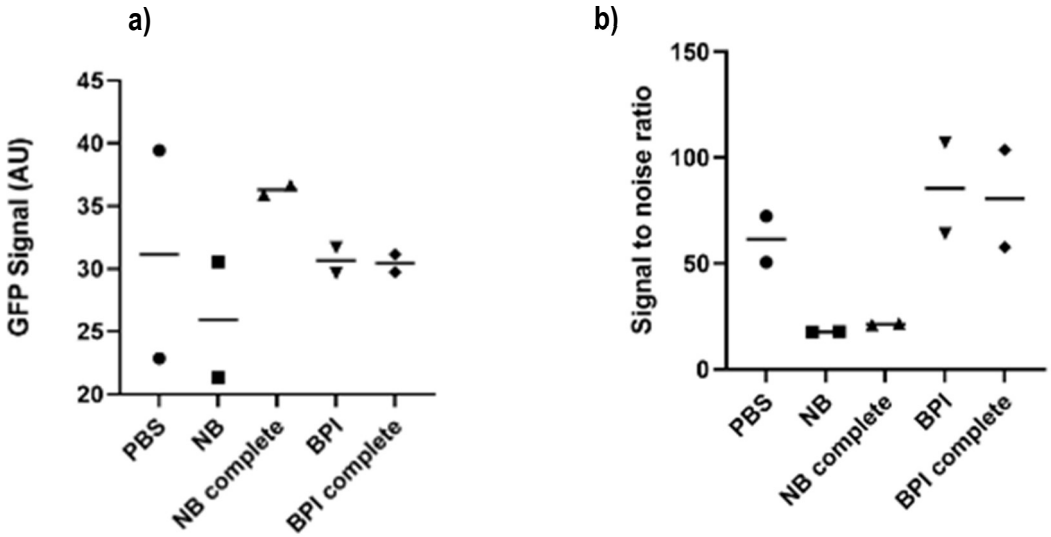

Figure 16. Results of media autofluorescence testing for single plane images. Graph (a) represents the GFP signal intensity in each of the media testes. Image (b) represents de Signal to Noise (S/N) ratio for each of the media tested.

Moreover, Figure 17 displays the results obtained using z-stack image acquisition, where the microscope collects a series of optical sections through the sample along the Z-axis. The distance between planes was set according to the optical resolution limit of the system taking together the imaging set up.

To generate a representative 2D image from the 3D stack, a maximum intensity projection was performed. This technique selects the brightest pixel at each XY coordinate across all Z-planes, effectively capturing the most prominent fluorescent signal within the scanned volume. In our case, this is particularly useful for highlighting weak or spatially variable signals, such as SeNCYT-GFP, which may not be consistently visible in a single optical plane due to variations in cell thickness or signal distribution. It can also be used better detect the background if non-specific fluorescence is present across multiple planes.

As shown in figure 17, both BrainPhys and BrainPhys complete resulted in greater image clarity and SeNCYT signal intensity, as well as a higher S/N ratio compared to the other medias tested. Furthermore, in the max image acquisition. The quantification of the GFP signal intensity (SeNCYT intensity) and S/N ration demonstrated a very similar result between to two BrainPhys conditions. (Figure 18).

Altogether, these results indicate that BrainPhys Imaging(BPI) medium, supplemented with N2 and SM1, is the most effective imaging medium among all those tested,. It consistently provided a higher S/N ratio and maximized SeNCYT signal intensity acquisition. Therefore, BPI complete was selected as the media for all subsequent image acquisition.

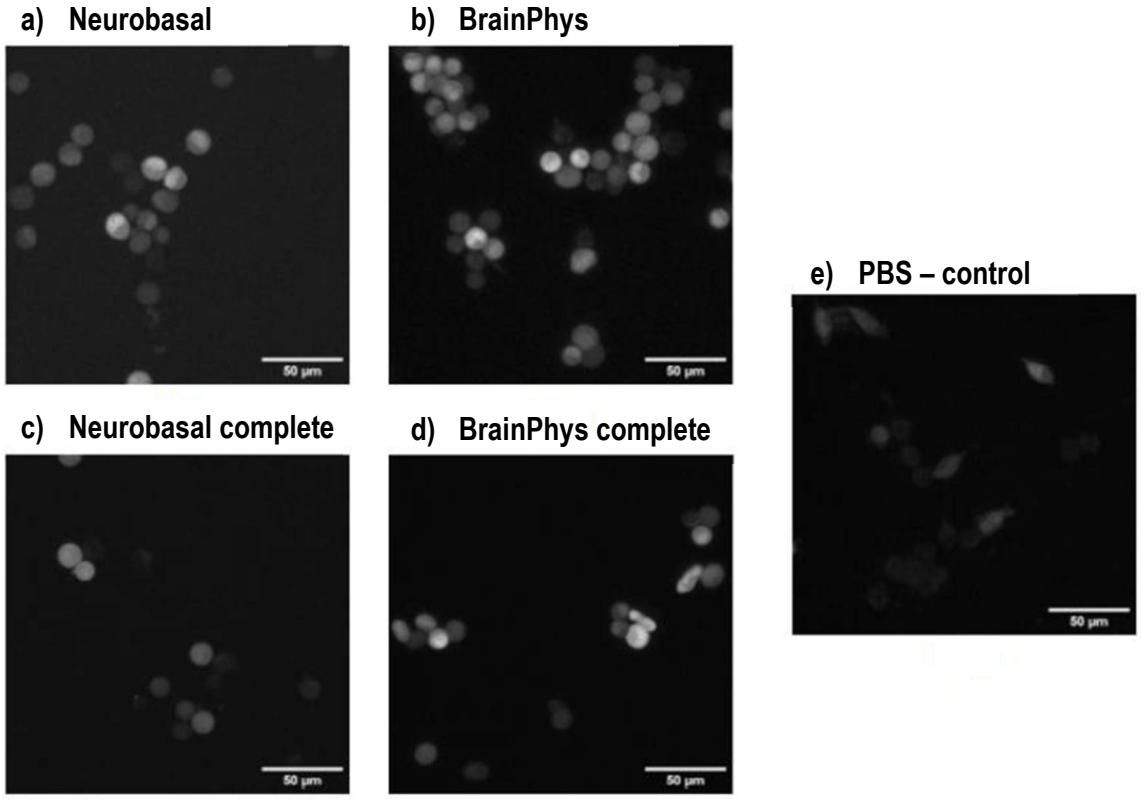

Figure 17. Maximum projection intensity of Z-stack confocal images of SH-SY5Y cells imaged in (a) Neurobasal, (b) BrainPhys, (c)Neurobasal Complete, (d) BrainPhys complete, (e) PBS, Scale bars: 50 µm

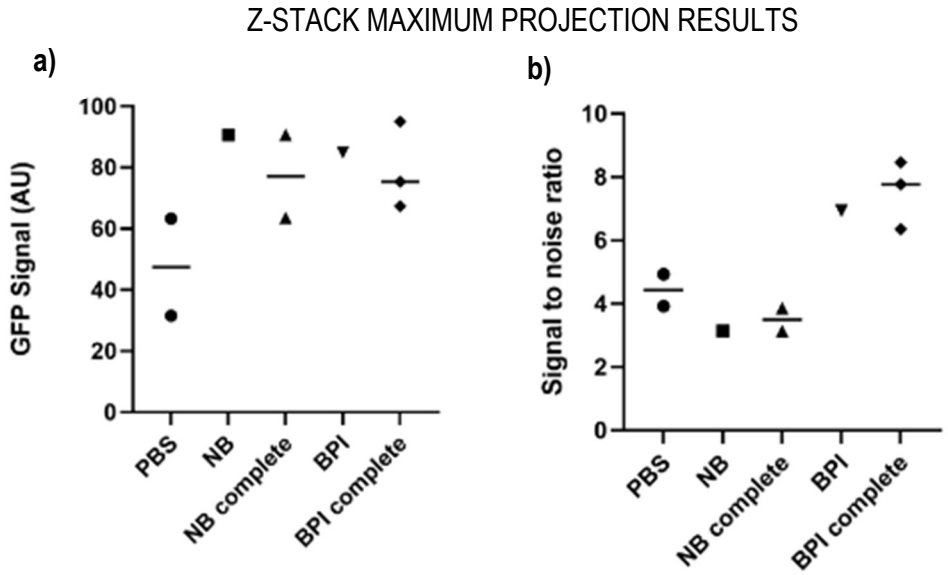

Figure 18. Results of media autofluorescence testing for z-stack maximum projections. Graph (a) represents the GFP signal intensity in each of the media testes. Image (b) represents de Signal to Noise (S/N) ratio for each of the media tested.

5.2.2. CHARACTERIZATION OF THE MEDIA OSMOLARITY

In parallel with the experiments aimed at identifying the imaging medium that provided the highest GFP signal intensity and signal-to-noise (S/N) ratio, we also validated the osmolality of the prepared media used for osmotic shock experiments. The targeted osmolality values—approximately 66% for hypoosmotic and 204% for hyperosmotic conditions—were chosen based on previous work by a former lab member [56] and as outlined in Section 4.2.7.

Confirming these values was essential to ensure that the osmotic shocks were applied correctly and reproducibly, while maintaining conditions that support cell viability and compatibility with imaging.

To ensure measurement accuracy and rule out outliers, three independent measurements were performed for each condition using a freezing point osmometer. The resulting mean osmolality, standard deviation (SD), and percentage deviation from the target values were calculated and are summarized in Table 3.

The differences between conditions can be more clearly visualized in the graph presented in Figure 19, which provides a straightforward comparison across the different media and osmotic states.

Table 3. Osmolarity measures results

Media		Repetition (mOsmol/kg)			Results		
		1	2	3	mean	SD	%
Basal	**NB**	285	280	287	284.00	3.61	-
Hyper-	**NB + Mannitol**	486	489	496	490.33	5.13	172.65
Hypo-	**NB + Ca^{2+} + Mg^{2+}**	116	119	112	115.97	3.51	59.27
Basal	**BPI**	308	310	311	309.67	1.53	-
Hyper-	**BPI + Mannitol**	514	522	529	521.67	7.51	168.46
Hypo-	**BPI + Ca^{2+} + Mg^{2+}**	140	132	133	135.00	4.36	56.41

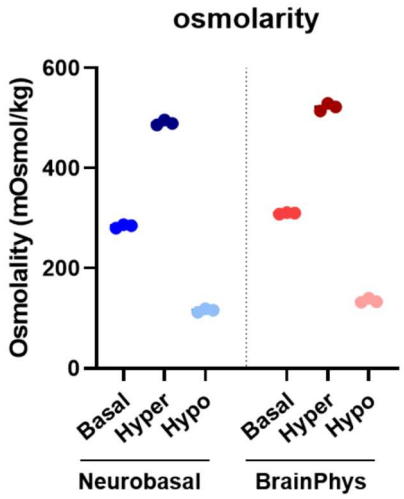

Figure 19. Plot of the different osmolalities. Comparison of NB-A and BPI mediums

The minimal SD among the datapoints reflects the robustness of the assay and media preparation. The data also confirms the osmolarities reported for the different medias. According to the BrainPhys patent sheet, the media has an osmolarity of around 310 mOsmol/L, which resembles the cerebrospinal fluid from healthy human brain. Considering the almost equivalence between osmolarity and osmolality in aqueous solutions, our results perfectly matched this value (309.67 ±1.53 mOsmol/kg). This same report indicated that Neurobasal media is formulated to reach around 220-250 mOsmol/L. Our results are a bit higher (284.00±3.61 mOsmol/kg), but those values do not take into account the addition of KCL, L-glutamine or B27, which surely increase those values.

More importantly, these experiments allowed to measure the apmplitude of the osmolarity changes when the proportion of hypo-and hypoosmotic solutions were applied as displayed.

In the case of HypoOsmotic shocks, the reduction was very close to the target value (66%), reaching 59.27% and 56.41% for Neurobasal and BrainPhys, respectively. However, the volume added, and the nature of the hyperosmotic solution did not allow the medium to reach a 204% increase. Instead, the osmolarity rose to 172.65% in the case of Neurobasal and 168.46% in BrainPhys Imaging medium. Nevertheless, we decided to work with these values, given that

Taken together, these findings support the use of BrainPhys Imaging (BPI) as the most suitable medium for live-cell experiments. Its superior signal-to-noise (S/N) ratio ensures excellent

visualization in fluorescence-based applications, which is particularly important for detecting weak signals such as those emitted by SeNCYT. Based on the consistent and reproducible modulation observed in both hypo- and hyperosmotic conditions, we concluded that the tested solutions provide a valid and reliable model for inducing osmotic shocks. Therefore, we will use the tested concentrations in our subsequent experiments, even though the hyperosmotic condition did not reach the initially intended 204% increase. We consider this acceptable because the achieved osmolarity increase was sufficient to elicit a clear and measurable cellular response, while also avoiding potential artifacts or cytotoxic effects that may arise from excessively high osmolarity levels.

5.2.3. HYDROGEL FUNCTIONALIZATION METHOD

As part of the gel optimization process, two functionalization strategies were tested for covalently binding laminin (50 µg/mL) to the PAA surface: sulfo-SANPAH and acrylic acid incorporation during polymerization. Although no quantitative comparison was performed, qualitative observations showed that the acrylic acid method consistently supported a higher number of adherent cells after seeding. In contrast, the sulfo-SANPAH method occasionally produced crystalline deposits on the gel surface, likely due to precipitation, which were observed to be auto-fluorescent under imaging conditions—interfering with signal clarity. Based on these observations, the acrylic acid-based functionalization was selected for all subsequent experiments due to its greater consistency and apparent efficiency.

Subsequent to the selection of the optimal protocol for cell differentiation and successful fabrication of PAA gels with defined stiffness values, seeding neuron-like SH-SY5Y cells onto the substrates with different rigidity and acquire images in order to determine morphological responses to the opposite mechanical environments. Two stiffness conditions were considered, 0.5kPa (soft) and 15kPa (stiff).

5.3. NUCLEOCYTOPLASMIC TRANSPORT ANALYSIS

Once the experimental conditions—including imaging medium, gel functionalization, and construct expression—were optimized, we proceeded to perform live-cell imaging of SH-SY5Y cells using confocal microscopy. Both undifferentiated and fully differentiated cells expressing the SeNCYT construct were imaged to validate construct expression and nuclear staining before applying experimental perturbations.

As shown in Figure 20, dual-channel confocal imaging confirmed that SeNCYT, tagged with green fluorescent protein (GFP), was successfully expressed and detectable in living cells (Figure 20a). In parallel, the nuclear compartment was clearly identified using Hoechst 33258 staining (Figure 20b), enabling accurate segmentation of nuclear and cytoplasmic regions.

Z-stack acquisition allowed for clear spatial resolution across cell volumes, and maximum intensity projections provided composite images showing both signals. These preliminary images confirmed that the system was ready for the quantitative analysis of nucleocytoplasmic transport (NCT) under different experimental conditions, including osmotic shock and substrate stiffness.

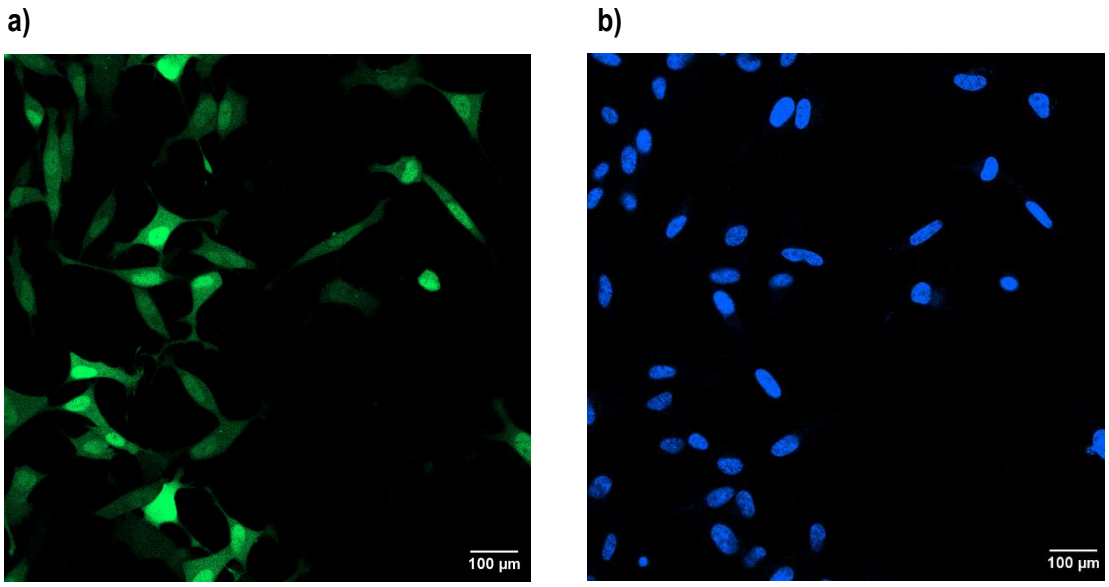

Figure 20. Confocal microscopy images of undifferentiated SH-SY5Y cells expressing SeNCYT. Maximum intensity projection of a z-stack acquisition showing both fluorescence channels. (a) GFP signal indicating SeNCYT localization. (b) Hoechst staining of the nuclei. Scale bar: 100µm

5.3.1. EFFECT OF OSMOTIC SHOCKS ON NUCLEOCYTOPLASMIC TRANSPORT

To assess how osmotic stress affects nucleocytoplasmic transport, SH-SY5Y cells, both undifferentiated and differentiated into neuronal-like cells, were subjected to either hypoosmotic or hyperosmotic conditions. Two custom osmotic solutions were used, as previously optimized (see Section 4.2.3): the hyperosmotic medium consisted of 96.9 g/L D-mannitol, while the hypoosmotic solution contained 264 mg/L $CaCl_2 \cdot 2H_2O$ and 164.67 mg/L $MgCl_2 \cdot 6H_2O$. When added to the imaging media in the appropriate proportions (as described in [56]), these formulations induced changes in osmolality of +168.46% (hyperosmotic) and −56.41% (hypoosmotic) relative to baseline values.

The expected result is that hypoosmotic treatment would result in cell and nuclear swelling due to water influx, while hyperosmotic conditions would trigger water efflux, causing shrinkage. These changes are known to modulate the mechanical tension of the nuclear envelope and potentially alter the permeability of nuclear pore complexes (NPCs), thereby influencing NCT dynamics.

A relevant consideration in these experiments is the time required for image acquisition during live confocal imaging. The use of z-stacks and multiple acquisition positions across the well extends the duration needed to capture each time point. As a result, the exact time intervals between baseline and post-treatment images may vary slightly across samples. Nonetheless, pilot experiments demonstrated that changes in SeNCYT signal following osmotic stress occurred within minutes and remained stable for at least 30 minutes. Thus, under the tested conditions, the timing variation introduced by image acquisition did not significantly affect the reliability of the observed responses.

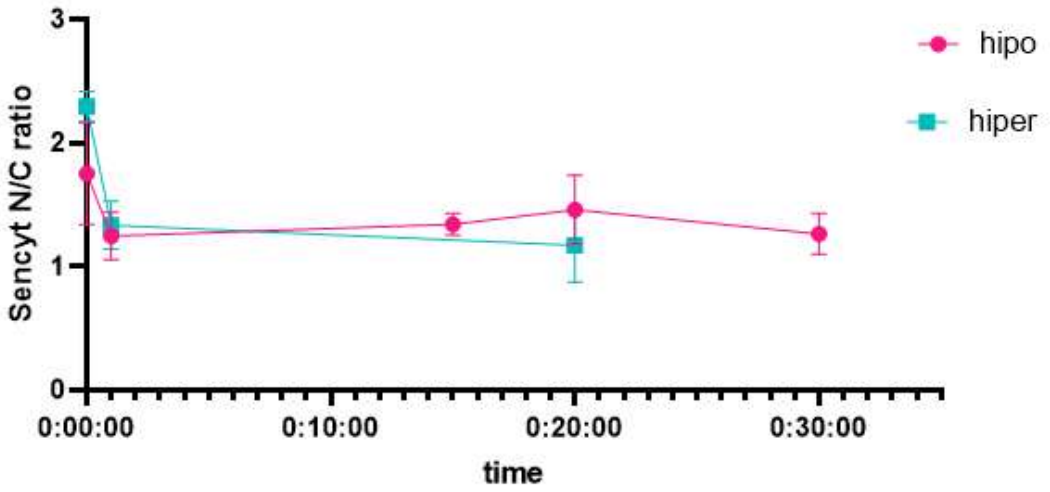

Figure 21. Time course of SeNCYT nuclear-to-cytoplasmic (N/C) ratio following osmotic shock. Undifferentiated SH-SY5Y cells expressing SeNCYT were subjected to either hypoosmotic (pink circles) or hyperosmotic (blue squares) conditions, and the SeNCYT N/C fluorescence ratio was quantified over time using live confocal imaging. Each point represents the mean ± SEM of n = 10 cells per time point, from N = 2 independent experiments

5.3.1.1 EFFECT OF OSMOTIC SHOCKS ON NUCLEOCYTOPLASMIC TRANSPORT ON SH-SY5Y CELLS

To initiate the analysis, we first examined the response of undifferentiated SH-SY5Y cells to **hypoosmotic stress**, serving as a reference population for later comparison with differentiated cells. Cells were imaged by live confocal microscopy before and 30 minutes after treatment, and both SeNCYT localization and nuclear morphology were evaluated. For improved precision, the analysis focused on a curated set of single cells rather than bulk quantification across all imaged positions. This allowed for cell-specific adjustment of nuclear and cytoplasmic regions, enhancing the reliability of SeNCYT intensity measurements without introducing selection bias.

Although subtle changes in nuclear shape were observed in some cells (Figure 22), quantitative single-cell analysis revealed no significant differences in either the SeNCYT nuclear-to-cytoplasmic (N/C) ratio or the nuclear projected area after treatment (Figure 23). While a slight upward trend in N/C ratio was seen in a subset of cells, the average change was not statistically significant ($p = 0.2237$). Similarly, nuclear area showed a mild increase in several cells, but the variation remained non-significant ($p = 0.3265$).

These results suggest that hypoosmotic treatment does not significantly alter SeNCYT distribution or nuclear morphology in undifferentiated SH-SY5Y cells within the 30-minute timeframe tested. One possible explanation for the limited morphological and NCT response is that undifferentiated cells were seeded on stiff substrates, which are known to promote extensive cell spreading and increased cytoskeletal tension. In these conditions, cells often adopt a flattened morphology with a well-developed actin cytoskeleton, which can impose mechanical constraints on the nucleus. As a result, the nuclear envelope may already be under a state of elevated tension, limiting its ability to undergo further deformation in response to osmotic swelling.

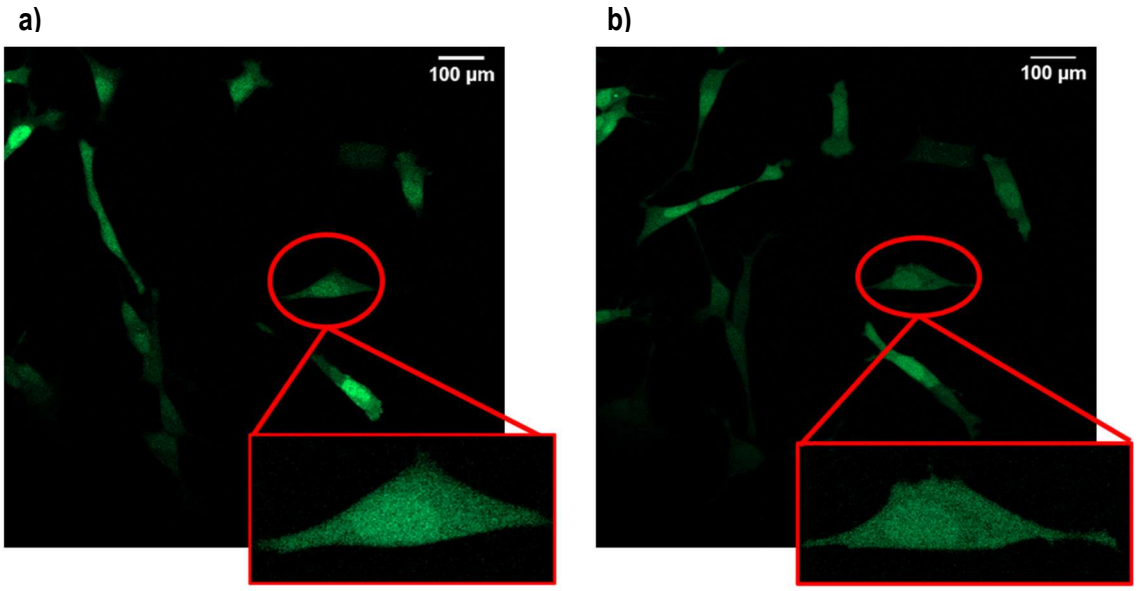

Figure 22. Confocal images of undifferentiated SH-SY5Y cells expressing SeNCYT before and after hypoosmotic treatment. Panels show maximum intensity projections of z-stacks acquired before (a) and 20 minutes after (b) exposure to a hypoosmotic shock. GFP fluorescence indicates SeNCYT localization. Insets highlight a representative cell. Scale bar: 100 µm.

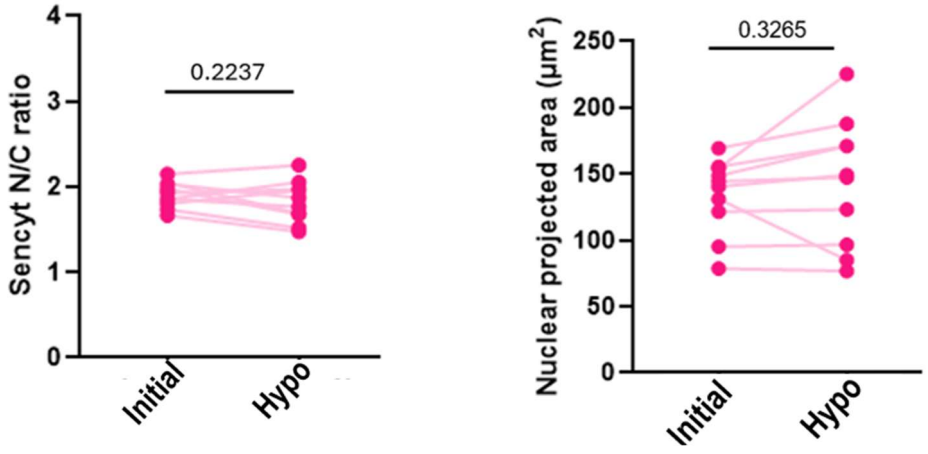

Figure 23. Quantitative analysis of SeNCYT distribution and nuclear size in undifferentiated SH-SY5Y cells before and after hypoosmotic shock. (a) Nuclear-to-cytoplasmic (N/C) ratio of SeNCYT fluorescence before and after treatment. (b) Nuclear projected area (µm²) of the same cells across the same conditions. Each dot represents a single cell; n = 10 cells per condition, from N = 2 independent experiments. Statistical analysis was performed using a paired t-test.

We next evaluated the response of SH-SY5Y undifferentiated cells to **hyperosmotic shock**. The same experimental setup was used, with the osmotic composition adjusted by adding D-mannitol to achieve the target osmolality.

As shown in Figure 24, hyperosmotic treatment led to a visible reduction in the contrast between nuclear and cytoplasmic SeNCYT signal, along with an apparent decrease in nuclear size, consistent with nuclear shrinkage. To validate these observations, a quantitative single-cell analysis was performed (Figure 25). Panel a) shows a significant decrease in the SeNCYT nuclear-to-cytoplasmic (N/C) fluorescence ratio after treatment, suggesting a redistribution of SeNCYT out of

the nucleus. Panel b confirms the morphological response, showing a statistically significant reduction in nuclear projected area.

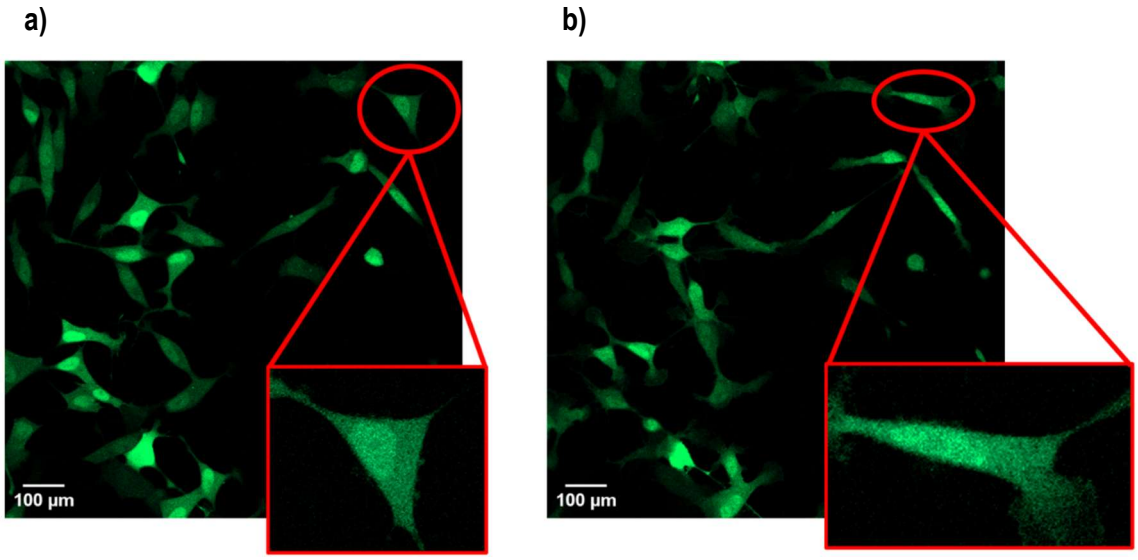

Figure 24. Confocal images of undifferentiated SH-SY5Y cells expressing SeNCYT before and after hyperosmotic treatment. Panels show maximum intensity projections of z-stacks acquired before (a) and after (b) exposure to a hyperosmotic shock. GFP fluorescence indicates SeNCYT localization. Insets highlight a representative cell. Scale bar: 100 µm.

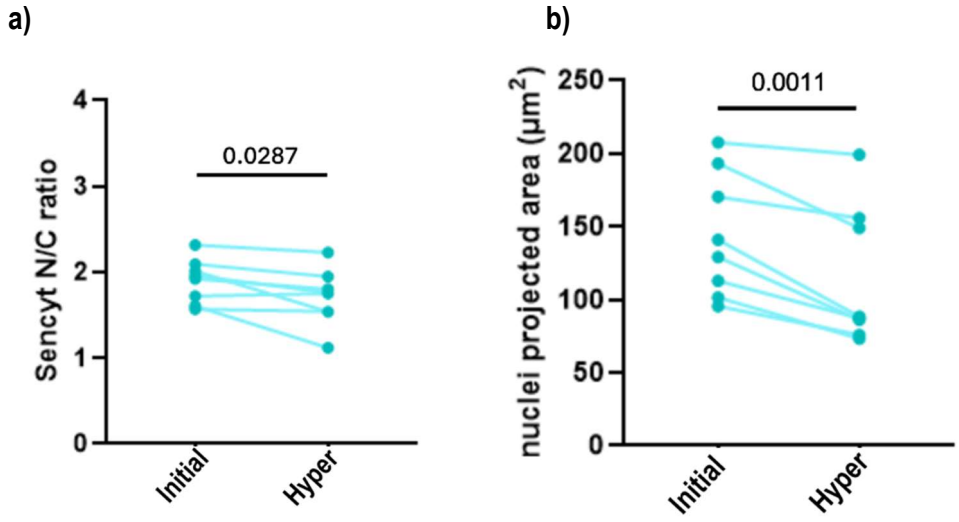

Figure 25. Quantitative analysis of SeNCYT distribution and nuclear size in undifferentiated SH-SY5Y cells before and after hyperosmotic shock. (a) Nuclear-to-cytoplasmic (N/C) ratio of SeNCYT fluorescence before and after treatment. (b) Nuclear projected area (µm²) of the same cells across the same conditions. Each dot represents a single cell; n = 10 cells per condition, from N = 2 independent experiments. Statistical analysis was performed using a paired t-test.

Unlike the hypoosmotic condition, the effects of hyperosmotic stress were statistically significant for both parameters, with p-values below 0.05. These findings confirm that hyperosmotic shock elicits a robust biological response, impacting both nuclear morphology and nucleocytoplasmic transport in undifferentiated SH-SY5Y cells.

5.3.1.2. EFFECT OF OSMOTIC SHOCKS ON NUCLEOCYTOPLASMIC TRANSPORT (NCT) ON NEURONAL-LIKE CELLS

To investigate the response of **neuron-like SH-SY5Y-derived cells** to **hypoosmotic stress**, the experiment was repeated under the same shock conditions. In this case, however, image

acquisition was performed after 45 minutes. This extended time point was determined not by biological reasons, but rather due to technical constraints: we needed to acquire multiple positions and full z-stacks across the sample to ensure sufficient cell numbers for analysis.

As shown in Figure 26, confocal images before (a) and after (b) the hypoosmotic treatment reveal subtle morphological changes, such as a slight increase in soma spreading. However, no obvious difference in SeNCYT localization is apparent by visual inspection.

To confirm these observations, single-cell quantitative analysis was conducted. As summarized in Figure 27, neither the SeNCYT nuclear-to-cytoplasmic (N/C) intensity ratio nor the nuclear projected area showed statistically significant changes after 45 minutes of hypoosmotic exposure. These findings are consistent with those obtained in undifferentiated cells, suggesting that under the same osmotic conditions, neuron-like cells also do not exhibit substantial NCT modulation or nuclear morphological alterations.

This reinforces the notion that the osmotic challenge applied may be too mild to disrupt the nuclear transport equilibrium or nuclear morphology in these cells. This could be due to the mechanical properties of the neuronal phenotype, able to buffer the mechanical expansion, or the stiffness of the underlying substrate.

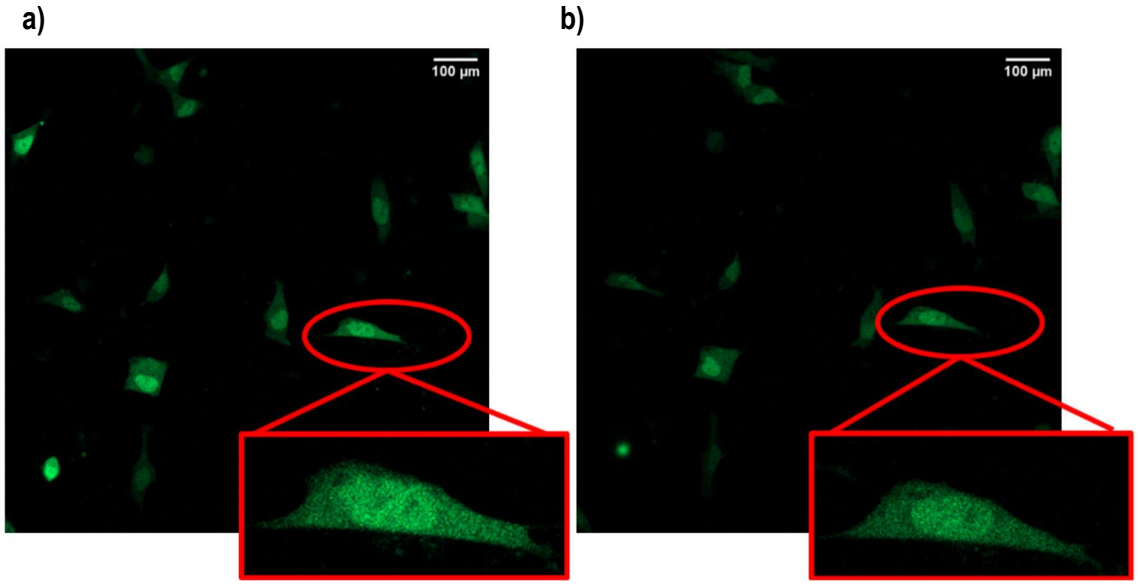

Figure 26. Confocal images of SH-SY5Y-derived neuronal-like cells expressing SeNCYT before and after hypoosmotic treatment. Panels show maximum intensity projections of z-stacks acquired before (a) and 20 minutes after (b) exposure to a hypoosmotic shock. GFP fluorescence indicates SeNCYT localization. Insets highlight a representative cell. Scale bar: 100 µm.

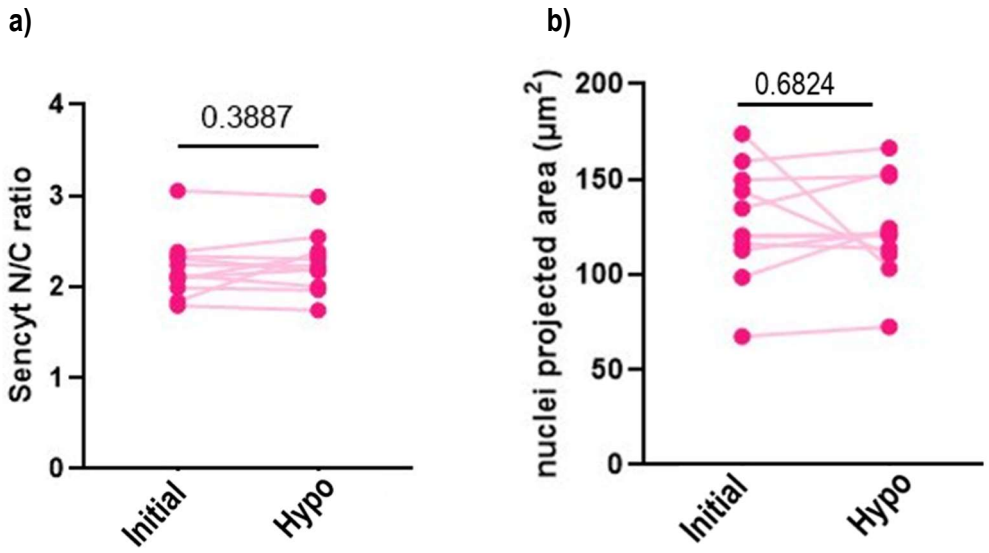

Figure 27. Quantitative analysis of SeNCYT distribution and nuclear size in SH-SY5Y-derived neuronal-like cells before and after hypoosmotic shock. (a) Nuclear-to-cytoplasmic (N/C) ratio of SeNCYT fluorescence before and after treatment. (b) Nuclear projected area (µm²) of the same cells across the same conditions. Each dot represents a single cell; n = 10 cells per condition, from N = 2 independent experiments. Statistical analysis was performed using a paired t-test

Similar to the response observed in undifferentiated SH-SY5Y cells, **hyperosmotic treatment** of neuron-like cells induced evident changes in both SeNCYT distribution and nuclear morphology. Visual inspection of the confocal images suggests a reduction in nuclear size and a drop in the SeNCYT nuclear-to-cytoplasmic (N/C) intensity contrast, consistent with cellular shrinkage and altered nucleocytoplasmic transport.

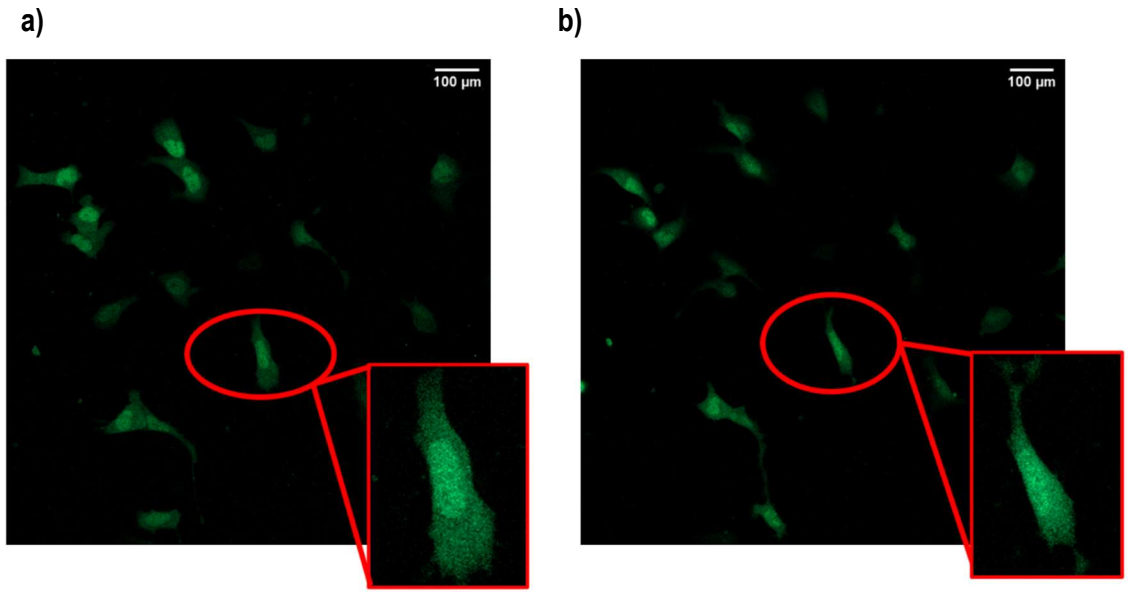

Figure 28. Confocal images of SH-SY5Y-derived neuronal-like cells expressing SeNCYT before and after hyperosmotic treatment. Panels show maximum intensity projections of z-stacks acquired before (a) and 20 minutes after (b) exposure to a hyperosmotic shock. GFP fluorescence indicates SeNCYT localization. Insets highlight a representative cell. Scale bar: 100 µm.

These observations were confirmed through quantitative single-cell analysis (Figure 29). Panel (a) shows a significant decrease in the SeNCYT N/C ratio, indicating reduced nuclear signal relative to the cytoplasm. Panel (b) displays a significant reduction in the nuclear projected area, reflecting

nuclear shrinkage. Both results were statistically significant ($p < 0.05$), confirming a consistent biological response to hyperosmotic stress.

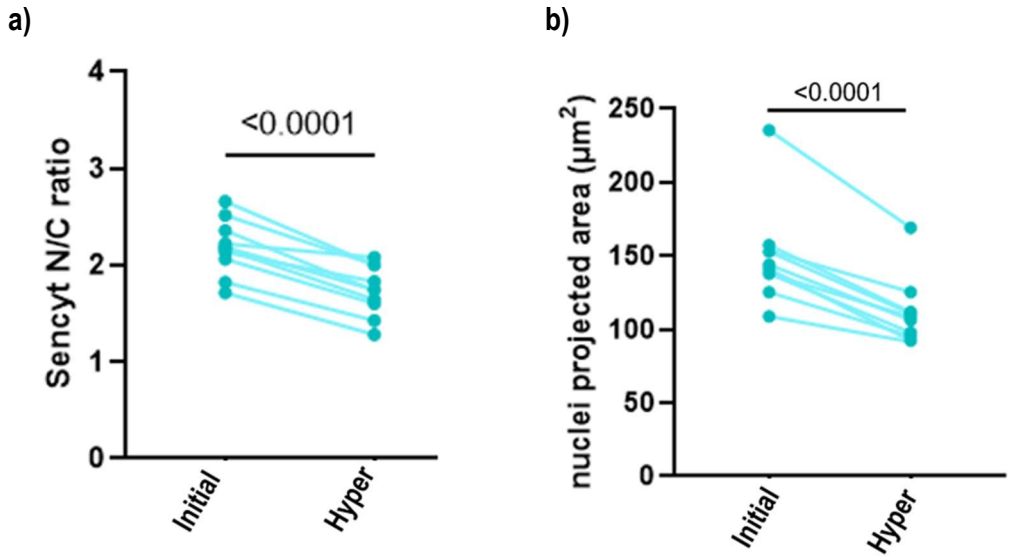

Figure 29. Quantitative analysis of SeNCYT distribution and nuclear size in SH-SY5Y-derived neuronal-like cells before and after hyperosmotic shock. (a) Nuclear-to-cytoplasmic (N/C) ratio of SeNCYT fluorescence before and after treatment. (b) Nuclear projected area (µm²) of the same cells across the same conditions. Each dot represents a single cell; n = 10 cells per condition, from N = 2 independent experiments. Statistical analysis was performed using a paired t-test

These findings demonstrate that neuron-like cells are sensitive to osmotic changes, and under hyperosmotic conditions, nucleocytoplasmic transport is disrupted, as evidenced by the reduction in SeNCYT nuclear accumulation. This supports the notion that the nuclear environment and transport dynamics are tightly linked to external mechanical and osmotic cues.

5.3.2. EFFECT OF TISSUE RIGIDITY ON NUCLEOCYTOPLASMIC TRANSPORT ON NEURONAL-LIKE CELLS

To assess the effect of ECM mechanical cues on neuron-like SH-SY5Y cells, we first examined how substrate stiffness influences cellular morphology. As shown in Figure 30, cells cultured on **soft matrices (0.5 kPa)** exhibit characteristic features: rounded somas, limited spreading, and reduced neurite extension, generally forming short projections that connect only to nearby cells. In many cases, neurons tend to aggregate into clusters, likely due to the low mechanical resistance of the substrate. These observations are consistent with reported behaviours of neurons grown in compliant environments.

In contrast, cells grown on **stiffer substrates (15 kPa)** display markedly different morphology. They appear more spread and flattened, with a more homogeneous distribution across the gel surface, showing no signs of clustering. Neurites are visibly longer, forming dense and organized networks that connect cells across wider distances. This behaviour suggests that neuron-like cells respond to increased matrix stiffness by enhancing cytoskeletal tension, promoting adhesion, and supporting extended neurite outgrowth.

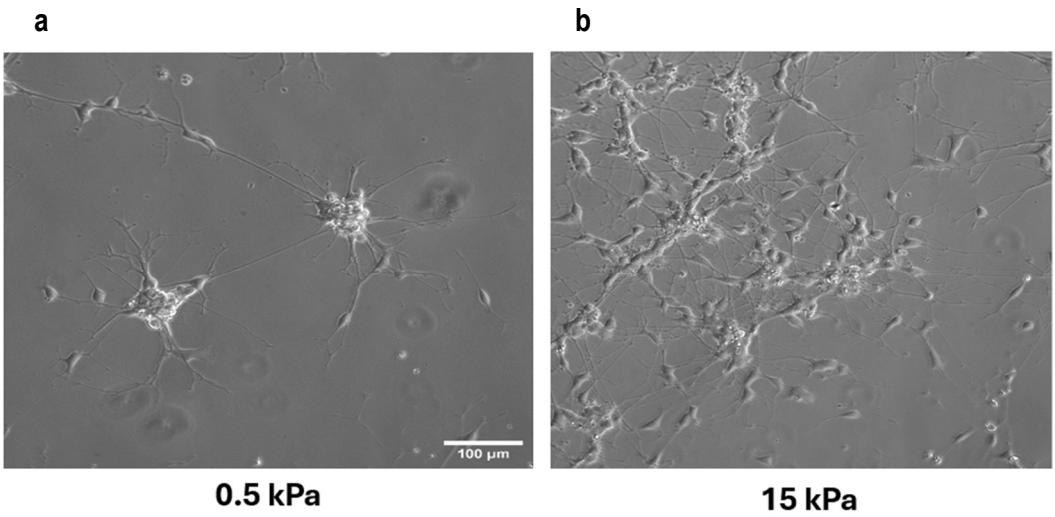

Figure 30. Bright field images of neuron-like SH-SY5Y cells cultured on PAA gels of (a) 0.5 and (b) 15kPa.

To quantitatively assess these morphological changes, we compared the projected area of the soma, nucleus, and neurites in neurons grown on soft vs. stiff gels. As shown in Figure 31, all measured compartments exhibited a significant increase in area on the stiffer substrate. This behaviour is expected, as cells typically expand and flatten more in response to rigid environments. However, it is worth noting that the magnitude of the difference was moderate, and neurite areas displayed substantial variability between individual cells. These measurements were kindly provided by Dr. Jorge Oliver de la Cruz, who used fluorescein-conjugated WGA membrane staining and Hoechst DNA staining to generate these morphometric data.

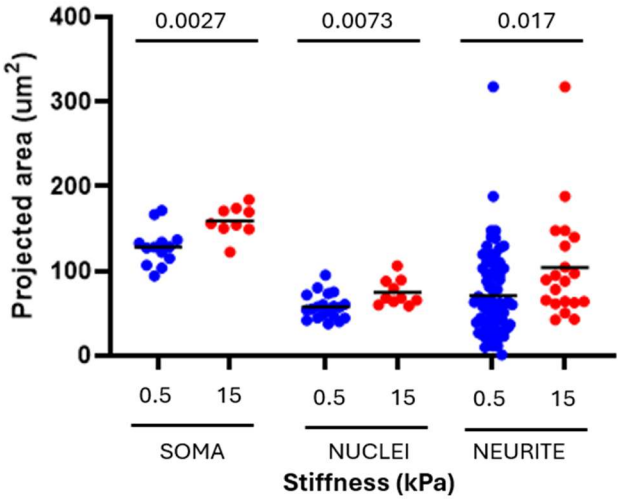

Figure 31. Quantification of soma, nuclear, and neurite projected areas in neuron-like SH-SY5Y cells cultured on soft (0.5 kPa) and stiff (15 kPa) polyacrylamide gels. Each dot represents a single cell measurement. p-values from unpaired t-tests are indicated for each comparison.

Having confirmed that neuron-like cells respond morphologically to substrate stiffness, we next assessed whether **nucleocytoplasmic transport (NCT)** is also influenced by mechanical cues. To do this, we measured the **SeNCYT nuclear-to-cytoplasmic (N/C) fluorescence ratio** in neurons cultured on substrates of these two different stiffnesses (0.5 kPa and 15 kPa).

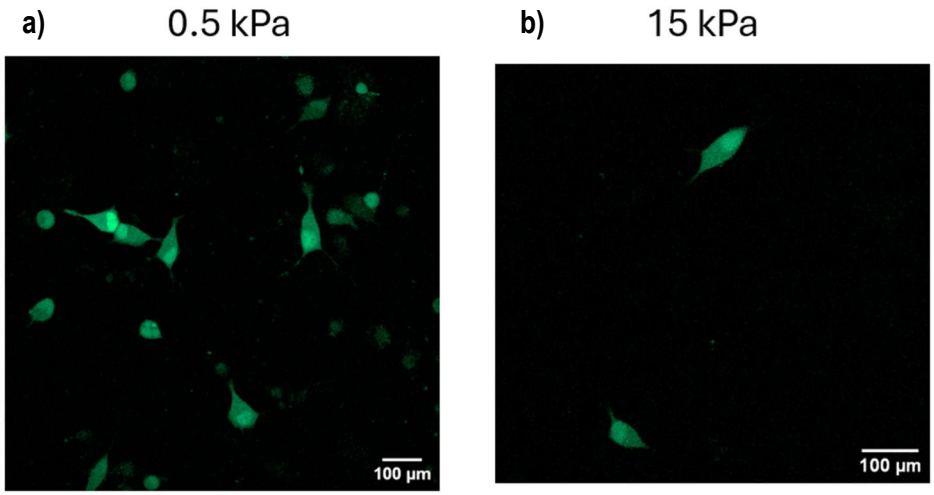

Figure 32. Confocal images of SH-SY5Y-derived neuronal-like cells expressing SeNCYT culture onto (a) soft (0.5Kpa) or (b) stiff PAA gels. Scale bar: 100 µm

As shown in Figure 32, neurons seeded on softer substrates (0.5 kPa) exhibit a lower N/C ratio compared to those grown on stiffer gels (15 kPa). This indicates that higher matrix stiffness promotes increased SeNCYT nuclear accumulation, potentially reflecting more active or permissive NCT under those conditions. This trend aligns with previous morphological findings, as neurons on stiff substrates display a more flattened and spread phenotype, which may affect nuclear tension and pore dynamics. Importantly, the observed differences in SeNCYT N/C ratio did not reach statistical significance in this dataset. This is likely due to the limited number of cells analysed. Although additional image data were acquired, time constraints during the preparation of this report prevented the completion of a full quantitative analysis.

To extend this analysis, a comparison with glass substrates was also included. Neurons seeded on glass, which has a stiffness in the gigapascal (GPa) range, showed only a slightly higher SeNCYT N/C ratio compared to those on 15 kPa gels. These results suggest a potential saturation of the NCT response around 15 kPa, indicating that SH-SY5Y-derived neurons may be sensitive to a narrower stiffness range than other cell types. However, further testing across additional stiffness levels and with larger datasets is needed to confirm this.

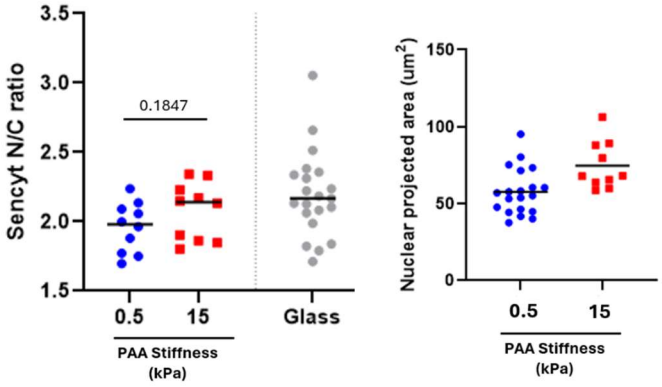

Figure 33. Effect of substrate stiffness on SeNCYT localization and nuclear area. Left) SeNCYT nuclear-to-cytoplasmic (N/C) ratio in neuron-like cells cultured on 0.5 kPa, 15 kPa, and glass substrates. (Right) Nuclear projected area for 0.5 kPa and 15 kPa

Altogether, our results suggest a role for substrate stiffness in modulating not only the morphology but also the nucleocytoplasmic transport of neuronal cells. Although not all differences reached statistical significance, the observed trends consistently support a mechanosensitive behaviour of

NCT, where stiffer environments might promote greater nuclear accumulation of proteins with similar characteristics to SeNCYT.

6. EXECUTION SCHEDULE

To accomplish the goals of the project accurately, hence offering methodological advances and exhaustive explanation of the project a Work Breakdown Structure (WBS) is detailed. By the WBS implementation activities are thoroughly evaluated and exposed. Moreover, PERT and GANTT diagrams, which show understandably the activity sequence and flexible outcomes, are also enclosed below. This organized and ordered approach enables always having the project under control, also considering unexpected events.

6.1. WORK BREAKDOWN STRUCTURE (WBS)

Before detailing the WBS dictionary with all the task exhaustively analysed, a proper WBS structure has been framed. Figure 34 depicts tasks developed during the project.

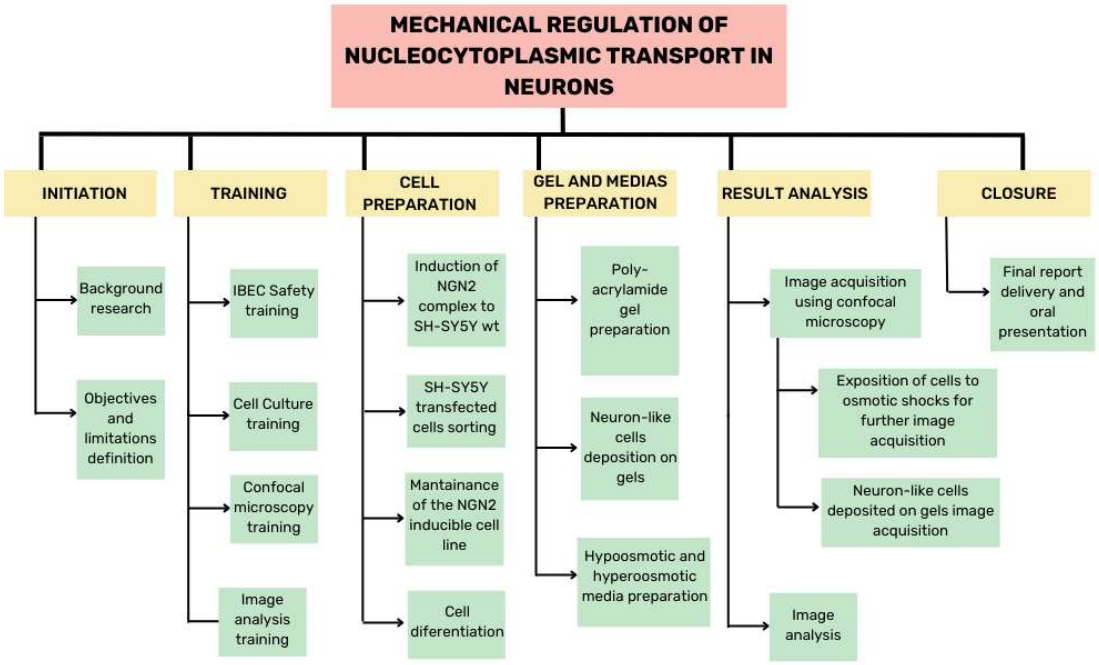

Figure 34. WBS structure of the project. Generated with https://www.canva.com/

As Figure 34 shows, tasks are divided into work packages following a hierarchical architecture. This division allows reaching maximum activity specificity and execution. WBS distribution helps defining a viable program and best budget. On the top of the scheme the overall project is defined. From it we will divide the project into six different work packages, corresponding each one to concept engineering, plan designing, resource management and final delivery of the research. Once we have these blocks defined, we enter in more detail breaking them down into more specific activities. Hence, the whole goal of developing a WBS is stablishing the direction of the project depending on each task.

6.1.1. WBS DICTIONARY

Next step to WBS structure creation is WBS dictionary development. This shows in scrupulously every activity previously defined in the scheme of the project. The dictionary is displayed as a table and incorporates all the relevant and crucial aspects of the tasks defined in each work package.

Table 4. 'Initiation' work package WBS dictionary package

INITIATION			
Nº	**Name**	**Duration**	**Description**
1.1	Background research	7 days	Based on the research of information on the background of the project, the state of the art (situation and motivations) and doing an exhaustive market analysis.
1.2	Objectives and limitations definition	7 days	Determine the aims of the project, and its scope. Also, the characteristics it must fulfil, and outline which are the limitations we are exposed to.

Table 5. 'Training' WBS dictionary work package

TRAINING			
Nº	**Name**	**Duration**	**Description**
2.1	IBEC safety training	7 days	Program to understand the potential hazards in a bioengineering lab and take measures to reduce risks and prevent accidents. It ensures that researchers know how to keep a safe and secure environment.
2.2	Cell culture training	7 days	Develop the skills to perform cell cultures efficiently. The training includes cell transfer and fixation techniques, creation of culture media, managing with culture hoods, and material localization.
2.3	Confocal microscopy training	4 days	Learn how to use a confocal microscope, the software behind it and get used to its working.
2.4	Image analysis training	3 days	Achieve the skills to work with ImageJ's program functioning.

Table 6. 'Cell preparation' WBS dictionary work package

CELL PREPARATION			
Nº	**Name**	**Duration**	**Description**
3.1	Induction of NGN2 complex into SH-SY5Y wild type (WT)	5 days	Insert the N2G2 viral complex to the wild type of SH-SY5Y cell line, to enable cells to differentiate into neuron-like cells
3.2	SH-SY5Y transfected cells sorting	2 days	Analyse thanks to sorting tools which of the cells have included the NGN2-dox complex
3.3	Maintenance of the NGN2-inducible cell line	15 days	Maintaining the SH-SY5Y cell-line with the introduction of the NGN2 protein previously cultured by another colleague.
3.3	Cell differentiation	28 days	Carry out the differentiation of SH-SY5Y cells into neuron-like cells

Table 7. 'Gel preparation' WBS dictionary work package

GEL AND MEDIAS PREPARATION			
Nº	**Name**	**Duration**	**Description**
4.1	Polyacrylamide gel preparation	2 days	Production of different stiffness gels, 0.5kPa and 15kPa, by following a given protocol.
4.2	Neuron-like cells deposition on gels	2 days	Displaying the previously differentiated neuron-like cells onto the gels of different stiffness. Hence, making them to adhere and interact with each of the gels respectively.
4.3	Hypoosmotic and Hyperosmotic media preparation	1 day	Mixture of Milli-Q water with high and low salinity reagents to generate hyperosmotic and hypoosmotic medias respectively.

Table 8. 'Results analysis' WBS dictionary work package

RESULTS ANALYSIS			
Nº	**Name**	**Duration**	**Description**
5.1	Image acquisition using confocal microscopy	30 days	Obtain the images of differentiated SH-SY5Y cells into neurons using confocal microscopes.
5.2	Expose cells to both hyper- and hypoosmotic medias and acquire images	1 days	Add the respective solution to the already generated cell line and acquire images of the effects of the osmotic changes using confocal microscopes.
5.3	Acquire images of the neurons seeded onto the PAA gels	3 days	Acquire images of the cells seeded over different stiffness PAA gels (0.5kPa and 15kPa) using confocal microscopes.
5.4	Image analysis	15 days	Analyse the images obtained on 5.1, 5.2, and 5.3 and define the final hypotheses.

Table 9. 'Closure' WBS dictionary work package

CLOSURE			
Nº	**Name**	**Duration**	**Description**
6.1	Delivery of the final report and oral presentation	15 days	Hand the work developed throughout all the projects.

6.2. PERT DIAGRAM

Above we have defined all the activities carried out and the times each one needs to be completed. Right away we must determine the interdependences between tasks. Thus, a Program Evaluation and Review Technique (PERT) is undertaken. With this tool, we can detail the schedule, plan and organize properly the different project tasks.

Table 10. Time and predecessor's matrix to compute PERT diagram.

ID	Name	Predecessor	Duration (days)
A	Background research	-	7
B	Objectives and limitations definition	A	7
C	IBEC safety training	B	7
D	Cell culture training	C	7
E	Confocal microscopy training	D	4
F	Image analysis training	E	3
G	Induction of NGN2 complex into SH-SY5Y wild type (WT)	F	5
H	SH-SY5Y transfected cells sorting	G	2
I	Maintenance of the N2G2-inducible cell line	H	15
J	Cell differentiation	I	28
K	Polyacrylamide gel preparation	J	2
L	Neuron-like cells deposition on gels	K	2
M	Image acquisition using confocal microscopy	L	30
N	Expose cells to both hyper- and hypoosmotic medias and acquire mages	M	1
O	Acquire images of the neurons seeded onto PAA gels	M	3
P	Image analysis	O, N	15
Q	Delivery of the final report and oral presentation	P	15

Figure 35 corresponds to the PERT diagram, where all activities are depicted. The critical path is defined by the activities in red. It is depicted in green that task N has a 2-day margin for fulfilling the activity. PERT diagram sequential solution indicates the progression of the tasks in the project. Each of the tasks depend on the accomplishment of the previous task, leading to a linear dependence sequence. For instance, before performing cell differentiation (task J), a proper maintenance of NGN2-induced cells had to be done previously. In fact, if the predecessor of a task is not completed, the task can't be performed, and the project will be delayed. Nevertheless, tasks like N that are not critical to develop the whole process have a time margin to be completed. Moreover, PERT present fictitious tasks represented by dashed arrows which do not consume time but are essential to the development of the following task. This scheme highlights the need to have a pre-established design where activities and tasks are accurately organized.

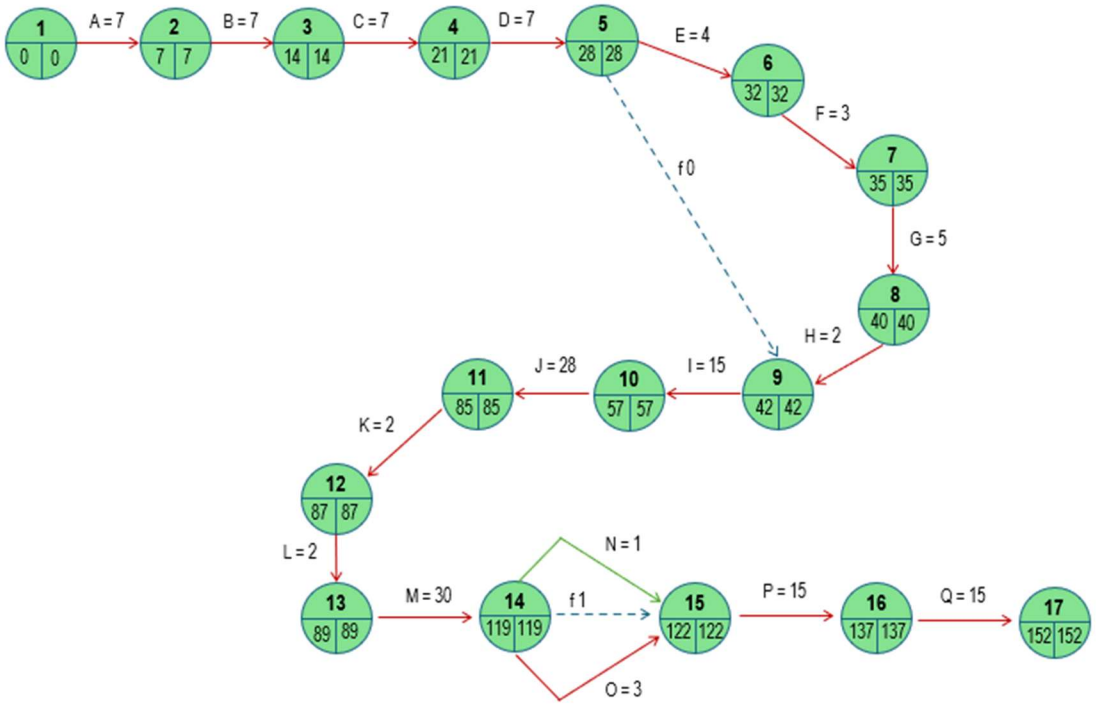

Figure 35. PERT diagram

6.3. GANTT DIAGRAM

Next project management tool presented is a Gantt chart. This diagram allows illustrating the whole project over a certain time space related to the planned time to develop it. There are represented start and ending dates. In fact, Gantt diagram illustrates the activities defined in the WBS dictionary on the x- axis, while the timeline in days is represented on the y-axis. PERT diagram conclusions are also depicted in Gantt chart. The total duration of the project is 152 days, which is an investment of 5 months, from February to June. For instance, Gantt chart includes all the tasks performed by the student, indeed all trainings assisted, and meetings with the supervisor implying constant project revisions. However, these last have not been defined as tasks before but is a time investment to perform all the project accurately.

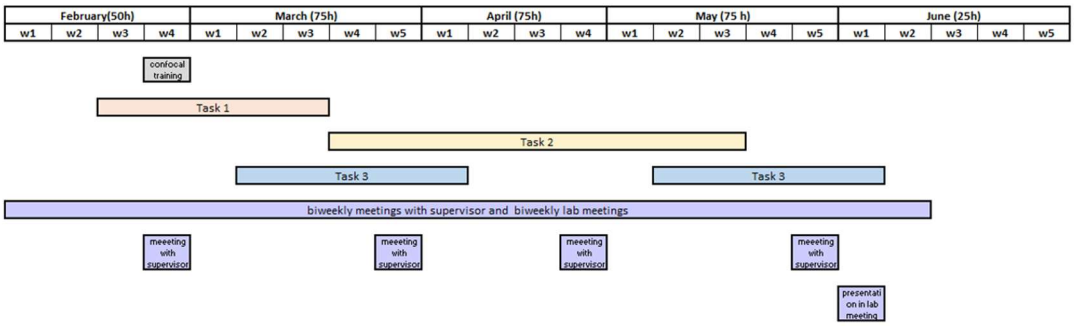

Figure 36. First Gantt diagram sketch.

Figure 36 represents the time dedicated each moth to the specific tasks one, two, three or four. Each task encompasses different work packages. By a way of illustration, Task 1, includes Initiation and Training work packages. In any case, a Gantt diagram illustrated more in detail is presented in Figure 37.

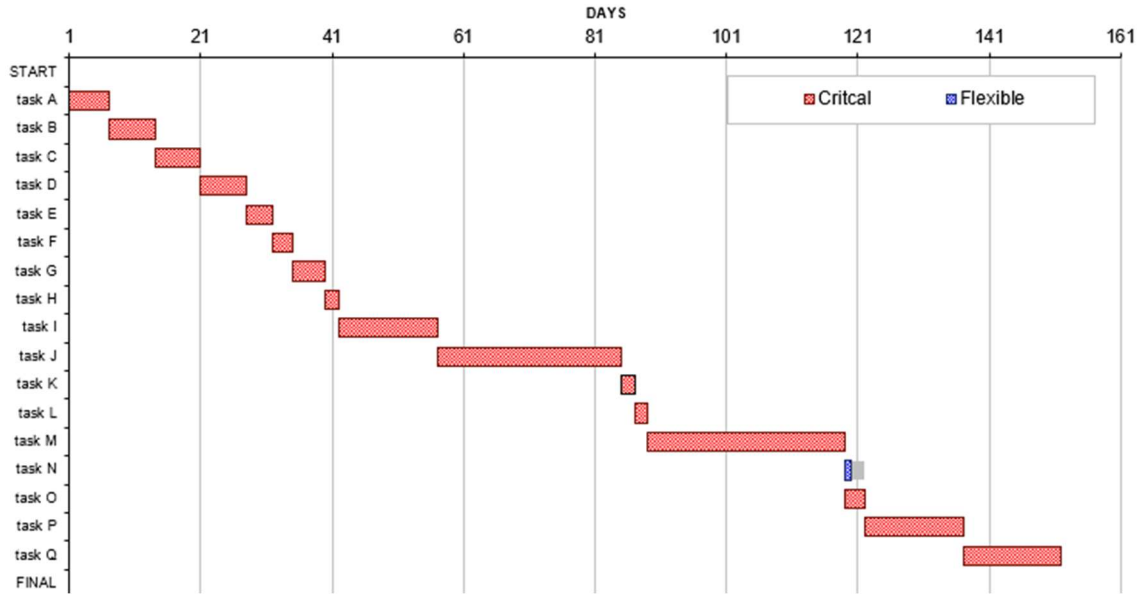

Figure 37. Gantt diagram

7. TECHNICAL VIABILITY

Fulfilling a SWOT analysis is fundamental for ensuring the success of this project, as well as any project regardless its objective. This strategic tool enables the prevention of potential challenges and eases a comprehensive and exhaustive assessment of the project's overall outcome.

In addition, a SWOT analysis provides a structured approach to evaluating either the internal or external factors that can eventually potentially influence the project. Internal factors refer to the available resources of the laboratory, team member's expertise, and organizational abilities. In contrast, external factors include opportunities and threats such as market dynamics or variations, competing entities, funding accessibility, and technological improvements. By continuously identifying these factors, the project can strategically focus on its strengths, overcome its weaknesses, explore external opportunities and lighten potential burdens.

Table 11. SWOT representation

STRENGTHS	WEAKNESSES
Innovative research field. It is studied a cutting-edge topic relatively low considered. Combines engineering aspects with biology knowledge, leading to an exhaustive understanding. Exist a lot of theoretical founds in neuroscience, which the project can be based on having a start point. Highly developed methodologies and technologies available at the laboratory. Findings among the project can contribute into neurodegenerative understanding, helping medical advances. Funding and resources provided to the research.	No previous experience by the student performing some tasks. Insufficient theoretical background by the student. Hence, previous literature research is needed. Inability to perform the project with absence of reagents or material. Limited time to fulfil the scope of the study.
OPPORTUNITIES	**THREATS**
Technological advances in imaging and molecular biology fields enhance data collection, giving better and more accurate results. Access to limited databases and literature by the institute. Collaboration and fundings with other companies interested in the subject. Assistance to conferences to spread the new information acquired.	Possibility of facing unforeseen technical difficulties. Lack of supplied due to chain disruption for essential material or equipment. High experience required. Changes in the availability of funding and resources.

Throughout the project what we were more concerned about was the lack of experience the student had related to the techniques and experiments developed. Moreover, the time limits did not help at all as the trainings and abilities require time to acquire. In addition, we were also conscious of the external threats we might struggle with, like the possibility of material and equipment unavailability.

For instance, the project faced several internal weaknesses and threats that impacted on the scope of the findings exposed in Section 5. One of the most important limitations included restricted access to laboratory equipment and material resources, the technical level of the procedures, and the initial learning curve in order to feel familiar with the project needs and techniques. Externally, the dominant threat was the limited range of substrate stiffness tested, which limited the physiological relevance of the model analysed. Performing the technique exclusively with static hydrogels fails to reproduce the dynamic changes, and the reliability of SeNCYT sensor expression when live imaging. This last constraint was accompanied by a reduced sample size and lack of

reproducibility. In addition, time constraints supposed a major problem throughout the development of the whole project, as experimental procedures need time to be performed properly. All these factors mentioned limit the generalization of the results and claim the need for future studies with methodological improvements.

Nevertheless, we took advantage of the opportunities the market gave us and the strength we had. The fundings allowed the team to enjoy of technological advanced resources and a strong updated laboratory tools and spaces. Furthermore, the amount of literature related to neuroscience and some of the similar projects developed also helped to the progress of the whole study by far. At long last, there was expected collaborations and contributions to the research given the relevance and innovation of the topic it is focused on.

8. ECONOMICAL VIABILITY

A deep analysis of the resources employed during the project is key to evaluate its financial feasibility and overall economic viability. Since the purpose of this study is generating academic knowledge anticipated benefits before the ending of the study are not expected.

Table 12 presents a detailed breakdown of project-related expenses, including the cost of experimental reagents, laboratory supplies, like gloves, and equipment use, which has been calculated based on the usage time of the machinery. It also takes into account human resources involved, especially the hours invested in the project by the director and the student. These lasts are valued at 20€ and 8€, respectively.

Table 12. Description of materials, respective quantity used and final price.

ITEM	QUANTITY USED	FINAL PRICE (€)
Reagents		
DMSO (Invitrogen™, D12345)	1 mL	3.87
70% ethanol (Sigma-Aldrich™, 470198)	2 L	191.75
DMEM/F12 (Gibco™, 11320033)	1 L	68.8
Fetal Bovine Serum heat inactivated (Gibco™, 10082147)	112 mL	155.46
Pen/Strep*L-Glut (Invitrogen™, 10378016)	100 mL	42.17
PBS (Gibco™, 10010002)	2 L	72.8
TrypLE Express™ (Gibco™, 12604013)	15 mL	3.08
Trypan Blue (Gibco™, 15250061)	0,1 mL	0.04
Plasmid NGN2 (Addgene, 34999)	5000 ng	85$
Plasmid pLenti PGK-SV40A4-eGFP-2PrA	5000 ng	85$
pMD2.G (Addgene, 12259)	1750 ng	85$
psPAX2 (Addgene, 12260)	3250 ng	85$
HEK 293T cells (CLS, 300189)	1x	375
OptiMEM (Gibco™, 11058021)	1 mL	0.1
DMEM High glucose (Gibco™, 10569010)	500 µL	0.04
Lenti-X™ Concentrator (Takara, 631232)	9 mL	16.09
Polybrene (Sigma-Aldrich™, TR-1003-G)	0,32 µL	0.02
Puromycin (Thermo Scientific Chemicals, J66301.MC)	4 µg	0.02
PrestoBlue® (Thermofisher, A13261)	450 µL	4.01
Matrigel (Corning, FAL356231)	6,4 mL	222.26
EC23 (Biotechne, 4011)	100 µL	6.42

Neurobasal-A-Media (Gibco™, 12348017)	250 mL	46
BDNF (Peprotech, 450-02)	500 µL	94.5
KCl (Sigma-Aldrich™, P5405)	100 µL	0
B27 (Gibco Life Technologies, 17564-044)	200 µL	2.14
Doxycycline (Thermo Scientific Chemicals, J67043.AE)	500 µL	1.1
Laminin (Gibco™, A29249)	500 µL	3.28
Acetic Acid (Sigma-Aldrich™, 338826)	2 mL	3.54
Bind Silane (Sigma-Aldrich™, 440159)	2 mL	1.18
Ethanol 96% (Panreac, 131085.1612)	100 mL	2.86
40% Acrylamide (Biorad, 161-0140)	4 mL	1.11
2% Bis Acrylamide (Biorad, 1610142)	1 mL	0.24
Beads (Invitrogen™, F8811)	72 µL	4.88
APS (Sigma-Aldrich™, A3678)	90 µL	0
TEMED (Sigma-Aldrich™, T9281-25ML)	9 µL	0.02
HEPES (Sigma-Aldrich™, H0887)	360 µL	0.63
Sulfo-SANPAH (Thermofisher)	3 mL	1.82
MilliQ Water (IBEC)	500 mL	2.5
Fibronectin (Gibco™, 33016015)	880 µL	2.9
4% PFA (Thermo Scientific Chemicals, 047392.9L)	10 mL	19
Triton X (Sigma-Aldrich™, T8787)	20 µL	0.02
2.5% BSA (Invitrogen™, A23017)	20 mL	11.04
Hoechst 33342 DNA stain	50 µL	1
$MgCl_2$	13.33 mg	0.01
$CaCl_2 \cdot 2H_2O$	22.64 mg	0.01
D-Manitol	10 g	4.81
BrainPhys	100 mL	30.8
Employed Material		
Sigma-Aldrich™ 10 µl pipette tips	200 units	5.45
Sigma-Aldrich™ 200 µl pipette tips	200 units	5.53
Sigma-Aldrich™ 1000 µl pipette tips	300 units	5.67
Sigma-Aldrich™ 2 ml serological pipettes	50 units	28.75
Sigma-Aldrich™ 5 ml serological pipettes	50 units	19.68
Sigma-Aldrich™ 10 ml serological pipettes	70 units	28.04
Sigma-Aldrich™ 25 ml serological pipettes	70 units	52.15
Sigma-Aldrich™ Eppendorf Conical tubes	20 units	1.33
Sigma-Aldrich™ Eppendorf Conical tubes	15 units	1.13
Sigma-Aldrich™ Corning 50 mL Centrifuge Tube	35 units	21
Sigma-Aldrich™ Corning 15 mL Centrifuge Tube	50 units	18.83
Sigma-Aldrich™ Cell culture flasks 75 cm^2	20 units	45.8
Sigma-Aldrich™ Cell Culture 96-wells plate	4 units	13.13
Sigma-Aldrich™ Cell Culture 8 chamber slide	4 units	50
Sigma-Aldrich™ Cell Culture 6 wells	1 unit	32.8
Sigma-Aldrich™ Microscope slide	10 units	14.72
Sigma-Aldrich™ Nitrile Santex Gloves	1000 units	99
18 mm diameter coverslips (Paul Marienfield)	10 units	2.65
24 x 40 mm coverslips #1.5 (VWR) (Menzel-Gläser)	6 units	0.6
MatTek's 35mm Glass Bottom Dishes	30 units	153$
Equipment		
Neubauer chamber (BLAUBRAND®)	5 hours	0.05

Confocal Microscope (Zeiss LSM900)	3 hours	0.2
Biological culture hood (Telstar bio2 advance)	10 hours	272
Infinite M200 PRO Multimode Microplate Reader from Tescan	70 hours	5.32
Cell culture inverted optical microscope (TS100; Nikon)	20 minutes	0.15
Cell incubator (ThermoScientific forma steri-cycle i160)	5 hours	0.11
Fridge (liebherr profiline)	4 months	466.6
Cell culture centrifuge (Eppendorf Centrifuge 5702)	4 months	31
Flow hood (flores valles)	3 hours	0.16
Mr Frosty container	10 hours	0.32
Human Resources		
Undergraduate Student	500 h	4400
Research Director	550 h	11000
	TOTAL	**18512,49**

A substantial portion of the budget is destinated for reagents used in experimental procedures, particularly the ones required for specialized techniques, such as cell differentiation and imaging.

In any case, it is important to hallmark that the project received fundings from IBEC. Consequently, the final disbursement varies as a great portion of all the expenses related to material and equipment is provided by the institution and shared with other investigations.

9. REGULATION AND LEGAL ASPECTS

For successfully aligning this research project with a legally compliant and ethically responsible research, a proper alignment with data protection laws, biosafety standards, funding obligations, and principles of transparency must be undergone. At IBEC, all scientific activities are regulated by the *European Code of Conduct for Research Integrity (ALLEA, 2023) [*58], which enhances values as reliability, honesty, accountability and appreciation for professional standards. Fulfilment with this code boost the credibility of the researchers as well as their work. In addition, it contributes to the trustworthiness of scientific knowledge as it follows the research community expectations. IBEC also includes an institutional commitment to Open Science, guided by recent initiatives like the *Barcelona Declaration on Open Research Information (*2024) [59]. Within the most important legal frameworks that supporting open science, Law 17/2022, which is an update of Law 14/2011 on Science, Technology and Innovation (BOE, 2022) [60] and Organic Law 2/2023 on the Spanish University System, which boost transparency (BOE, 2023) are considered. In the regional context, Catalonia's Law 9/2022 strengthen these principles by making official open science obligations across the territory (DOGC, 2022) [61]. These legal constraints are consistent with the principles defined in the *Charter of Fundamental Rights of the EU* (European Union, 2012), and with national laws such as Spanish law 19/2013 (BOE, 2013) [62] which ensures that scientific activity is financed with public funds and remains open to society.

Another important field to consider are ethical regulations. For instance, projects involving human biomedical material, such as human embryonic or iPSCs, must fulfil Law 14/2007 on Biomedical Research and Royal Decree 1527/2010 (BOE, 2007; BOE, 2010) [63], [64]. In such cases, the approval from national and regional ethic committees is needed before the initiation of the experimental procedures, and in Catalonia, must be also authorized by the Department of Health of the Generalitat. This project involves dealing with tumour cells, SH-SY5Y, which are considered a hazardous substance. As a consequence, is essential to follow the Royal Decree 66/1997 [65], which sets protection measures for workers (BOE, 1997). Furthermore, to enhance protection

during the experiment's performance, IBEC offers a complete training course of risk prevention. This training, knowledge and skills for safe laboratory practices are included.

Eventually, recently, additional developments have reshaped the research fields. As an example, the EU Artificial Intelligence Act (2024) [66] aimed the regulation of artificial intelligence, as well as the enhancement of regulation of transparency, and documentation of experimental methods, and risk management protocols (European Commission 2012) [67]. Additionally, the Spanish Government made an investment in order to improve research infrastructure, talent, and enhance open science within the national system (Ministerio de Ciencia, Innovación y Universidades, 2024) [68].

Altogether, these legal, and institutional commitment reveals IBEC dedication to ensure that their projects are in line with ethical standards, public responsibility, and updated legal standards.

10. CONCLUSIONS AND FUTURE LINES

Our results were built upon previous studies undertaken in the laboratory which demonstrated that NGN2 overexpression efficiently induces neuronal differentiation in SH-SY5Y cells. In addition, these differentiated cells exhibit mechanosensitive behaviour by responding to mechanical cues such as substrate stiffness. Following these findings, we explored the mechanoregulation of nucleocytoplasmic transport using SeNCYT construct as a fluorescent reporter of nucleocytoplasmic dynamics

After a 10-day differentiation process, SH-SY5Y cells unveil neuron-like morphology and behaviour. In order to ensure experimental strength, essential optimizations were undertaken, including reduction of media autofluorescence, enrichment of cells expressing high levels of SeNCYT expression, and accurate fabrication of polyacrylamide (PAA) gels to control substrate stiffness and enhance cell adhesion. Altogether, this workflow enabled the reliable study of NCT dynamics in response to environmental mechanical and osmotic changes.

We observed that hyperosmotic treatments led to a clear reduction in nuclear area and a decrease in SeNCYT nuclear to cytoplasmic (N/C) ratio, which indicates an increase of SeNCYT presence on the cytoplasmic regions of the cells, finding consistent with an alteration of the nuclear transport. Unlikely, hypoosmotic conditions did not yield a significative morphological or localization change. This fact it might possibly be due to physical constraints set by the substrate, glass surface, or due to cellular limitations in expansion. In order to understand the reason of this behaviour Future experiments using softer gels may help determine whether this insensitivity is an intrinsic cellular limitation or a result of mechanical saturation.

In addition, regarding the analysis of neurons seeded onto PAA gels, neurons on stiffer substrates increased nuclear area and SeNCYT nuclear accumulation. These results are in line with the literature showing that for stiffer substrates cell spreading and nuclear expansion is enhanced. Consequently, the promotion of nuclear import of complexes is intensified. Although some results did not reach statistical significance due to limited sample size, the observed trends consistently support a mechanosensitive regulation of NCT in neuronal cells.

Furthermore, while SeNCYT served as a sensitive reporter for passive nucleocytoplasmic diffusion, extending this analysis to mechanosensitive proteins will be essential. This will probably require an initial screening, because neurons typically express low levels of canonical mechanosensors like

YAP. For instance, proteins like TDP-43, which are mislocalized in neurodegenerative conditions, could help establish how mechanical cues influence active transport pathways.

To further prove the physiological relevance of these findings, similar experiments should be conducted using more representative models such as iPSC-derived neurons, which better recapitulate the cellular complexity and mechanical properties of human brain tissue. These models could also facilitate the study of patient-specific responses, particularly in the context of neurodegenerative diseases, where both cytoskeletal architecture and nuclear transport are known to be compromised.

Finally, understanding the functional consequences of altered NCT, such as its effects on transcriptional regulation, stress response, and long-term neuronal viability, will be key to determining its broader biological impact. This could open new research directions aimed at identifying therapeutic strategies targeting the mechanotransduction pathways that modulate nuclear-cytoplasmic dynamics.

In summary, this work lays a robust foundation for the systematic investigation of how physical forces shape the behaviour of neuronal cells at the molecular level. By integrating mechanobiology, imaging, and neurobiology, it provides a stepping stone toward future studies on disease mechanisms and potential regenerative or protective strategies for nervous system disorders.

11. REFERENCES

[1] Institute for Bioengineering of Catalonia Cellular and molecular mechanobiology - Institute for Bioengineering of Catalonia. Available at: https://ibecbarcelona.eu/cellmolmech

[2] Zhu C, Lee CY, McIntire LV. From cellular to molecular mechanobiology. APL Bioeng. 2020 Feb 14;4(1):010902. doi: 10.1063/1.5129937. PMID: 32095735; PMCID: PMC7021513. Available at: https://www.ncbi.nlm.nih.gov/pmc/articles/PMC7021513/

[3] Kamkin, A. (2005g) Mechanosensitivity of Cells from Various Tissues. Available at: https://www.ncbi.nlm.nih.gov/books/NBK7493/

[4] Adminpcb Contact - Parc Científic de Barcelona. Available at: https://www.pcb.ub.edu/en/contact/

[5] Scheltens, P., De Strooper, B., Kivipelto, M., Holstege, H., Chételat, G., Teunissen, C. E., Cummings, J., & van der Flier, W. M. (2021). Alzheimer's disease. Lancet (London, England), 397(10284), 1577–1590. Available at: https://doi.org/10.1016/S0140-6736(20)32205-4

[6] Iqbal, K., Liu, F., Gong, C. X., & Grundke-Iqbal, I. (2010). Tau in Alzheimer disease and related tauopathies. Current Alzheimer research, 7(8), 656–664. Available at: https://doi.org/10.2174/156720510793611592

[7] Martino, F., Perestrelo, A. R., Vinarský, V., Pagliari, S., & Forte, G. (2018). Cellular Mechanotransduction: From Tension to Function. *Frontiers in physiology*, *9*, 824. Available at: https://doi.org/10.3389/fphys.2018.00824

[8] Hall, C. M., Moeendarbary, E., & Sheridan, G. K. (2021). Mechanobiology of the brain in ageing and Alzheimer's disease. The European journal of neuroscience, 53(12), 3851–3878. Available at: https://doi.org/10.1111/ejn.14766

[9] Zheng, Q., Liu, H., Yu, W., Dong, Y., Zhou, L., Deng, W., & Hua, F. (2023). Mechanical properties of the brain: Focus on the essential role of Piezo1-mediated mechanotransduction in the CNS. *Brain and behavior*, *13*(9), e3136. Available at: https://doi.org/10.1002/brb3.3136

[10] Donnaloja, F., Limonta, E., Mancosu, C., Morandi, F., Boeri, L., Albani, D., & Raimondi, M. T. (2023). Unravelling the mechanotransduction pathways in Alzheimer's disease. Journal of biological engineering, 17(1), 22. Available at: https://doi.org/10.1186/s13036-023-00336-w

[11] Hutten, S., & Dormann, D. (2020). Nucleocytoplasmic transport defects in neurodegeneration — Cause or consequence? Seminars in Cell &Amp; Developmental Biology, 99, 151-162. Available at: https://doi.org/10.1016/j.semcdb.2019.05.020

[12] Andreu, I., Granero-Moya, I., Garcia-Manyes, S., & Roca-Cusachs, P. (2022). Understanding the role of mechanics in nucleocytoplasmic transport. *APL bioengineering*, *6*(2), 020901. Available at: https://doi.org/10.1063/5.0076034

[13] Ding, B., & Sepehrimanesh, M. (2021). Nucleocytoplasmic Transport: Regulatory Mechanisms and the Implications in Neurodegeneration. International journal of molecular sciences, 22(8), 4165. Available at: https://doi.org/10.3390/ijms22084165

[14] Korgiopoulou, Christina. "Modelling Alzheimer's Disease in Cells and Animals". StressMarq Biosciences.17 of March of 2020. Available at: https://www.stressmarq.com/modelling-alzheimers-disease-cells-animals/

[15] Oprea, D., Sanz, C. G., Barsan, M. M., & Enache, T. A. (2022). PC-12 Cell Line as a Neuronal Cell Model for Biosensing Applications. Biosensors, 12(7), 500. Available at: https://doi.org/10.3390/bios12070500

[16] Slanzi, A., Iannoto, G., Rossi, B., Zenaro, E., & Constantin, G. (2020). In vitro Models of Neurodegenerative Diseases. Frontiers in cell and developmental biology, 8, 328. Available at: https://doi.org/10.3389/fcell.2020.00328

[17] Qian, X., Song, H., & Ming, G. L. (2019). Brain organoids: advances, applications and challenges. *Development (Cambridge, England)*, *146*(8), dev166074. Available at: https://doi.org/10.1242/dev.166074

[18] Elosegui-Artola, A., Andreu, I., Beedle, A. E. M., Lezamiz, A., Uroz, M., Kosmalska, A. J., Oria, R., Kechagia, J. Z., Rico-Lastres, P., Le Roux, A. L., Shanahan, C. M., Trepat, X., Navajas, D., Garcia-Manyes, S., & Roca-Cusachs, P. (2017). Force Triggers YAP Nuclear Entry by Regulating Transport across Nuclear Pores. Cell, 171(6), 1397–1410.e14. Available at: https://doi.org/10.1016/j.cell.2017.10.008

[19] Stewart, M. P., Langer, R., & Jensen, K. F. (2018). Intracellular Delivery by Membrane Disruption: Mechanisms, Strategies, and Concepts. *Chemical reviews*, *118*(16), 7409–7531. Available at: https://doi.org/10.1021/acs.chemrev.7b00678

[20] Ngo, M. T., & Harley, B. A. C. (2021). Progress in mimicking brain microenvironments to understand and treat neurological disorders. *APL bioengineering*, *5*(2), 020902. Available at: https://doi.org/10.1063/5.0043338

[21] Tortorella, I., Argentati, C., Emiliani, C., Morena, F., & Martino, S. (2022). Biochemical Pathways of Cellular Mechanosensing/Mechanotransduction and Their Role in Neurodegenerative Diseases Pathogenesis. Cells, 11(19), 3093. Availale at: https://doi.org/10.3390/cells11193093

[22] Alzheimer's Disease Diagnostics and Therapeutics Market Size & Share Analysis - Growth Trends & Forecasts (2024 - 2029) Available at: https://www.mordorintelligence.com/industry-reports/alzheimers-diagnosis-and-drugs-market

[23] Alzheimer's Therapeutics Market Size, Share, Competitive Landscape and Trend Analysis Report by Drug Class, by Distribution Channel: Global Opportunity Analysis and Industry Forecast, 2021-2031. Available at: https://www.alliedmarketresearch.com/alzheimers-therapeutics-market-A10535

[24] 2023 Alzheimer's disease facts and figures. (2023). *Alzheimer's & dementia: the journal of the Alzheimer's Association*, *19*(4), 1598–1695. Available at: https://doi.org/10.1002/alz.13016

[25] Yang, H. D., Kim, D. H., Lee, S. B., & Young, L. D. (2016). History of Alzheimer's Disease. Dementia and neurocognitive disorders, 15(4), 115–121. Available at: https://doi.org/10.12779/dnd.2016.15.4.115

[26] Pistollato, F., Ohayon, E. L., Lam, A., Langley, G. R., Novak, T. J., Pamies, D., Perry, G., Trushina, E., Williams, R. S., Roher, A. E., Hartung, T., Harnad, S., Barnard, N., Morris, M. C., Lai,

M. C., Merkley, R., & Chandrasekera, P. C. (2016). Alzheimer disease research in the 21st century: past and current failures, new perspectives and funding priorities. Oncotarget, 7(26), 38999–39016. Available at: https://doi.org/10.18632/oncotarget.9175

[27] Kerwin, D., Abdelnour, C., Caramelli, P., Ogunniyi, A., Shi, J., Zetterberg, H., & Traber, M. (2022). Alzheimer's disease diagnosis and management: Perspectives from around the world. Alzheimer's & dementia (Amsterdam, Netherlands), 14(1), e12334. Available at: https://doi.org/10.1002/dad2.12334

[28] van der Flier, W.M., de Vugt, M.E., Smets, E.M.A. et al. Towards a future where Alzheimer's disease pathology is stopped before the onset of dementia. Nat Aging 3, 494–505 (2023). Available at: https://doi.org/10.1038/s43587-023-00404-2

[29] Kumarasinghe, U., Fox, L. N., & Staii, C. (2022). Combined Traction Force-Atomic Force Microscopy Measurements of Neuronal Cells. *Biomimetics (Basel, Switzerland)*, *7*(4), 157. Available at: https://doi.org/10.3390/biomimetics7040157

[30] Aron N. Horvath, Andreas A. Ziegler, Stephan Gerhard, Claude N. Holenstein, Benjamin Beyeler, Jess G. Snedeker, Unai Silvan, Focus on time: dynamic imaging reveals stretch-dependent cell relaxation and nuclear deformation, Biophysical Journal, Volume 120, Issue 5, 2021, Pages 764-772, ISSN 0006-3495. Available at: https://doi.org/10.1016/j.bpj.2021.01.020.

[31] Eimear B. Dolan, Stefaan W. Verbruggen, Rebecca A. Rolfe, Chapter 1 - Techniques for studying mechanobiology, Editor(s): Stefaan W. Verbruggen, Mechanobiology in Health and Disease, Academic Press, 2018, Pages 1-53, ISBN 9780128129524. Available at: https://doi.org/10.1016/B978-0-12-812952-4.00001-5.

[32] Liu, Y., Wu, W., Feng, S. *et al.* Dynamic response of the cell traction force to osmotic shock. *Microsyst Nanoeng* **9**, 131 (2023). Available at: https://doi.org/10.1038/s41378-023-00603-2

[33] Finan, J. D., & Guilak, F. (2010). The effects of osmotic stress on the structure and function of the cell nucleus. *Journal of cellular biochemistry*, *109*(3), 460–467. Available at: https://doi.org/10.1002/jcb.22437

[34] Granero-Moya, I., Venturini, V., Belthier, G., Groenen, B., Molina-Jordán, M., González-Martín, M., Trepat, X., van Rheenen, J., Andreu, I., & Roca-Cusachs, P. (2024). Nucleocytoplasmic transport senses mechanical forces independently of cell density in cell monolayers. *Journal of cell science*, *137*(17), jcs262363. Available at: https://doi.org/10.1242/jcs.262363

[35] Kelley, J. B., & Paschal, B. M. (2007). Hyperosmotic stress signaling to the nucleus disrupts the Ran gradient and the production of RanGTP. *Molecular biology of the cell*, *18*(11), 4365–4376. Available at: https://doi.org/10.1091/mbc.e07-01-0089

[36] Eva-Maria Hock, Zuzanna Maniecka, Marian Hruska-Plochan, Stefan Reber, Florent Laferrière, Sonu Sahadevan M.K., Helena Ederle, Lauren Gittings, Lucas Pelkmans, Luc Dupuis, Tammaryn Lashley, Marc-David Ruepp, Dorothee Dormann, Magdalini Polymenidou, Hypertonic Stress Causes Cytoplasmic Translocation of Neuronal, but Not Astrocytic, FUS due to Impaired Transportin Function, Cell Reports, Volume 24, Issue 4, 2018, Pages 987-1000.e7, ISSN 2211-1247. Available at: https://doi.org/10.1016/j.celrep.2018.06.094.

[37] Pouria Moshayedi, Gilbert Ng, Jessica C.F. Kwok, Giles S.H. Yeo, Clare E. Bryant, James W. Fawcett, Kristian Franze, Jochen Guck, The relationship between glial cell mechanosensitivity and foreign body reactions in the central nervous system, Biomaterials, Volume 35, Issue 13, 2014, Pages 3919-3925, ISSN 0142-9612. Available at: https://doi.org/10.1016/j.biomaterials.2014.01.038.

[38] Ozgun, A. et al. (2021) "Substrate stiffness effects on SH-SY5Y: The dichotomy of morphology and neuronal behavior," Journal of Biomedical Materials Research Part B, 109(1), pp. 92–101. Available at: https://doi.org/10.1002/jbm.b.34684.

[39] Leipzig, N. D., & Shoichet, M. S. (2009). The effect of substrate stiffness on adult neural stem cell behavior. *Biomaterials*, *30*(36), 6867–6878. Available at: https://doi.org/10.1016/j.biomaterials.2009.09.002

[40] Qiao, Y., Gong, J., Jin, Z., Tu, Y., & Yang, X. (2024). An optimized method of culturing neurons based on polyacrylamide gel. *Biophysics reports*, *10*(1), 41–47. Available at: https://doi.org/10.52601/bpr.2023.230033

[41] Lei, M., Wang, W., Zhang, H., Gong, J., Wang, Z., Cai, H., Yang, X., Wang, S., & Ma, C. (2023). Cell-cell and cell-matrix adhesion regulated by Piezo1 is critical for stiffness-dependent DRG neuron aggregation. *Cell reports*, *42*(12), 113522. Available at: https://doi.org/10.1016/j.celrep.2023.113522

[42] Song, S., Ashok, A., Williams, D., Kaufman, M., Duff, K., & Sproul, A. (2021). Efficient Derivation of Excitatory and Inhibitory Neurons from Human Pluripotent Stem Cells Stably Expressing Direct Reprogramming Factors. *Current protocols*, *1*(6), e141. Available at: https://doi.org/10.1002/cpz1.141

[43] Dravid, A. et al. (2021) "Optimised techniques for high-throughput screening of differentiated SH-SY5Y cells and application for neurite outgrowth assays," Scientific Reports, 11(1). Available at: https://doi.org/10.1038/s41598-021-03442-1

[44] Overbaugh, J., Mangold, C.A., and Szpara, M.L. (2016) "Differentiation of the SH-SY5Y Human Neuroblastoma Cell Line," Journal of Visualized Experiments [Preprint], (108). Available at: https://doi.org/10.3791/53193

[45] Christie, V.B. et al. (2010) "Retinoid supplementation of differentiating human neural progenitors and embryonic stem cells leads to enhanced neurogenesis in vitro," Journal of Neuroscience Methods, 193(2), pp. 239–245. Available at: https://doi.org/10.1016/j.jneumeth.2010.08.022

[46] Clemens, G. et al. (2013) "The action of all-trans-retinoic acid (ATRA) and synthetic retinoid analogues (EC19 and EC23) on human pluripotent stem cells differentiation investigated using single cell infrared microspectroscopy," Molecular BioSystems, 9(4), p. 677. Available at: https://doi.org/10.1039/c3mb25505k

[47] Nucleocytoplasmic transport senses mechanics independently of cell density in cell monolayers. Ignasi Granero-Moya, Guillaume Belthier, Bart Groenen, Marc Molina-Jordán, Miguel González-Martín, Xavier Trepat, Jacco van Rheenen, Ion Andreu, Pere Roca-Cusachs. bioRxiv 2024.01.11.575167. Available at:https://doi.org/10.1101/2024.01.11.575167

[48] Andreu, I., Granero-Moya, I., Chahare, N. R., Clein, K., Molina-Jordán, M., Beedle, A. E. M., Elosegui-Artola, A., Abenza, J. F., Rossetti, L., Trepat, X., Raveh, B., & Roca-Cusachs, P. (2022). Mechanical force application to the nucleus regulates nucleocytoplasmic transport. Nature cell biology, 24(6), 896–905. Available at: https://doi.org/10.1038/s41556-022-00927-7

[49] *Cell Sorting: Techniques, Applications and Future Directions | Danaher Life Sciences*. (n.d.). Danaher Life Sciences. Available at: https://lifesciences.danaher.com/us/en/library/cell-sorting.html

[50] Skarp, KP., Vartiainen, M.K. (2013). Actin as a Model for the Study of Nucleocytoplasmic Shuttling and Nuclear Dynamics. In: Shav-Tal, Y. (eds) Imaging Gene Expression. Methods in Molecular Biology, vol 1042. Humana Press, Totowa, NJ. Available at: https://doi-org.sire.ub.edu/10.1007/978-1-62703-526-2_18

[51] Elliott A. D. (2020). Confocal Microscopy: Principles and Modern Practices. *Current protocols in cytometry*, *92*(1), e68. Available at: https://doi.org/10.1002/cpcy.68

[52] BrainPhys™ Imaging Optimized Medium. Stemcell Technologies. Available at: https://www.stemcell.com/products/brainphys-imaging-optimized-medium.html

[53] Cellpose a generalist algorithm for cellular segmentation. cellpose. (n.d.). Available at: https://www.cellpose.org/

[54] Stringer, C., Wang, T., Michaelos, M. et al. Cellpose: a generalist algorithm for cellular segmentation. Nat Methods 18, 100–106 (2021). Availbale at: https://doi.org/10.1038/s41592-020-01018-x

[55] Schindelin, J., Arganda-Carreras, I., Frise, E., Kaynig, V., Longair, M., Pietzsch, T., … Cardona, A. (2012). Fiji: an open-source platform for biological-image analysis. *Nature Methods*, *9*(7), 676–682. doi:10.1038/nmeth.2019. Available at: https://imagej.net/ij/index.html

[56] Ignasi Granero-Moya, Guillaume Belthier, Bart Groenen, Marc Molina-Jordán, Miguel González-Martín, Xavier Trepat, Jacco van Rheenen, Ion Andreu, Pere Roca-Cusachs. *Nucleocytoplasmic transport senses mechanics independently of cell density in cell monolayers.* bioRxiv 2024.01.11.575167; Available at: https://doi.org/10.1101/2024.01.11.575167

[57] Protocol for Imaging. ThermoFisher Scientific. Available at: https://www.thermofisher.com/es/es/home/references/protocols/cell-and-tissue-analysis/protocols/hoechst-33342-imaging-protocol.html

[58] ALLEA. (2024, December 19). *The European Code of Conduct for Research Integrity - ALLEA*. Available at: https://allea.org/code-of-conduct/

[59] Peroni, S., & Metadata, R. C. F. O. S. (n.d.). *Home*. Research Centre for Open Scholarly Metadata. Available at: https://openscholarlymetadata.org/

[60] Boletín Oficial del Estado. (2022, septiembre 5). Ley 17/2022, de 5 de septiembre, por la que se modifica la Ley 14/2011, de 1 de junio, de la Ciencia, la Tecnología y la Innovación (BOE-A-2022-14581). Available at: https://www.boe.es/eli/es/l/2022/09/05/17

[61] Boletín Oficial del Estado. (n.d.). *Ley 9/2022, de 21 de diciembre, de la ciencia* (BOE-A-2023-467). Available at: https://www.boe.es/diario_boe/txt.php?id=BOE-A-2023-467

[62] Boletín Oficial del Estado. (2013, diciembre 9). Ley 19/2013, de 9 de diciembre, de transparencia, acceso a la información pública y buen gobierno (BOE-A-2013-12887). Available at: https://www.boe.es/eli/es/l/2013/12/09/19

[63] Boletín Oficial del Estado. (2007, julio 3). Ley 14/2007, de 3 de julio, de Investigación biomédica (BOE-A-2007-12945). Available at: https://www.boe.es/eli/es/l/2007/07/03/14

[64] Boletín Oficial del Estado. (2010, noviembre 15). Real Decreto 1527/2010, de 15 de noviembre, por el que se regulan la Comisión de Garantías para la Donación y Utilización de Células y Tejidos Humanos y el Registro de Proyectos de Investigación (BOE-A-2010-18654). Available at: https://www.boe.es/eli/es/rd/2010/11/15/1527

[65] Boletín Oficial del Estado. (1997, mayo 12). Real Decreto 664/1997, de 12 de mayo, sobre la protección de los trabajadores contra los riesgos relacionados con la exposición a agentes biológicos durante el trabajo (BOE-A-1997-11144). Available at: https://www.boe.es/eli/es/rd/1997/05/12/664

[66] Comisión Europea. (n.d.). Shaping Europe's digital future. Shaping Europe's Digital Future. Available at: https://digital-strategy.ec.europa.eu/en

[67] Unión Europea. (2012). Carta de los Derechos Fundamentales de la Unión Europea (2012/C 326/02). Available at: http://data.europa.eu/eli/treaty/char_2012/oj

[68] Gobierno de España. (2023). Plan Estatal de Investigación Científica, Técnica y de Innovación 2024-2027. Ministerio de Ciencia, Innovación y Universidades. Available at: https://www.ciencia.gob.es/InfoGeneralPortal/documento/80da28ed-be5b-431b-82d5-367d602b713c

12. ANNEXES

12.1. ANNEX 1: Cell Culture Protocols

All protocols mentioned below have been extracted from the laboratory or from other colleagues that have lend them. For instance, from Yara Hinojosa (2023) 'Optimization of SH-SY5Y Differentiation to Study Neuronal Mechanosensitivity'(https://hdl.handle.net/2445/199965), we took the differentiation protocol.

SH-SY5Y Medium Protocol

1. Add to a 500mL DMEM/F12 bottle FBS 10X and Pen/Strep*L-Glut 1x.
2. Mix thoroughly to ensure integration of the reagents.

SH-SY5Y Thawing Protocol

1. Get the cryovial containing frozen SH-SY5Y cells from the liquid nitrogen tank
2. Put the cryovial in a 37ºC water bath until its contents are thawed
3. Clean carefully the exterior of the cryovial with 70% ethanol and insert it inside the sterile cell culture hood.
4. Dilute the contents of the cryovial in 6mL of pre-warmed culture medium
5. Centrifuge the cell suspension at 300g for 4 minutes to obtain cell pelle.
6. Absorb the media and leave pellet, resuspend in 1mL of pre-warmed culture medium
7. Seed the desired amount of cell volume according to the following experiment needs in 12mL of culture medium, pre-warmed as well

SH-SY5Y Freezing Protocol

1. Detach SH-SY5Y cells from the flask with PBS and TrypLE Express™, following the established protocol
2. Resuspend the cell pellet after centrifuge in 1mL of culture medium
3. Prepare the adequate dilutions to achieve a volume of 1mL per cryovial, with a composition of 90% cell medium + cells and 10% of DMSO
4. Add 1mL of the final solution to each of the respective cryovials
5. Locate the cryovials in a Mr. frosty container and store it at -80ºC for 24 hours.
6. After 24 hours, transfer the cryovials to a liquid nitrogen tank for long-term conservation.

SH-SY5Y Passaging Protocol

For T75 cm^2 flasks at 90% cell confluency:

1. Absorb the cell culture medium and rinse the cells with 5mL of PBS, and leave for 5 minutes at RT
2. Aspirate PBS and add 1mL of TrypLE Express™ into the flask. Ensure proper coverage of TrypLE Express™ among all the surface of the flask.
3. Incubate the flask for 5 minutes in the incubator at 37ºC
4. Add 5mL of PBS to the flask and transfer the 6mL contained in the flask into a 15mL falcon tube
5. Centrifuge the mixture at 300g for 4 minutes
6. Aspirate the solution and leave the pellet
7. Add 1mL of cell culture medium pre-warmed and mix thoroughly
8. Prepare a T75 cm^2 flask and add 12mL of cell culture media pre-warmed
9. Add the desired amount of cell solution to the flask

SH-SY5Y Counting Protocol

1. Clean a Neubauer chamber exhaustively with 70% ethanol to guarantee sterility
2. Follow the cell detachment protocol detailed above Annex 1.4 to detach cells
3. Gather 10µL of the cell solution with 1mL of cell culture medium and mix with 10µL of erythrosine. Mix thoroughly
4. Cautiously add 10µL of the mixture to the chamber, inside the grid area between the coverslip and the bottom surface. Allow the sample to reach the edges of the chamber
5. Place the Neubauer chamber in the Automated Cell Counter. Adjust the focus until a clear image of the cells is shown. Set the proper protocol counting method and count
6. Repeat the focusing and counting process three times and average the number of total alive cells given after each counting

12.2. ANNEX 2: Lentivirus Transfection

Reagents:

- Plasmid of interest: pLenti PGK-SV40A4-eGFP-2PrA (Jacco van Rheenen

  Group, Netherlands Cancer Institute)

- Packaging plasmids
  - pMD2.G, Addgene #12259
  - psPAX2, Addgene #12260
- HEK 293T
- Lipofectamine 3000/ P3000 reagent (Thermofisher, Cat nº L3000015)
- OptiMEM (Thermofisher, Cat nº 11058021)
- Media for HEK
  - For normal conditions: DMEM High glucose + 1X Glutamine + 1X Pen/Strep

    (for hIPSCs only if the lentiviral supernatant is concentrated)
- For lentiviral concentration: Lenti-X™ Concentrator (Takara, ref 631232)

Protocol:

Day 0

1. Culture the HEK to get around 40-50% of confluence in normal media, HEK cells tend to grow in colonies, and that reduces lentiviral production, it is better to pass them the night or even in the morning before starting the protocol. At least one passage must be done after freezing. Between 3-4 million HEK seeded 24h before is a good number and usually does not require passage the following day.

Day 1

1. Change media to HEK to new media (with serum) around 1h before starting.
2. Put OptiMEM and Lipofectamine 3000/ reagent p3000 aliquot at RT.
3. Dilute the plasmids in 500µL of OptiMEM, vortex and spin.
   a. Plasmid of interest → 5000 ng
   b. pMD2.G → 1750 ng (J010 Plasmid #12259)
   c. psPAX2 → 3250 ng (J01, Plasmid #12260)

4. Add 20µL of p3000 reagent
5. In a second Eppendorf, mix 30µL of Lipofectamine 3000 to 500µL of OptiMEM, vortex and spin
6. Add the lipofectamine mix to the plasmids+p3000 reagent and mix by inversion (avoid foam formation). Incubate 15 minutes at RT
7. Apply dropwise to the well
8. Incubate overnight

Day 2

1. Change media.

Day 3, Day 4

1. Check the cells, they should remain attached
2. Carefully collect media (around 10 ml). centrifuge x 500g for 10min at 4ºC. Add new media to the cells
3. Filter with 0,45µM syringe filter
4. Store at +4ºC covered with parafilm

Day 5

1. Collect media (around 10mL). centrifuge 500g 10min at 4ºC. Discard cells according to the safety rules.
2. Filter with 0,45 µM syringe filter.
3. Mix with supernatant collected from day 1 and day 2. The last one, day 3, should be the one containing more particles, but if you plan to concentrate it is better to pull them all together)

CONCENTRATION WITH Lenti-X:

a. Transfer clarified supernatant to a sterile 50ml falcon and combine 1 volume of Lenti-X Concentrator with 3 volumes of clarified supernatant (usually 27mL + 9mL of Lenti-X)
b. Incubate mixture at 4°C for 30 minutes to overnight. We usually do at least 2h. It needs to get cold, so it's better when the supernatant of day 1 and 2 was on the fridge and lenti-X just came out from fridge.
c. Centrifuge sample at 1,500g for 45 minutes at 4°C. After centrifugation, an off-white pellet will be visible.
d. Carefully remove supernatant, taking care not to disturb the pellet. Residual supernatant can be removed with either a pipette tip or by brief centrifugation at 1,500 x g.
e. Gently resuspend the pellet from 1/10 to 1/100th of the original volume using complete DMEM, PBS, or TNE. The pellet can be somewhat sticky at first but will go into suspension quickly.
f. Store at +4ºC, better if you use it immediately.

INFECTION

Prepare a solution of Polybrene + lentivirus with normal media. We apply to apply the equivalent to 4mL for a flask of 25 cm^2 for Sh-SY5Y. Add Polybrene so the final concentration is 8µg/mL. Apply the solution dropwise the solution and incubate overnight.

Change to normal media the following morning.

CELL SELECTION

SORTER

12.3. ANNEX 3: Media autofluorescence optimization method

Objective:

Test which of the medias compatible with neurons have lower autofluorescence. There are several components in media diff 2 (NB+b27) that contains fluorescent subsnates (e.g. riboflavine). It has been already tested that BrainPhys is the best, but also quite expensive.

Also, it has been found that BrainPhys is compatible and actually improves SH-SY5Y differentiation: Satir, T. M. et al. (2020). Author Correction: Accelerated neuronal and synaptic maturation by BrainPhys medium increases Aβ secretion and alters Aβ peptide ratios from iPSC-derived cortical neurons. *Scientific reports*, *10*(1), 3993.

Materials

- SH-SY5Y cells + doxNGN2+ SenCYT, sorted for GFP high and culture with puromycin
- Differentiation media 1 basal (no EC27, no puromycin)
- Neurobasal -A
- BrainPhys
- Chamber slides

Method

Seed 20.000 cells/well in 8 well/ chamberslide without coating, using Stage 1 differentiation media and prepare the medias from the table below for tomorrow:

		Repetition					
		1	2	3	mean	SD	%
Basal	NB	285	280	287	284,00	3,606	---
Hyper	NB + Mannitol	486	489	496	490,33	5,132	172,6526
Hypo	NB +Ca/mg	116	119	112	115,67	3,512	59,2723
Basal	BPI	308	310	311	309,67	1,528	---
Hyper	BPI + Mannitol	514	522	529	521,67	7,506	168,4607
Hypo	BPI +Ca/mg	140	132	133	135,00	4,359	56,40474
		Units = mOsmol/kg					

Change medias take 500µL of each media, add 1:2000 Hoechst (0.25µl each). Then change medias in the chamber slide following the pattern below:

L	PBS	1	3	Media 1
	Media 1	2	4	Media 1

Afterwards, incubate for 10 minutes in the incubator at 37ºC.

Eventually, Image with microscope 6, 40x glycerol:

- single plane images: 2048x2048, 6 speed, 2 averaging

- z-stack: 1024x1024, 6 speed, no averaging, change every track, 0,42µm/plane
- z-stack: 1024x1024, 6 speed, 2 averaging, change every track, 0,42µm/plane

→Hoechst: detector CH1 (493-595)

→ EGFP: detector Ch2 GaAsp (more sensitive)

→ High laser power on 488 lasers: 50 power, 650 gain

12.4. ANNEX 4: Media composition for hyper- and hypoosmotic treatments

Objective:

To prepare hyperosmotic and hypoosmotic solutions /medias to optimize the response of sh-sy5y with SeNCYT. Taking as reference Granero-Moya's paper: https://www.biorxiv.org/content/10.1101/2024.01.11.575167v1

"Cell medium has an osmolarity of ∼340 mOsm. ∼113 mOsm hypo-osmotic shocks (66%) were performed by mixing the 500µL of medium with 1.5x de-ionized water with Ca2+ and Mg2+ ion concentration corrected to match those of the medium (264mg/L CaCl2 · 2H2O, 164.67mg/L MgCl2 · 6H2O). ∼695 mOsm hyper-osmotic shocks (204%) were performed by adding 1mL of 1.5x solution containing 96.9g/L D-mannitol (Sigma) to the medium."

The osmolarity of Neurobasal and BrainPhys is around 310 mOs and Neurobasal-A around 257

https://patentimages.storage.googleapis.com/14/7b/2f/f4911d7d95719a/EP2986715B1.pdf

	BrainPhys medium	Ingredient function	Ingredient class	Imgredient	BrainPhys (CB2) mM	*Ranges of BrainPhys (CB2) mM*	Neurobasal-A (mM)	Neurobasal (mM)	DMEM/F12, Glutamax #10565 (mM)
5	BrainPhys Basal		Vitamin	i-Inositol	0.07000000	*<0.07*	0.04000000	0.04000000	0.07000000
5	BrainPhys Basal		Vitamin	Niacinamide (B3)	0.01660000	*<0.02*	0.03280000	0.03280000	0.01660000
5	BrainPhys Basal		Vitamin	Pyridoxine hydrochloride	0.00986000	*<0.010*	0.01960000	0.01960000	0.00986000
5	BrainPhys Basal		Vitamin	Thiamine hydrochloride	0.00644000	*<0.007*	0.01190000	0.01190000	0.00644000
5	BrainPhys Basal		Vitamin	Vitamin B12 (cyanocobalamin)	0.00050200	*<0.0006*	0.00000500	0.00000500	0.00050200
5	BrainPhys Basal [o]		Vitamin	Riboflavin (B2)	0.00058200	*<0.0006*	0.00106000	0.00106000	0.00058200
6									
6.1	BrainPhys Basal [o]	pH	pH buffer	HEPES	5.00000000	*<10*	10.92000000	10.92000000	0.00000000
6.2	BrainPhys Basal [a]	pH	pH Indicator	Phenol Red	0.02150000	*<0.07*	0.07360000	0.02150000	0.02150000
10									
10.5	*BrainPhys Basal*	*QC*	*Properties*	*Osmolarity*	*310 mOsmol/L*	*280-330 mOsmol/L*	*257 mOsmol/L*	*220 mOsmol/L*	315 *mOsmol/L*
10.5	*BrainPhys Basal*	*QC*	*Properties*	*pH*	*7.40000000*	7.3-7.5			
10.6									
20	BrainPhys supplements		Protein (Neurotrophic factors)	Human Brain Derived Neurotrophic Factor (BDNF)	20 ug/L	*<40 ug/L*	0.0000000	0.0000000	0.0000000

The concentrations of Mg2+ (MgSO4) and Ca2+ (CaCl2) are the following:

	BrainPhys medium	Ingredient function	Ingredient class	Imgredient	BrainPhys (CB2) mM	*Ranges of BrainPhys (CB2) mM*	Neurobasal-A (mM)	Neurobasal (mM)	DMEM/F12 Glutamax #10565 (mM)
0	BrainPhys Basal	neuroactive	Inorganic Salt	Sodium Chloride (NaCl)	121.00000000	*>70 and <150*	68.97000000	51.72000000	120.68000000
0.1	BrainPhys Basal	neuroactive	Inorganic Salt	Potassium Chloride (KCl)	4.20000000	*<5*	5.33000000	5.33000000	4.16000000
0.2	BrainPhys Basal	neuroactive	Inorganic Salt	Calcium Chloride (CaCl2) (anhyd.)	1.10000000	*>0.8 and <2*	1.80000000	1.80000000	1.05000000
0.3	BrainPhys Basal	neuroactive	Inorganic Salt	Magnesium Sulfate (MgSO4) (anhyd.)	1.00000000	*<2*	0.00000000	0.00000000	0.40700000
0.4	BrainPhys Basal	neuroactive	Inorganic Salt	Magnesium Chloride (anhydrous)	0.00000000	*<2*	0.81400000	0.81400000	0.30100000
0.5	BrainPhys Basal	neuroactive	Inorganic Salt	Ferric Nitrate (Fe (NO3)3"9H2O)	0.00012400	*<0.0004*	0.00024800	0.00024800	0.00012400
0.6	BrainPhys Basal	neuroactive	Inorganic Salt	Zinc sulfate ($ZnSO_4$-$7H_2O$)	0.00150000	*<0.002*	0.00067400	0.00067400	0.00150000
1	BrainPhys Basal	neuroactive	Inorganic Salt	Cupric sulfate (CuSO4-5H2O)	0.00000000	*<0.00001*	0.00000000	0.00000000	0.00000520
1	BrainPhys Basal	neuroactive	Inorganic Salt	Ferric sulfate (FeSO4-7H2O)	0.00000000	*<0.0015*	0.00000000	0.00000000	0.00150000
1	BrainPhys Basal	pH	Inorganic Salt	Sodium Bicarbonate (NaHCO3)	29.00000000	*<35*	26.19000000	26.19000000	29.02000000
1	BrainPhys Basal	pH	Inorganic Salt	Sodium Phosphate dibasic (Na2HPO4) anhydrous	0.50000000	*<1*	0.00000000	0.00000000	0.50000000

We did not have available (MgSO4) at the start of the experiment, so we worked with MgCl2. We obtained at day MgSO4 heptahydrated (M2773, sigma) from Joaquín Martínez Cambella (Nanoprobes and Nanoswitches Group).

Materials:

- Osmometer OM807. It is a type of Freezing point osmomenter with Adriano Caliari from Bioinspired Interactive Materials and Protocellular Systems Group
- MgCl2
- CaCl2*2 H20
- D-Mannitol
- Milli-Q water

Methods:

Hypoosmotic solution

Mixing 500µL of medium with 1.5x Mili-Q water with Ca2+ and Mg2+ concentration corrected to match those of the medium.

For instance, BrainPhys:

ION	[Mm]
Ca^{2+}	1.1
Mg^{2+}	1

Ions are found in CaCl2 and MgSO4 molecules. Thus, the solution will be done by adding the disponible reagents:

- Ca2+ (CaCl2 ·2H2O)
- MgCl2. Even though, the desired reagent was MgSO4 there was no disponibility.

The calculus performed to obtain the amounts needed were:

- Mili-Q water :$500\mu L \cdot 1.5 = 750\mu L$

- To obtain medium molarity: $n\ moles = C \cdot V$
- Ca^{2+} ($CaCl2 \cdot 2H2O$):

$$n = 1.1 \cdot 10^{-3} M \cdot 700 \cdot 10^{-6} L = 7.7 \cdot 10^{-7}\ mols\ Ca2+$$

$$7.7 \cdot 10^{-7} mols\ CaCl2 \cdot 2H2O \cdot \frac{147.01\ g\ CaCl2 \cdot 2H2O}{1\ mol\ CaCl2 \cdot 2H2O} = 113.20\ \mu g\ CaCl2 \cdot 2H2O$$

- Mg^{2+} ($MgCl2$):

$$n = 1 \cdot 10^{-3} M \cdot 700 \cdot 10^{-6} L = 7 \cdot 10^{-7} mols\ MgCl2$$

$$7 \cdot 10^{-7} mols\ MgCl2 \cdot \frac{95.211 g\ MgCl2}{1\ mol\ MgCl2} = 6.665 \cdot 10^{-5} g\ MgCl2$$

All these calculi are performed for a determined amount of solution. However, the dilutions we need to prepare are of 100mL. Hence, we need to do a conversion to obtain the definite amount of solute we need for each solution.

$$113.20\ \mu g\ CaCl2 \cdot 2H2O \cdot \frac{100\ mL}{500 \cdot 10^{-3}\ mL} = 22.64\ mg\ CaCl2 \cdot 2H2O$$

$$66.65\ \mu g\ MgCl2 \cdot \frac{100\ mL}{500 \cdot 10^{-3}\ mL} = 13.33\ \ mg\ MgCl2$$

$$0.0969\ g\ D-Mannitol \cdot \frac{100\ mL}{1\ mL} = 9.69\ g\ D-Mannitol$$

Hyperosmotic solution

Performed by adding 1mL of 1.5x solution containing 96.9g/L D-mannitol (Sigma) to the medium.

$$V\ medium = \frac{1\ mL}{1.5} = 666.67\ \mu L\ BrainPhys$$

For 1mL of de-ionized water:

$$1 \cdot 10^{-3}\ L \frac{\cdot 96.9\ g\ D-mannitol(Sigma)}{1L} = 0.0969\ g\ D-mannitol(Sigma)$$

Hence, to make solutions hyperosmotic and perform an hyperosmotic shock to analyse SeNCYT shuttling we may add 0.0969 g of D-Mannitol (Sigma) to 666.67µL of medium.

12.5. ANNEX 5: Differentiation of SH-SY5Y into neuron-like cells protocol

Protocol obtained from: Dravid, A. et al. (2021b) "Optimised techniques for high-throughput screening of differentiated SH-SY5Y cells and application for neurite outgrowth assays" Scientific Reports, 11(1). Available at: https://doi.org/10.1038/s41598-021-03442-1.

Reagents

- Dulbecco's Modified Eagle's Medium (DMEM)
- Heat-inactivated fetal bovine serum (hiFBS)
- Glutamax-I
- Penicillin/streptomycin

- Matrigel (1:100 dilution)
- Retinoic acid (RA)
- Neurobasal-A media
- Brain-derived neurotrophic factor (BDNF)
- Potassium chloride (KCl)
- B27

Protocol

1. Seed cells on Matrigel-coated dishes (1:1000) dilution at the necessary density for the following experiment
2. After 24h change the media to Stage 1 media, which includes DMEM supplemented with hiFBS (2.5%), 1 × glutamax-I, 1 × penicillin/streptomycin, Retinoic acid (RA) (10μM)
3. On day 5, switch to Stage 2 media, which includes Brain-derived neurotrophic factor (BDNF) (50 ng/mL), Potassium chloride (KCl) (20 mM), 1 × B27, 1 × glutamax-I, 1 × penicillin/streptomycin
4. On day 10, cells are considered to be differentiated.

Note: maintain cultivated cells at 37ºC with 5% CO_2 in an incubator

12.6. ANNEX 6: Reagents amount for ~0.5kPa and ~15/18kPa PAA gel production

Gel mix

N.S (kPa)	**0.5**	**15/18**
M.S (kPa)	0.64	16.8
Acrylamide 40% (μL)	50	94.4
BisAcrylamide 2% (μL)	7.5	40
Acrylic acid (μL)	0.3	
Beads (μL)	10	10
APS (μL)	2.5	2.5
TEMED (μL)	0.25	0.25
PBS (μL)	429.75	351.35
Final Volume (μL)	500	500